Cover Page

Universiteit Leiden

Leiden University
Repository

The handle https://hdl.handle.net/1887/3158748 holds various files of this Leiden University dissertation.

Author: Loeff, F.C.
Title: Alemtuzumab: the mechanisms of differential sensitivity and resistance
Issue Date: 2021-04-08

ALEMTUZUMAB

THE MECHANISMS OF DIFFERENTIAL SENSITIVITY
AND RESISTANCE

Floris C. Loeff

ALEMTUZUMAB

THE MECHANISMS OF DIFFERENTIAL SENSITIVITY AND RESISTANCE

Proefschrift

ter verkrijging van de graad van doctor aan
de Universiteit Leiden,

op gezag van rector magnificus prof.dr.ir. H. Bijl,
volgens besluit van het college voor promoties
te verdedigen op donderdag 8 april 2021 klokke 16.15 uur

door

Floris Christian Loeff
geboren te Willemstad in 1986

Alles wat een ander kan, kun jij ook!
Hoogstens, duurt het wat langer.

Fred Loeff

CHAPTER 1

Introduction and aims of the thesis
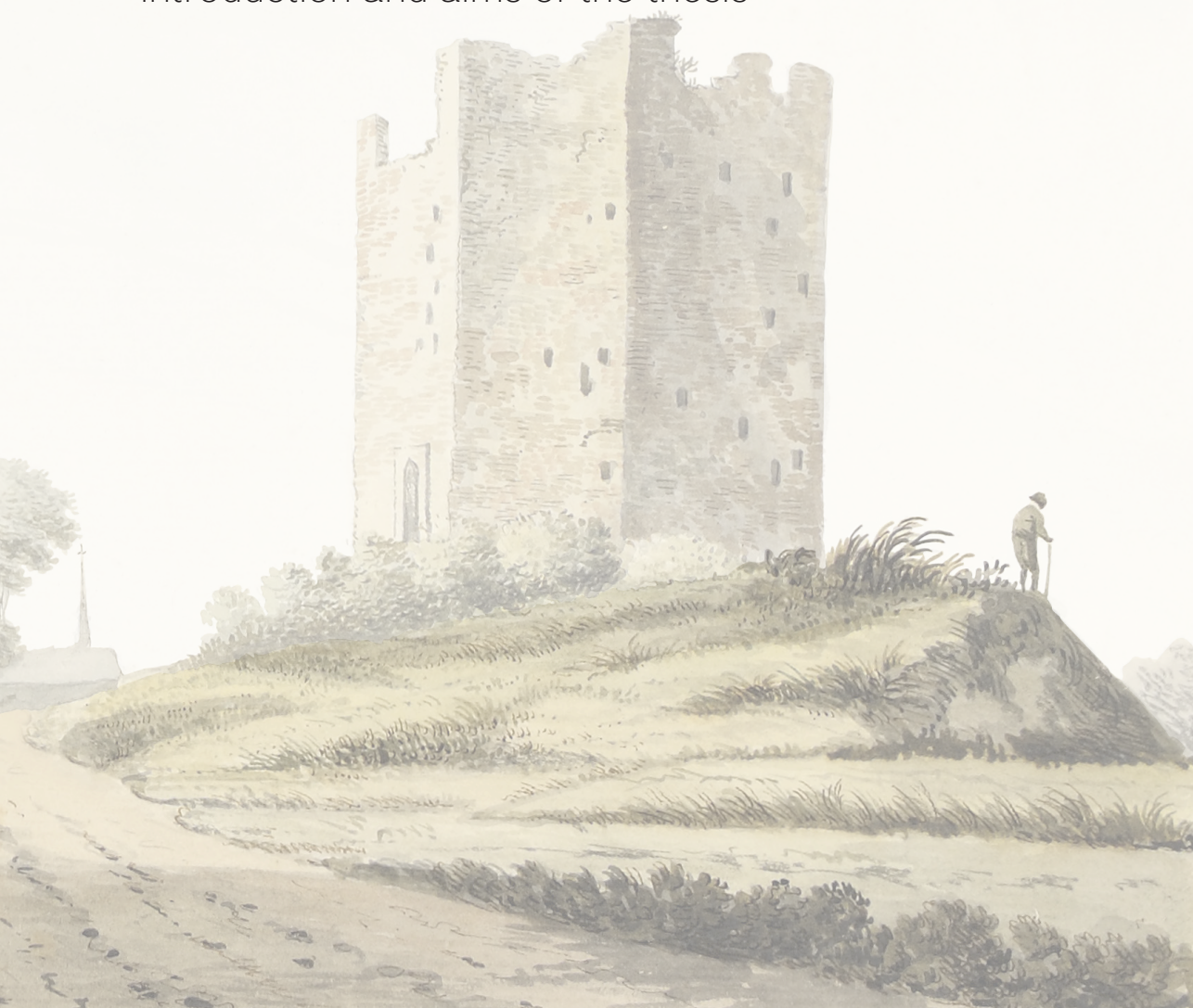
Therapeutic monoclonal antibody alemtuzumab

Immune therapy has been successfully introduced as treatment modality in the fields of hematology, oncology and autoimmune diseases. Monoclonal antibody therapy is a prime member of this class of treatments. Alemtuzumab (ALM) was one of the first monoclonal antibodies commercially available for therapeutic use. ALM is the final product of the Campath project that was started in 1979 by Herman Waldmann and colleagues at the pathology department of Cambridge University. The goal of this project was to create a monoclonal antibody for the purpose of depleting lymphocytes from bone marrow allografts, thereby preventing graft-versus-host disease (GvHD).[1] Immunization of rats with human lymphocytes generated various antibody clones directed against the membrane-associated protein CD52.[2] CD52 is expressed on the cell membrane of all mature lymphocytes, but not (or only marginally) on hematopoietic stem cells, red blood cells, or non-hematopoietic tissue.[2-5] The exact biological function of CD52 is not known. Clinical tests with various variants of CD52-targeting antibodies demonstrated that CD52 was a suitable target to achieve the goals that had been set with limited accompanying toxicity.[2,6,7] To prevent immunogenicity and to realize optimal recruitment of effector mechanisms (see below), a humanized IgG1 variant of anti-CD52 was created resulting in the final format of the therapeutic antibody ALM.[8,9]

Clinical applications of ALM

In 2001, ALM was approved by the European Medicine Agency (EMA) and the US Food and Drug Administration (FDA) as a second-line monotherapy for B-cell chronic lymphocytic leukemia (CLL). Based on its mechanism of action (depletion of CD52-expressing lymphocytes), additional off-label uses have been developed. These include T-cell depletion before allogeneic hematopoietic stem cell transplantation (alloSCT), treatment of B-cell (e.g. B-lymphoblastic leukemia, follicular lymphoma, Waldenström's macroglobulinemia)[10] and T-cell malignancies (e.g. cutaneous T-cell lymphoma, T-cell prolymphocytic leukemia, T-cell acute lymphoblastic leukemia, Sézary syndrome)[11], B-cell or T-cell depletion in the setting of auto-immune diseases (e.g. rheumatoid arthritis[12] and multiple sclerosis[13]) and as immunoprophylaxis in solid organ transplant.[14] In 2012, the original Campath formulation of ALM was withdrawn from the market. Rebranded as Lemtrada, ALM was shortly after approved by the FDA and EMA for the purpose of T-cell depletion in patients suffering from multiple sclerosis. Despite this change, the original Campath formulation is still provided by the manufacturer within compassionate-use programs.

ALM-based T-cell depletion in alloSCT

AlloSCT is a potentially curative treatment for patients who suffer from hematological malignancies or from non-malignant hematological diseases. The goal of the treatment is to replace the patient's diseased hematopoiesis with normal hematopoiesis by infusion of hematopoietic stem cells from a healthy donor. The therapeutic effect and toxicity of alloSCT are determined by closely related mechanisms which are based on the genetic disparities between the donor and patient and are especially mediated via mature T cells that are infused with the donor stem cell graft.[15,16] Recognition and elimination of residual malignant cells by these donor T cells conveys the therapeutic effect, termed graft-versus-tumor effect (GvT).[17] On the other hand, recognition and destruction of non-hematopoietic healthy patient tissue (e.g. skin, liver, or gut) by donor T cells results in toxicity, known as GvHD.[18,19] The clinical relevance of GvHD is reflected in the numbers with up to 35-50% of patients developing ≥grade 2 GvHD [20,21] and accounting for approximately 10% of deaths following alloSCT according to worldwide census data.[22] To mitigate GvHD, strategies have been developed to remove donor T cells during the initial phase of alloSCT. One of the strategies relies on depletion of T cells by addition of ALM to the patient's conditioning regimen (in-vivo depletion).[23] Administration of ALM as part of the patient's conditioning regimen serves two purposes; depletion of patient T cells to prevent graft rejection and depletion of donor T cells upon their infusion with the graft to prevent GvHD.[24] Following in-vivo depletion of T cells by addition of 100 mg ALM to the conditioning regimen, incidence of ≥grade 2 GvHD in large cohort studies typically decreased to less than 10% in non-myeloablative conditioned patients transplanted with a sibling donor graft and to less than 20% of patients transplanted with an unrelated (matched or mismatched) donor graft.[25-28] As an alternative, donor T cells can be removed from the donor graft before infusion (In-vitro depletion, various techniques reviewed in Daniele et al.[29]). In-vitro depletion of T cells by administration of 20 mg ALM to the bag containing the stem cell graft resulted in reduction of ≥grade 2 GvHD to 22% of myeloablative conditioned patients receiving an HLA-identical sibling graft.[30] A combination of in-vivo and in-vitro T-cell depletion in non-myeloablative conditioned patients receiving a graft from an HLA-matched unrelated donor resulted in almost complete absence of severe GvHD (6.7% of patients).[31] Together these clinical data illustrate the effectiveness of reducing GvHD through ALM-based T-cell depletion before alloSCT.

1

Treatment of B-lymphoblastic leukemia with ALM

A second clinical application of ALM is treatment of hematological malignancies. The shared characteristic of the malignancies treated with ALM is expression of the ALM target antigen CD52. One of these

malignancies is B-lymphoblastic leukemia (B-ALL). B-ALL is characterized by rapid and uncontrolled proliferation of B-lymphocyte progenitor cells within the bone marrow.[32] Within The Netherlands, around 165 new cases are diagnosed yearly and approximately 1160 patients suffer from B-ALL.[33] Treatment of B-ALL has been shown to be challenging due to accumulation of additional genetic abnormalities upon progression of the malignancy, resulting in a complex subclonal architecture of the malignancy.[34-37] Nearly all subtypes of B-ALL display high levels of CD52 membrane expression, with the only exception being the B-ALL subtype carrying the mixed lineage leukemia (MLL)-translocation t(4;11).[38] As such, ALM was considered a promising new treatment modality for patients with B-ALL resulting in their inclusion in the earliest clinical trials that were conducted with ALM.[39] Unfortunately, despite initial good clinical responses, most patients who received ALM as a monotherapy relapsed early after treatment.[40-42]

Mechanisms of target-cell depletion by ALM

To understand the factors that determine the effectiveness of ALM as a therapeutic agent, it is necessary to understand how ALM exerts its function. ALM is an unconjugated cytotoxic antibody. Other well-known therapeutic agents in this category are the CD20-targeting antibodies rituximab (RTX) and ofatumumab (OFA). Upon binding to target antigens expressed on the surface of a cell, unconjugated cytotoxic antibodies recruit and activate the patient's own immune effector mechanisms to induce death of the targeted cell. Immune mechanisms that have been recognized to be able to induce antibody-mediated target-cell death are antibody-dependent cellular cytotoxicity (ADCC), antibody-dependent cellular phagocytosis (ADCP), and complement-dependent cytotoxicity (CDC).[43-47] In ADCC, clustered antibodies on the surface of a target cell recruit via their Fc-tails effector cells that express Fc-receptors (e.g. natural killer cells). Crosslinking of Fc-receptors activates the effector cell, which is further enhanced in the presence of additional stimulatory signals, resulting in directional release of perforins and granzymes. Perforins are able to form pores in the target-cell membrane which allows granzymes to enter the cell and initiate apoptosis by cleavage of the apoptosis pathway proteins caspases and bid. In ADCP, antibody-opsonized target cells are recognized by macrophages which are able to engulf, take up, and enzymatically digest the cells. In CDC, clustering of antigen-bound antibodies (for IgG at least 2, but ideally 6)[48] on the cell surface of target cells recruits C1q, the first component of the complement pathway. Upon recruitment of C1q, the complement pathway is activated resulting in a proteolytic cleavage cascade which ends with the formation of the membrane attack complex (MAC). This MAC consists of multiple membrane spanning C9 proteins that together form a pore in the membrane of the target cell resulting in an ion flux and ultimately osmotic lysis.

Factors that contribute to differential target-cell depletion by ALM

Many factors have been documented to influence the potential of cytotoxic antibodies to induce target-cell depletion mediated via the immune effector mechanisms. These factors may thereby influence the overall efficacy of the treatment. Depending on the degree that they can be manipulated, better understanding of these factors may allow treatment optimization. In addition, factors that are patient or target-cell specific may allow us to understand why some patients are or become non-responsive to the treatment or experience side effects. Factors that are within the scope of this thesis were selected and described below.

Antibody concentration

One of the primary factors that influences effectiveness of treatment with therapeutic antibodies is antibody concentration. Higher concentrations allow more therapeutic antibodies to be bound to the target cell, leading to more efficient recruitment and activation of the individual immune effector mechanisms.[5,49] The relevant antibody concentration range for effective induction of cell death is likely to be different for the various immune effector mechanisms. Based on in-vitro studies, the cell-mediated effector mechanisms ADCC and ADCP are anticipated to efficiently induce target-cell death at 10 to 100 fold lower antibody concentrations than CDC (1-10 µg/mL).[8] Whether similar concentrations also effectively trigger these mechanisms in-vivo remains under debate.

It is generally accepted that antibody concentration is an important variable affecting the efficacy of treatment with monoclonal antibodies. However, implementing strategies to optimize in-vivo antibody concentration by adjusting the treatment dose for individual patients has proven to be difficult. As a result most therapeutic antibody therapies, including ALM, are dosed according to a fixed schedule and with fixed amounts for all adult patients. Since most monoclonal antibody therapies are accompanied by no or only limited direct toxicity, most schedules use a relatively high antibody dose. To optimize antibody concentration it would be advantageous to be able to correctly estimate the antibody level at the site of the target cells as it would allow for an easier establishment of the correlation between antibody concentration and clinical effect. Since in the hematological setting target cells are directly in circulation or in well perfused tissue, blood plasma concentration is an accurate proxy for the antibody concentration near the target cells. As such, various clinical applications in which ALM is used would be appropriate candidates for patient-specific dose optimization. Implementing such approaches would require two yet to be established factors, (1) the optimal concentration range for clinical efficacy and (2)

1

patient-specific factors that could be used as predictors for plasma concentration.

CD52 antigen expression

Expression of target antigen on the membrane of the target-cell population is essential for treatment with cytotoxic therapeutic antibodies. Variation in antigen density has been shown to affect the effectiveness of antibody-mediated target-cell lysis, with higher antigen levels resulting in higher levels of ADCC, ADCP, and CDC.[3,4,50,51] In terms of antigens per cell, CD52 is one of the highest expressed membrane-associated antigens on lymphocytes. Expression levels are typically 5 to 20 fold higher than for other membrane-associated antigens targeted by therapeutic antibodies, such as CD3, CD19, and CD20.[52,53] CD52 is expressed on all mature lymphocytes subsets, but at different levels. In general, B and T cells express high CD52 levels whereas only low levels are present on NK cells and monocytes. Within these hematopoietic cell lineages, CD52 expression levels further differ between the various subsets. Within the T cell lineage, CD52 expression is highest on naive and memory CD4 cells and naive CD8 T cells followed by CD4 effector T cells and is lowest on memory and effector CD8 cells.[4] For B cells, CD52 expression is high on memory and naive B cells, but is almost completely absent on plasma cells.[4,54] Upon malignant transformation, antigen expression levels for CD52 were shown to remain relatively stable in relation to the healthy cell population from which they originate.[50,54,55]

Inhibition of CDC by complement inhibitors

Complement inhibitors may affect the level of target-cell death induced via the mechanism of CDC. Complement activation is a complex multi-step pathway and various regulatory processes are known to be able to interfere with this pathway, ultimately blocking formation of the MAC. Most of the regulators of complement reside in the plasma and therefore convey protection to all host cells. Decay accelerating factor (DAF, CD55) and membrane inhibitor of reactive lysis (MIRL, CD59) are membrane-bound complement regulatory proteins (mCRP) and their expression level may vary considerably on cells. These mCRP may function as target-cell specific down-regulators of CDC.[56-58] These proteins normally protect healthy human cells from the effect of spontaneous and bystander complement pathway activation. The level of protection conveyed by these mCRP to target cells from antibody-induced cell death via CDC, especially in relation to antibody concentration and antigen expression level, is currently not fully understood.

Resistance to ALM treatment

Following treatment with therapeutic antibodies, loss of antigen expression has frequently been observed. In many cases this is the result of biological variation in the level of target antigen expression on different cells within the original target population and subsequent treatment evasion of cells with low expression. Upon termination of the treatment, target antigen expression on the population may revert to original levels. However, in some cases loss of target antigen expression is permanent and outgrowth of these cells results in disease relapse resistant to this specific treatment. Following ALM treatment, loss of CD52 antigen expression has been observed intriguingly frequent.

Loss of CD52 membrane expression

The exact incidence of development of these CD52 loss variants following the various ALM treatment regimens is largely unknown due to the absence of cohort studies. One exception is a study in which ALM was used for T-cell depletion before alloSCT, reporting presence of CD52-negative T cells early after transplantation in 23 of 26 patients.[59] Other studies have also reported loss of CD52 expression following ALM-based T-cell depleted alloSCT,[60,61] but not quantitatively. In the setting of treatment of T-cell malignancies, loss of CD52 expression following ALM treatment has been described in two case reports concerning Sézary syndrome and T-cell prolymphocytic leukemia.[62,63] Remarkably, in several studies where ALM was used for the purpose of B-cell depletion, e.g. treatment of patients with rheumatoid arthritis,[64] B-cell non-Hodgkin lymphoma,[65] and chronic lymphocytic leukemia,[66,67] loss of CD52 antigen expression from the membrane of T cells and not the B cells was described, despite these cells not being the target of treatment. Only two studies reported on CD52-negative cells other than T cells. These studies showed the presence of small populations of CD52-negative B cells present at diagnosis in patients with B-ALL.[68,69] Interestingly, most reports describe permanent loss of CD52 membrane expression, suggesting an underlying genetic involvement.

GPI-anchor expression is essential for CD52 membrane expression

CD52 is encoded by a single copy gene located on chromosome 1 (1p36) and is initially expressed as a 61 amino acid (aa) transmembrane protein. Subsequently, in the lumen of the endoplasmic reticulum, recognition of a glycophosphatidylinositol (GPI)-attachment signal at the carboxyl-terminus of CD52 by the GPI-transamidase complex results in removal of the transmembrane domain and transfer of the residual 12aa core peptide sequence (GQNDTSQTSSPS) onto the GPI anchor.[70,71] As a consequence of this posttranslational modification, CD52 is marked for translocation to the plasma membrane where

it is mainly confined to membrane lipid rafts.[72,73] Since the epitope of ALM includes part of the CD52 peptide as well as part of the GPI anchor, GPI-anchor expression is essential for ALM binding.[70]

Besides CD52, at least 150 different proteins are attached to the plasma membrane via the GPI anchor. Correct synthesis of the GPI anchor is essential for membrane expression of these proteins. This is most evident for the rare acquired blood disorder paroxysmal nocturnal hemoglobinuria (PNH) wherein a single crippling mutation in the *PIGA* gene in a hematopoietic stem cell results in loss of GPI-anchor expression and consequently complement-mediated hemolysis of erythrocytes that lack membrane expression of GPI-anchored complement inhibitors CD55 and CD59.[74,75] In total, 26 different genes are involved in the GPI-anchor biosynthesis pathway, of which almost all are essential for expression of the mature GPI anchor.[76] Except for the *PIGA* gene which is located on the X-chromosome, all GPI genes are encoded on autosomal chromosomes. These GPI genes are expressed in all major tissues of the human body and are essential for normal tissue development as suggested by knock-out experiments performed in mice.[77] An intriguing exception to this rule are cells from hematopoietic origin which were able to mature normally in the absence of GPI-anchor expression.[77] Loss of GPI-anchor expression from the membrane of lymphocytes did not result in intrinsic survival or growth benefits compared to GPI-anchor-positive lymphocytes,[78] indicating that loss of GPI-anchor expression is relatively neutral in its effect on differentiation and proliferation of hematopoietic cells in the absence of artificially introduced selective pressure.

Loss of GPI-anchor expression following ALM treatment

The mechanisms that result in loss of CD52 target antigen expression following ALM treatment have been the topic of several studies. Interestingly, these studies showed that the common cause of loss of CD52 membrane expression was loss of expression of the GPI anchor. This was concluded based on simultaneous loss of membrane expression of multiple GPI-anchored proteins such as CD55, CD59, or CD48,[59,64-66,68,69] and by absence of direct staining with the fluorescently labeled GPI-anchor specific inactivated toxin pro-aerolysin (FLAER).[62] In three case studies, concerning patients with Sézary syndrome, non-Hodgkin lymphoma, or CLL, additional analyses were performed to elucidate how GPI-anchor expression was lost. Genetic aberrations in the *PIGA* gene were found in all cases.[62,65,66] Since *PIGA* is X-linked, only one mutation (in women due to genomic imprinting) can be sufficient to result in a non-functional protein, thereby explaining its frequent association with a GPI-anchor-negative phenotype. Remarkably, in GPI-anchor-negative malignant B cells found in patients with B-ALL no aberrations in the

PIGA gene were found.[69] This indicates that a yet to be established mechanism other than a genetic aberrations in the *PIGA* gene resulted in loss of GPI-anchor expression in these B-ALL cells.

Challenges that hamper the clinical use of ALM

Adoption of ALM-based T-cell depleted alloSCT by the transplantation community has been limited, which is in part due to the difficulty of performing large randomized clinical trials to demonstrate the feasibility and efficacy of the approach. Solid scientific support for ALM-based T-cell depleted alloSCT from studies on the mechanistics of this approach may aid its acceptance.

Application of ALM in treatment regimens for adults with B-ALL have been unsatisfactory. Little improvement was observed following the implementation of ALM monotherapy. The extent to which various factors contribute to effective activation of the immune effector mechanisms by ALM remain unknown. In addition, lack of molecular understanding of the mechanism that leads to relapse following ALM monotherapy prevents the use of this treatment as an effective therapy. Solving these issues could allow revival of this treatment modality, potentially by co-administration of synergistic drugs.

1

Aims of the thesis

To optimally exploit the therapeutic potential of ALM it is essential to understand which factors contribute to the effectiveness of ALM-induced target-cell depletion. Despite being one of the first monoclonal antibodies to be used for clinical purposes, many basic questions on this topic remained unanswered. In this thesis we examined the relative contribution of several key factors that result in differential sensitivity of target cells for ALM-induced lysis in the clinical setting of T-cell depletion before alloSCT and treatment of B-ALL.

ALM is successfully being used for in-vitro T-cell depletion before alloSCT to decrease the incidence of severe GvHD. However, in a small subset of patients acute GvHD is still observed. Also, it was anticipated that residual ALM after alloSCT delays T-cell reconstitution which may negatively affect protection against viral infections. To investigate the extent to which these processes are impacted by ALM levels, in **CHAPTER 2** we set out to measure ALM serum levels and the numbers of circulating T cells in a cohort of patients who had received an allogeneic in-vitro T-cell depleted graft with or without prior ALM as part of the conditioning regimen. Patient specific variables were tested for their effect on ALM serum level during and after transplantation. Pharmacokinetic modeling was used to predict ALM clearance within individual patients over time and to relate this to reconstitution of CD52-negative and CD52-positive T cells. Finally, the impact of post-transplant ALM peak levels and total ALM exposure was related to the incidence of GvHD and occurrence of viral infections.

CDC is a potent mechanism by which therapeutic monoclonal antibodies are able to kill target cells, but the effect and interplay of factors such as antibody concentration, antigen expression, and expression of the membrane-bound complement inhibitors, such as CD55 and CD59, on the efficiency of antibody-induced target-cell lysis remained debated. In **CHAPTER 3** we aimed to investigate the interplay of these factors using B-ALL as a model. To broaden the relevance of the potential findings, therapeutic antibodies RTX and OFA that are frequently used in the treatment of B-cell malignancies were assessed alongside ALM. The effect of natural variation in the expression levels of the complement inhibiting factors was also assessed using primary malignant cells to examine their potential to serve as a predictor for effective CDC.

Following ALM-based T-cell depleted alloSCT, relatively rapid recovery of circulating T cells with a CD52-negative phenotype was observed in graft recipients (**CHAPTER 2**). To establish the extent to

which CD52-negative cells contribute to reconstitution following ALM-based T-cell depleted alloSCT, a comprehensive phenotypic analysis of lymphocytes was done using samples taken from a cohort of patients who had received alloSCT for the treatment of various malignant and non-malignant hematological diseases. Results from this analysis are described in **CHAPTER 4**. To establish the origin of the CD52-negative cells and to elucidate the mechanism resulting in their loss of CD52 membrane expression, chimerism analysis and an extensive genetic analysis was performed. Since CD52-negative T cells may be important in the early protection of alloSCT recipients against viral infections, we lastly studied the functional potential of CD52-deficient virus-specific T cells.

In patients with B-ALL, outgrowth of pre-existing malignant cells that are deficient for CD52 membrane expression may explain the short-lived treatment success of ALM-monotherapy. However, the extent to which these cells are present in patients was not known. In **CHAPTER 5** we aimed to determine the prevalence and frequency of these cells in a cohort of patients with B-ALL. Further, we set out to elucidate the mechanism by which these cells had become CD52 target antigen negative. Based on the newly gained insights we tested whether we could revert the phenotype by stimulation of the malignant B-ALL cells with a compound already established for clinical use.

In **CHAPTER 6**, the results that are presented in **CHAPTERS 2-5** are summarized and discussed based on current knowledge. We discuss the potential implication of these findings in relation to the various therapies in which ALM is applied and we discuss potential implications for future settings in which ALM, or medication targeting other GPI-anchored antigens, may be used.

1

REFERENCE LIST

1.   Hale G. The CD52 antigen and development of the CAMPATH antibodies. *Cytotherapy*. 2001;3(3):137-143.

2.   Hale G, Bright S, Chumbley G, et al. Removal of T cells from bone marrow for transplantation: a monoclonal antilymphocyte antibody that fixes human complement. *Blood*. 1983;62(4):873-882.

3.   Ratzinger G, Reagan JL, Heller G, Busam KJ, Young JW. Differential CD52 expression by distinct myeloid dendritic cell subsets: implications for alemtuzumab activity at the level of antigen presentation in allogeneic graft-host interactions in transplantation. *Blood*. 2003;101(4):1422-1429.

4.   Rao SP, Sancho J, Campos-Rivera J, et al. Human peripheral blood mononuclear cells exhibit heterogeneous CD52 expression levels and show differential sensitivity to alemtuzumab mediated cytolysis. *PLoS One*. 2012;7(6):e39416.

5.   Novitzky N, Davison G, Abdulla R, Mowla S. Definition of the variables affecting efficacy of immunodepletion ex vivo of peripheral blood progenitor cell grafts by alemtuzumab (Campath in the bag). *Biol Blood Marrow Transplant*. 2013;19(12):1753-1759.

6.   Waldmann H, Polliak A, Hale G, et al. Elimination of graft-versus-host disease by in-vitro depletion of alloreactive lymphocytes with a monoclonal rat anti-human lymphocyte antibody (CAMPATH-1). *Lancet*. 1984;2(8401):483-486.

7.   Hale G, Cobbold S, Waldmann H. T cell depletion with CAMPATH-1 in allogeneic bone marrow transplantation. *Transplantation*. 1988;45(4):753-759.

8.   Riechmann L, Clark M, Waldmann H, Winter G. Reshaping human antibodies for therapy. Nature. 1988;332(6162):323-327.

9.   Bruggemann M, Williams GT, Bindon CI, et al. Comparison of the effector functions of human immunoglobulins using a matched set of chimeric antibodies. *J Exp Med*. 1987;166(5):1351-1361.

10. Moreton P, Hillmen P. Alemtuzumab therapy in B-cell lymphoproliferative disorders. *Semin Oncol*. 2003;30(4):493-501.

11. Zinzani PL, Corradini P, Gallamini A, et al. Overview of alemtuzumab therapy for the treatment of T-cell lymphomas. *Leuk Lymphoma*. 2012;53(5):789-795.

12. Matteson EL, Yocum DE, St Clair EW, et al. Treatment of active refractory rheumatoid arthritis with humanized monoclonal antibody CAMPATH-1H administered by daily subcutaneous injection. *Arthritis Rheum*. 1995;38(9):1187-1193.

13. Willis MD, Robertson NP. Alemtuzumab for Multiple Sclerosis. *Curr Neurol Neurosci Rep*. 2016;16(9):84.

14. Gundroo A, Zachariah M, Singh N, Sharma R. Alemtuzumab (Campath-1H) experience in kidney transplantation what we have learned; current practices; and scope for the future? *Curr Opin Organ Transplant*. 2015;20(6):638-642.

15. Little MT, Storb R. History of haematopoietic stem-cell transplantation. *Nat Rev Cancer*. 2002;2(3):231-238.

16. Thomas ED, Blume KG. Historical markers in the development of allogeneic hematopoietic cell transplantation. *Biol Blood Marrow Transplant*. 1999;5(6):341-346.

17. Miller JS, Warren EH, van den Brink MR, et al. NCI First International Workshop on The Biology, Prevention, and Treatment of Relapse After Allogeneic Hematopoietic Stem Cell Transplantation: Report from the Committee on the Biology Underlying Recurrence of Malignant Disease following Allogeneic HSCT: Graft-versus-Tumor/Leukemia Reaction. *Biol Blood Marrow Transplant*. 2010;16(5):565-586.

18. Goker H, Haznedaroglu IC, Chao NJ. Acute graft-vs-host disease: pathobiology and management. *Exp Hematol*. 2001;29(3):259-277.

19. Lee SJ, Vogelsang G, Flowers ME. Chronic graft-versus-host disease. *Biol Blood Marrow Transplant*. 2003;9(4):215-233.

20. Cutler C, Giri S, Jeyapalan S, Paniagua D, Viswanathan A, Antin JH. Acute and chronic graft-versus-host disease after allogeneic peripheral-blood stem-cell and bone marrow transplantation: a meta-analysis. *J Clin Oncol*. 2001;19(16):3685-3691.

21. Champlin RE, Schmitz N, Horowitz MM, et al. Blood stem cells compared with bone marrow as a source of hematopoietic cells for allogeneic transplantation. IBMTR Histocompatibility and Stem Cell Sources Working Committee and the European Group for Blood and Marrow Transplantation (EBMT). *Blood*. 2000;95(12):3702-3709.

22. (CIBMTR) CflBaMTR. Summery slides 2016; 2017.

23. Waldmann H, Polliak A, Hale G, et al. Elimination of graft-versus-host disease by in-vitro depletion of alloreactive lymphocytes with a monoclonal rat anti-human lymphocyte antibody (CAMPATH-1). *Lancet*. 1984;2(8401):483-486.

24. Hale G, Waldmann H. Control of graft-versus-host disease and graft rejection by T cell depletion of donor and recipient with Campath-1 antibodies. Results of matched sibling transplants for malignant diseases. *Bone Marrow Transplant*. 1994;13(5):597-611.

25. Perez-Simon JA, Kottaridis PD, Martino R, et al. Nonmyeloablative transplantation with or without alemtuzumab: comparison between 2 prospective studies in patients with lymphoproliferative disorders. *Blood*. 2002;100(9):3121-3127.

26. Kottaridis PD, Milligan DW, Chopra R, et al. In vivo CAMPATH-1H prevents GvHD following nonmyeloablative stem-cell transplantation. *Cytotherapy*. 2001;3(3):197-201.

27. Mead AJ, Thomson KJ, Morris EC, et al. HLA-mismatched unrelated donors are a viable alternate graft source for allogeneic transplantation following alemtuzumab-based reduced-intensity conditioning. *Blood*. 2010;115(25):5147-5153.

28. Chakraverty R, Peggs K, Chopra R, et al. Limiting transplantation-related mortality following unrelated donor stem cell transplantation by using a nonmyeloablative conditioning regimen. *Blood*. 2002;99(3):1071-1078.

1

29.   Daniele N, Scerpa MC, Caniglia M, et al. Overview of T-cell depletion in haploidentical stem cell transplantation. *Blood Transfus*. 2012;10(3):264-272.

30.   Barge RM, Starrenburg CW, Falkenburg JH, Fibbe WE, Marijt EW, Willemze R. Long-term follow-up of myeloablative allogeneic stem cell transplantation using Campath "in the bag" as T-cell depletion: the Leiden experience. *Bone Marrow Transplant*. 2006;37(12):1129-1134.

31.   von dem Borne PA, Beaumont F, Starrenburg CW, et al. Outcomes after myeloablative unrelated donor stem cell transplantation using both in vitro and in vivo T-cell depletion with alemtuzumab. *Haematologica*. 2006;91(11):1559-1562.

32.   Inaba H, Greaves M, Mullighan CG. Acute lymphoblastic leukaemia. *Lancet*. 2013;381(9881):1943-1955.

33.   Organisation NCC. The Netherlands Cancer Registry; 2016.

34.   Anderson K, Lutz C, van Delft FW, et al. Genetic variegation of clonal architecture and propagating cells in leukaemia. *Nature*. 2011;469(7330):356-361.

35.   Moorman AV. New and emerging prognostic and predictive genetic biomarkers in B-cell precursor acute lymphoblastic leukemia. *Haematologica*. 2016;101(4):407-416.

36.   Liu YF, Wang BY, Zhang WN, et al. Genomic Profiling of Adult and Pediatric B-cell Acute Lymphoblastic Leukemia. *EBioMedicine*. 2016;8:173-183.

37.   Yeoh EJ, Ross ME, Shurtleff SA, et al. Classification, subtype discovery, and prediction of outcome in pediatric acute lymphoblastic leukemia by gene expression profiling. *Cancer Cell*. 2002;1(2):133-143.

38.   Lozanski G, Sanford B, Yu D, et al. CD52 Expression in Adult Acute Lymphoblastic Leukemia (ALL): Quantitative Flow Cytometry Provides New Insights. Blood. 2006;108:2293-2293.

39.   Dyer MJ, Hale G, Hayhoe FG, Waldmann H. Effects of CAMPATH-1 antibodies in vivo in patients with lymphoid malignancies: influence of antibody isotype. *Blood*. 1989;73(6):1431-1439.

40.   Stock W, Sanford B, Lozanski G, et al. Alemtuzumab can be Incorporated Into Front-Line Therapy of Adult Acute Lymphoblastic Leukemia (ALL): Final Phase I Results of a Cancer and Leukemia Group B Study (CALGB 10102). *Blood*. 2009;114:838-838.

41.   Gorin NC, Isnard F, Garderet L, et al. Administration of alemtuzumab and G-CSF to adults with relapsed or refractory acute lymphoblastic leukemia: results of a phase II study. *Eur J Haematol*. 2013;91(4):315-321.

42.   Piccaluga PP, Martinelli G, Malagola M, et al. Anti-leukemic and anti-GVHD effects of campath-1H in acute lymphoblastic leukemia relapsed after stem-cell transplantation. *Leuk Lymphoma*. 2004;45(4):731-733.

43.   Glennie MJ, French RR, Cragg MS, Taylor RP. Mechanisms of killing by anti-CD20 monoclonal antibodies. *Mol Immunol*. 2007;44(16):3823-3837.

44.   Seidel UJ, Schlegel P, Lang P. Natural killer cell mediated antibody-dependent cellular cytotoxicity in

tumor immunotherapy with therapeutic antibodies. *Front Immunol*. 2013;4:76.

45.   Golay J, Introna M. Mechanism of action of therapeutic monoclonal antibodies: promises and pitfalls of in vitro and in vivo assays. *Arch Biochem Biophys*. 2012;526(2):146-153.

46.   Weiner LM, Surana R, Wang S. Monoclonal antibodies: versatile platforms for cancer immunotherapy. *Nat Rev Immunol*. 2010;10(5):317-327.

47.   Weiner GJ. Building better monoclonal antibody-based therapeutics. *Nat Rev Cancer*. 2015;15(6):361-370.

48.   Diebolder CA, Beurskens FJ, de Jong RN, et al. Complement is activated by IgG hexamers assembled at the cell surface. *Science*. 2014;343(6176):1260-1263.

49.   Reverberi R, Reverberi L. Factors affecting the antigen-antibody reaction. *Blood Transfus*. 2007;5(4):227-240.

50.   Golay J, Cortiana C, Manganini M, et al. The sensitivity of acute lymphoblastic leukemia cells carrying the t(12;21) translocation to campath-1H-mediated cell lysis. *Haematologica*. 2006;91(3):322-330.

51.   van Meerten T, van Rijn RS, Hol S, Hagenbeek A, Ebeling SB. Complement-induced cell death by rituximab depends on CD20 expression level and acts complementary to antibody-dependent cellular cytotoxicity. *Clin Cancer Res*. 2006;12(13):4027-4035.

52.   Bikoue A, George F, Poncelet P, Mutin M, Janossy G, Sampol J. Quantitative analysis of leukocyte membrane antigen expression: normal adult values. *Cytometry*. 1996;26(2):137-147.

53.   Rossmann ED, Lundin J, Lenkei R, Mellstedt H, Osterborg A. Variability in B-cell antigen expression: implications for the treatment of B-cell lymphomas and leukemias with monoclonal antibodies. *Hematol J*. 2001;2(5):300-306.

54.   Rawstron AC, Laycock-Brown G, Hale G, et al. CD52 expression patterns in myeloma and the applicability of alemtuzumab therapy. *Haematologica*. 2006;91(11):1577-1578.

55.   Ginaldi L, De Martinis M, Matutes E, et al. Levels of expression of CD52 in normal and leukemic B and T cells: correlation with in vivo therapeutic responses to Campath-1H. *Leuk Res*. 1998;22(2):185-191.

56.   Gao LJ, Ding L, Guo SY, et al. Role of decay-accelerating factor in regulating survival of human cervical cancer cells. *J Cancer Res Clin Oncol*. 2011;137(1):81-87.

57.   Golay J, Zaffaroni L, Vaccari T, et al. Biologic response of B lymphoma cells to anti-CD20 monoclonal antibody rituximab in vitro: CD55 and CD59 regulate complement-mediated cell lysis. *Blood*. 2000;95(12):3900-3908.

58.   Macor P, Tripodo C, Zorzet S, et al. In vivo targeting of human neutralizing antibodies against CD55 and CD59 to lymphoma cells increases the antitumor activity of rituximab. *Cancer Res*. 2007;67(21):10556-10563.

59.   Garland RJ, Groves SJ, Diamanti P, et al. Early emergence of PNH-like T cells after allogeneic stem cell transplants utilising CAMPATH-1H for T cell depletion. *Bone Marrow Transplant*. 2005;36(3):237-244.

60.   Meyer RG, Wagner EM, Konur A, et al. Donor CD4 T cells convert mixed to full donor T-cell chimerism and replenish the CD52-positive T-cell pool after alemtuzumab-based T-cell-depleted allo-transplantation. Bone

1

Marrow Transplant. 2010;45(4):668-674.

61. Bunjes D, Theobald M, Wiesneth M, et al. Graft rejection by a population of primed CDw52- host T cells after in vivo/ex vivo T-depleted bone marrow transplantation. *Bone Marrow Transplant*. 1993;12(3):209-215.

62. Halkes CJ, Zoutman WH, van der Fits L, Jedema I, Vermeer MH. Mutation in PIGA results in a CD52- negative escape variant in a Sezary syndrome patient during alemtuzumab treatment. *J Invest Dermatol*. 2015;135(4):1199-1202.

63. Birhiray RE, Shaw G, Guldan S, et al. Phenotypic transformation of CD52(pos) to CD52(neg) leukemic T cells as a mechanism for resistance to CAMPATH-1H. *Leukemia*. 2002;16(5):861-864.

64. Brett SJ, Baxter G, Cooper H, et al. Emergence of CD52-, glycosylphosphatidylinositol-anchor- deficient lymphocytes in rheumatoid arthritis patients following Campath-1H treatment. *Int Immunol*. 1996;8(3):325-334.

65. Hertenstein B, Wagner B, Bunjes D, et al. Emergence of CD52-, phosphatidylinositolglycan-anchor- deficient T lymphocytes after in vivo application of Campath-1H for refractory B-cell non-Hodgkin lymphoma. *Blood*. 1995;86(4):1487-1492.

66. Rawstron AC, Rollinson SJ, Richards S, et al. The PNH phenotype cells that emerge in most patients after CAMPATH-1H therapy are present prior to treatment. *Br J Haematol*. 1999;107(1):148-153.

67. Osterborg A, Werner A, Halapi E, et al. Clonal CD8+ and CD52- T cells are induced in responding B cell lymphoma patients treated with Campath-1H (anti-CD52). *Eur J Haematol*. 1997;58(1):5-13.

68. Araten DJ, Sanders KJ, Anscher D, Zamechek L, Hunger SP, Ibrahim S. Leukemic blasts with the paroxysmal nocturnal hemoglobinuria phenotype in children with acute lymphoblastic leukemia. *Am J Pathol*. 2012;181(5):1862-1869.

69. Nijmeijer BA, van Schie ML, Halkes CJ, Griffioen M, Willemze R, Falkenburg JH. A mechanistic rationale for combining alemtuzumab and rituximab in the treatment of ALL. *Blood*. 2010;116(26):5930-5940.

70. Xia MQ, Hale G, Lifely MR, et al. Structure of the CAMPATH-1 antigen, a glycosylphosphatidylinositol- anchored glycoprotein which is an exceptionally good target for complement lysis. *Biochem J*. 1993;293 (Pt 3):633-640.

71. Hale C, Bartholomew M, Taylor V, Stables J, Topley P, Tite J. Recognition of CD52 allelic gene products by CAMPATH-1H antibodies. *Immunology*. 1996;88(2):183-190.

72. Mone AP, Cheney C, Banks AL, et al. Alemtuzumab induces caspase-independent cell death in human chronic lymphocytic leukemia cells through a lipid raft-dependent mechanism. *Leukemia*. 2006;20(2):272-279.

73. Ermini L, Secciani F, La Sala GB, et al. Different glycoforms of the human GPI-anchored antigen CD52 associate differently with lipid microdomains in leukocytes and sperm membranes. *Biochem Biophys Res Commun*. 2005;338(2):1275-1283.

74. Ware RE, Rosse WF, Howard TA. Mutations within the Piga gene in patients with paroxysmal nocturnal hemoglobinuria. *Blood*. 1994;83(9):2418-2422.

75. Rosse WF. Paroxysmal nocturnal hemoglobinuria as a molecular disease. *Medicine* (Baltimore). 1997;76(2):63-93.

76. Koike-Yusa H, Li Y, Tan EP, Velasco-Herrera Mdel C, Yusa K. Genome-wide recessive genetic screening in mammalian cells with a lentiviral CRISPR-guide RNA library. *Nat Biotechnol*. 2014;32(3):267-273.

77. Keller P, Tremml G, Rosti V, Bessler M. X inactivation and somatic cell selection rescue female mice carrying a Piga-null mutation. *Proc Natl Acad Sci U S A*. 1999;96(13):7479-7483.

78. Kulkarni S, Bessler M. The effect of GPI-anchor deficiency on apoptosis in mice carrying a Piga gene mutation in hematopoietic cells. *J Leukoc Biol*. 2002;72(6):1228-1233.

1

Floris C. Loeff[1]

H.M. Esther van Egmond[1]

Dirk J.A.R. Moes[2]

Charissa Wijnands[1]

Peter A. Von Dem Borne[1]

Hendrik Veelken[1]

J.H. Frederik Falkenburg[1]

Inge Jedema[1]*

Constantijn J.M. Halkes[1]*

CHAPTER 2

Impact of alemtuzumab pharmacokinetics on T-cell dynamics, graft-versus host disease and viral reactivation in patients receiving allogeneic stem cell transplantation with an alemtuzumab-based T-cell-depleted graft

[1] Department of Hematology - Leiden University Medical Center - Leiden - the Netherlands
[2] Department of Clinical Pharmacy and Toxicology - Leiden University Medical Center - Leiden - the Netherlands
* I.J. and C.J.H. share senior authorship

ABSTRACT

Administration of alemtuzumab (targeting the CD52 antigen) to the patient (in-vivo) or to the graft (in-vitro) before allogeneic stem cell transplantation (alloSCT) decreases the incidence of graft-versus-host disease (GvHD). Effectiveness of this treatment relies on depletion of donor T cells. Currently, no data are available on alemtuzumab pharmacokinetics and pharmacodynamics in patients who received combined in-vivo and in-vitro alemtuzumab-based T-cell depletion. In this prospective study, we analyzed alemtuzumab pharmacokinetics and its effect on the circulating T cells in 36 patients who received an allogeneic T-cell-depleted graft by addition of 20 mg alemtuzumab "to the bag" with or without prior alemtuzumab (30 mg cumulative dose intravenously) as part of the conditioning regimen. Effective T-cell depletion was shown for all patients, even though alemtuzumab plasma levels varied considerably. Peak alemtuzumab levels were observed directly after graft infusion and were not associated with the number of circulating T cells pre-infusion, but with plasma volumes of the patients. All patients engrafted, confirming feasibility of this transplantation protocol. Only three patients with low alemtuzumab levels developed acute GvHD (grade II in 2 patients and grade III in 1 patient). Persistence of circulating alemtuzumab at 3 weeks after transplantation had prevented reconstitution of CD52-positive T cells when alemtuzumab plasma levels were above 0.7 μg/mL. However, overall T-cell reconstitution did not correlate with the levels of alemtuzumab exposure, due to early reconstitution of CD52-negative alemtuzumab-resistant T cells. The protective effect of these cells likely explains the low incidence of Epstein-Barr-virus- and cytomegalovirus-related disease despite circulating alemtuzumab.

INTRODUCTION

Allogeneic stem cell transplantation (alloSCT) is a potentially curative treatment for a variety of malignant and non-malignant hematological diseases. However, treatment related morbidity and mortality as a result of graft-versus-host disease (GvHD) remains a challenge. GvHD is caused by an immune reaction against non-hematopoietic healthy tissue mediated by donor T cells infused with the graft. Depletion of donor T cells can prevent the development of GvHD. The therapeutic graft-versus-tumor effect, which results from recognition of residual malignant cells by the donor T cells, is also diminished by donor T-cell depletion,[1] but can be restored by postponed application of donor lymphocyte infusions.[2-5]

Alemtuzumab (Campath-1H) is a humanized IgG1 antibody which targets the glycophosphatidylinositol (GPI)-anchored protein CD52 that is expressed on lymphocytes, but not (or only marginally) on hematopoietic stem cells.[6,7] Alemtuzumab efficiently depletes CD52-expressing cells through antibody-dependent cellular cytotoxicity (ADCC), complement-dependent cytotoxicity (CDC), and potentially by direct activation of pro-apoptotic pathways. Addition of alemtuzumab to the pre-transplant conditioning regimen to deplete donor T cells upon their infusion with the graft (in-vivo depletion), decreases the incidence of severe acute GvHD from 35-50% to 10-20%.[8-11] Even more efficient prevention of GvHD is achieved when alemtuzumab is added directly to the stem cell graft (in-vitro depletion , or alemtuzumab "in the bag").[5,12-15] The efficacy of alemtuzumab-induced depletion of potentially alloreactive T cells depends on their CD52 expression in relation to the amount of alemtuzumab. After graft infusion, persistence of lytic plasma levels of alemtuzumab will prevent T-cell reconstitution and thereby increase the risk for patients to develop infections.[16,17] Previously, we have shown that T cells that lost expression of CD52 due to loss of GPI-anchor expression have antiviral activity and expand early after alemtuzumab-based in-vitro T-cell-depleted alloSCT.[18] These CD52-negative T cells can contribute to the antiviral protection early after alemtuzumab-based T-cell-depleted alloSCT irrespectively of alemtuzumab levels.

Over the years, alemtuzumab pharmacokinetics have been evaluated in various conditioning regimens using in-vivo alemtuzumab-based T-cell depletion in combination with post-transplantation cyclosporine as GvHD prophylaxis.[8,9,19-21] However, the effect of combined in-vivo and in-vitro T-cell depletion on alemtuzumab pharmacokinetics has not been established. During in-vitro alemtuzumab incubation donor T cells are exposed to a high alemtuzumab concentration and upon graft infusion residual unbound alemtuzumab is co-infused into the circulation. In this study, we performed a comprehensive

analysis of alemtuzumab pharmacokinetics in relation to T-cell depletion, T-cell reconstitution, and the occurrence of GvHD and viral infections in 36 patients who had received an allogeneic graft depleted of T cells by addition of alemtuzumab "to the bag" with or without prior in-vivo patient T-cell depletion.

MATERIAL AND METHODS

Patients and samples

A cohort of 36 adult patients who received alemtuzumab-based T-cell-depleted alloSCT following one of four transplantation protocols (**Table 1**) at Leiden University Medical Center (LUMC, Leiden, the Netherlands) between November 2015 and February 2017 were included. Informed consent was obtained for treatment and scientific evaluation (LUMC protocol numbers P03.114, P04.003, P03.173). Sixteen patients received myeloablative (MA) conditioning, consisting of cyclophosphamide and either total body irradiation (TBI, n = 13) or busulfan (n = 3). In the case of an unrelated donor (UD, n = 8) 15 mg alemtuzumab (MabCampath, Sanofi Genzyme, Naarden, the Netherlands) intravenously (IV) at days -6 and -5 (relative to the day of graft infusion) was added to the conditioning regimen. Twenty patients received non-myeloablative (NMA) conditioning consisting of 15 mg alemtuzumab IV at days -4 and -3, fludarabine, and busulfan. In case of an UD (n = 11) 1 mg/kg anti-thymocyte globulin (ATG; thymoglobulin, Sanofi Genzyme) was added at day -2. All patients received an allogeneic, G-CSF-mobilized peripheral blood stem cell (PBSC, n = 35) or bone marrow (BM, n = 1) graft subjected to T-cell depletion by addition of 20 mg alemtuzumab "to the bag".[22] Cyclosporin as prophylactic immune suppression was only given to patients with an UD after MA conditioning, starting day -1 and tapered from day 30. GvHD was graded according to modified Glucksberg and Shulman criteria.[23] Peripheral blood (PB) samples were scheduled for collection immediately before, 30 min and 1 day after each alemtuzumab cycle and the graft infusion, and at weeks 1, 2, 3, 6, 9 after graft infusion. PB was collected in cell preparation tubes (CPT, BD, Becton Dickinson B.V., Breda, the Netherlands) to isolate mononuclear cells (MNC) and in EDTA tubes (BD) for direct flow cytometric analysis and for plasma isolation. MNC and plasma samples were cryopreserved at -180°C and -80°C, respectively.

Analysis of circulating alemtuzumab plasma levels

Alemtuzumab plasma levels were measured using a flow cytometry-based indirect immunofluorescence assay modified from the methodology described by Rebello and Hale.[24] The CD52-positive

B-lymphoblastic leukemia cell line Leiden-ALL-HP [25] was seeded in a 96 wells plate (20.000 cells/well) and incubated with 10 μL of patient plasma at 0, 5, 10, 20, and 40 fold dilutions (in PBS) or as a reference (in duplicate) with 10 μL healthy donor plasma containing serially diluted alemtuzumab ranging from 5.0-0.03 μg/mL. After incubation for 30 min at 4°C, cells were washed 4 times with PBS and incubated with phycoerythrin (PE)-conjugated F(ab')2-goat anti-Human IgG Fc (Thermo Fisher Scientific, Bleiswijk,

Table 1. Protocols, and patient and graft characteristics

Protocol	Patient-donor relation	Number of patients
Myeloablative, n	Sibling donor	8
	Unrelated donor	8
Non-myeloablative, n	Sibling donor	9
	Unrelated donor	11
Patients		
Age at alloSCT, y		54 (26 – 74)[a]
Gender, n	Male	27
	Female	9
BSA, m^2		2.06 (1.57 – 2.42)[a]
Weight, kg		85 (58 – 115)[a]
Initial diagnosis, n	AML	15
	MM	5
	T-NHL	4
	ALL	3
	MDS	3
	Myelofibrosis	2
	B-NHL	1
	MCL	1
	CMML	1
	WM	1
Grafts		
Stem cell source, n	G-CSF stimulated PB	35
	BM	1
HLA-match, n	10 out 10	32
	9 out 10	4
CD34 cells, 10^6 cells		496.2 (178.6 – 1414.4)[a,b]
TNC, 10^9 cells		63.8 (7.7 – 139.2)[a]

[a] *Median and range are given.*

[b] *One patient received a BM graft for whom the number of CD34 cells was not quantified.*

Abbreviations: AML, acute myeloid leukemia; MM, multiple myeloma; T-NHL, T-cell non-Hodgkin lymphoma; ALL; acute lymphoblastic leukemia; MDS, myelodysplastic syndrome; B-NHL, B-cell non-Hodgkin lymphoma; MCL, mantle cell lymphoma; CMML, chronic myelomonocytic leukemia; WM, Waldenström macroglobinemia; TNC, total nucleated cells.

the Netherlands) for 30 min at 4°C to detect bound alemtuzumab. Cells were washed twice with PBS and kept on ice until analysis. Fluorescence was measured on an LSRII analyzer (BD) and analyzed using FlowJo software (Treestar, Ashland, OR, USA). The alemtuzumab concentrations within the dilutions of the patient plasma sample were interpolated using the reference samples and multiplied by the respective dilution factor. Alemtuzumab plasma levels in patient samples were calculated from the average concentration from at least two sample dilutions. The lower detection limit of this assay was 0.03 µg/mL alemtuzumab. In 6 patients, non-specific (e.g. anti-HLA antibodies, as determined by testing the samples against a GPI-anchor-deficient subculture of Leiden-ALL-HP that lacks CD52 membrane expression)[26] low background levels (<0.176 µg/mL) were detected in the pre-treatment samples which were subtracted from subsequent measurements from the same patient. One patient who had received treatment with rituximab up to two months before alloSCT was excluded from this analysis as rituximab is also detected in this assay.

Flow cytometry

Absolute numbers of circulating CD4 T, CD8 T, B, and NK cells were determined by the clinical Laboratory for Specialized Hematology (LUMC) as part of routine immune monitoring after transplantation on anticoagulated fresh venous blood using Trucount tubes (BD, Becton Dickinson, Breda, the Netherlands) following the manufacturer's instructions. Samples were stained with allophycocyanin (APC)-conjugated anti-CD3, PacificBlue-conjugated anti-CD4, fluorescein isothiocyanate (FITC)-conjugated anti-CD8, APC-H7-conjugated anti-CD14, R-phycoerythrin (PE)-conjugated anti-CD16, PE-Cy7-conjugated anti-CD19, V500-conjugated CD45, and PE-conjugated CD56 (all from BD). Fluorescence was analyzed using a FACSCanto (BD). The lower detection limit for this analysis was 0.5×10^6 cells/L.

Absolute numbers of T cells in the graft were determined in samples taken before and after 30 min incubation with alemtuzumab. Cells were kept at 4°C throughout the following steps to prevent additional cell loss due to processing. For each sample, the absolute number of nucleated cells was determined using a Sysmex KX-21 N (Sysmex, Etten-Leur, the Netherlands). Samples were pelleted and resuspended in red blood cell lysis buffer (8.4 g/L NH4CL and 1 g/L KHCO3, pH 7.4) (LUMC pharmacy). After 10 min incubation, cells were pelleted and resuspended in 10% v/v inactivated human serum at a concentration of 1×10^6–2×10^6 cells/mL. For logistic reasons samples were stored overnight at 4°C. Afterwards, the percentages of viable cells were determined using a Bürker cell counter chamber and eosin staining. Cells were pelleted and resuspended in 600 µL PBS with pasteurized plasma

proteins 2% w/v (GPO, Sanquin, Amsterdam, the Netherlands) of which 150 μL was used to determine the percentages of T cells within the samples by flow cytometry after with APC-H7-conjugated anti-CD3 (BD). The total numbers of viable T cells in the grafts were calculated by multiplying the Sysmex measurement with the graft volume subtracting the percentage of non-viable cells and multiplying by the percentage of T cells.

GPI-anchor and CD52 membrane expression on CD4 and CD8 T cells was analyzed by flow cytometry on thawed MNC by staining with the GPI-anchor-specific inactivated toxin pro-aerolysin coupled to Alexa Fluor 488 (FLAER-AF488, Sanbio, Uden, the Netherlands), APC-conjugated anti-CD52 (ITK diagnostics, Uithoorn, the Netherlands), APC-H7-conjugated anti-CD3, v500-conjugated anti-CD4 (BD), PacificBlue-conjugated anti-CD8 (BD), and AlexaFluor700-conjugated anti-CD45 (ITK diagnostics). Fluorescence was analyzed using an LSRII (BD).

Population pharmacokinetics model building

Pharmacokinetic parameters were estimated using a developed population pharmacokinetic model based on the alemtuzumab plasma concentration-time data by non-linear mixed-effects modeling using NONMEM (V7.3, Icon Development Solutions, Ellicot City, MD, USA). The Perl-speaks-NONMEM toolkit version 4.7.0 (ref Lindbom et al.)[27] and Pirana version 2.8.0 (ref Keizer et al.)[28] were used as modeling environment. Results were plotted using R (V2.25.2, Boston, MA, USA) and RStudio (V0.97.248). First-order conditional estimation method with interaction was used throughout the analysis. One and two compartmental pharmacokinetic models with first order elimination or non-linear elimination were compared with the observed alemtuzumab plasma concentration-time data to find the optimal fit. Model selection was based on statistical significance, goodness of fit and stability. Throughout the model building process, an altered model was chosen over a pre-cursor model if the difference in the objective functions (−2 log likelihood) was >6.63 (P < 0.01, with 1 degree of freedom, assuming $\chi2$ distribution). To identify possible covariates influencing alemtuzumab pharmacokinetics, diagnostic plots were constructed of the random effects of clearance (Cl), distribution volume (V1) versus the demographic (gender, age, body weight, height, body surface area, body mass index) and clinical covariates (initial diagnosis, absolute number of circulating patient T cells per liter of blood before IV alemtuzumab infusions, absolute number of donor leukocytes in the graft, hematocrit, and plasma volume). Plasma volume was calculated from blood volume using the Nadler method [29] and corrected for the patients hematocrit (ht) (formulas in **Table S1**). The final population pharmacokinetic model was

validated by means of a prediction corrected visual predictive check (pcVPC, 500 runs) and bootstrap (1000 runs).[30]

EBV and CMV detection and management

Epstein-Barr virus (EBV)-reactivation was defined as a detectable EBV DNA load in the serum by qPCR. Rituximab treatment (375 mg/m2) for EBV-reactivation was initiated if EBV DNA load was above 10^3 copies/mL. Cytomegalovirus (CMV)-reactivation was defined as a DNA CMV load higher than 10^3 copies/mL in serum by qPCR.[31] Treatment for CMV-reactivation was initiated if the load was higher than 10^3 copies/mL at two consecutive measurements and consisted of oral valganciclovir (900 mg twice daily) or IV ganciclovir (5 mg twice daily) for 2 weeks. CMV-disease was defined as CMV-reactivation with proven organ involvement.

Statistical analysis

Statistical analyses were performed using Prism 6 (GraphPad, La Jolla, CA, USA) using tests as indicated.

RESULTS

In-vivo depletion of patient T cells by alemtuzumab before graft infusion

All 20 NMA-conditioned patients and all 8 MA-conditioned patients with an unrelated donor received two intravenous (IV) infusions of 15 mg alemtuzumab as part of the conditioning regimen. To examine the effectiveness of alemtuzumab-induced in-vivo patient T-cell depletion, we determined the absolute numbers of circulating T cells directly before the first alemtuzumab infusion and 30 min after the second alemtuzumab infusion using flow cytometry. 6 patients were excluded from this analysis as either the pre- or post-alemtuzumab infusion sample was absent. The median T-cell count before the alemtuzumab infusions was 50×10^6 cells/L (range 4×10^6–829×10^6 cells/L). After the alemtuzumab infusions, complete depletion of circulating T cells was observed in 18 out of 22 patients (**Figure 1A**), whereas in the remaining 4 patients minimal numbers of residual T cells were found (range 0.6×10^6–1.0×10^6 cells/L).

To establish the alemtuzumab levels after the IV alemtuzumab infusions, we measured alemtuzumab plasma concentrations in available samples taken from patients before and 30 min after each infusion. After infusion 1, the median alemtuzumab plasma level was 2.5 µg/mL (range 1.1–6.5 µg/mL, n = 25,

Figure 1. Efficient in-vivo patient T-cell depletion following IV alemtuzumab

(A) Absolute numbers of circulating T cells before IV alemtuzumab infusion 1 and after IV alemtuzumab infusion 2. Red symbols depict patients that displayed low numbers of residual T cells following infusion 2. The dotted line represents the detection limit for this analysis. **(B)** Alemtuzumab plasma levels 30 min after IV alemtuzumab infusion 1 and 2. Dotted lines connect measurements from the same patient. **(C)** Relation between the number of circulating T cells before IV alemtuzumab infusion 1 and the alemtuzumab plasma level directly after IV alemtuzumab infusion 1. **(D)** Correlation between the alemtuzumab plasma levels 30 min after IV alemtuzumab infusion 1 and the increase in alemtuzumab plasma levels by IV alemtuzumab infusion 2. The increase in alemtuzumab plasma levels following infusion 2 was calculated by subtracting the alemtuzumab plasma levels before (max 8h) infusion 2 and 30 min after infusion 2. **(E)** Correlation between the alemtuzumab plasma levels directly after IV alemtuzumab infusion 2 and the calculated patients' plasma volume. The solid line depicts a linear regression analysis and P values were generated by F test.
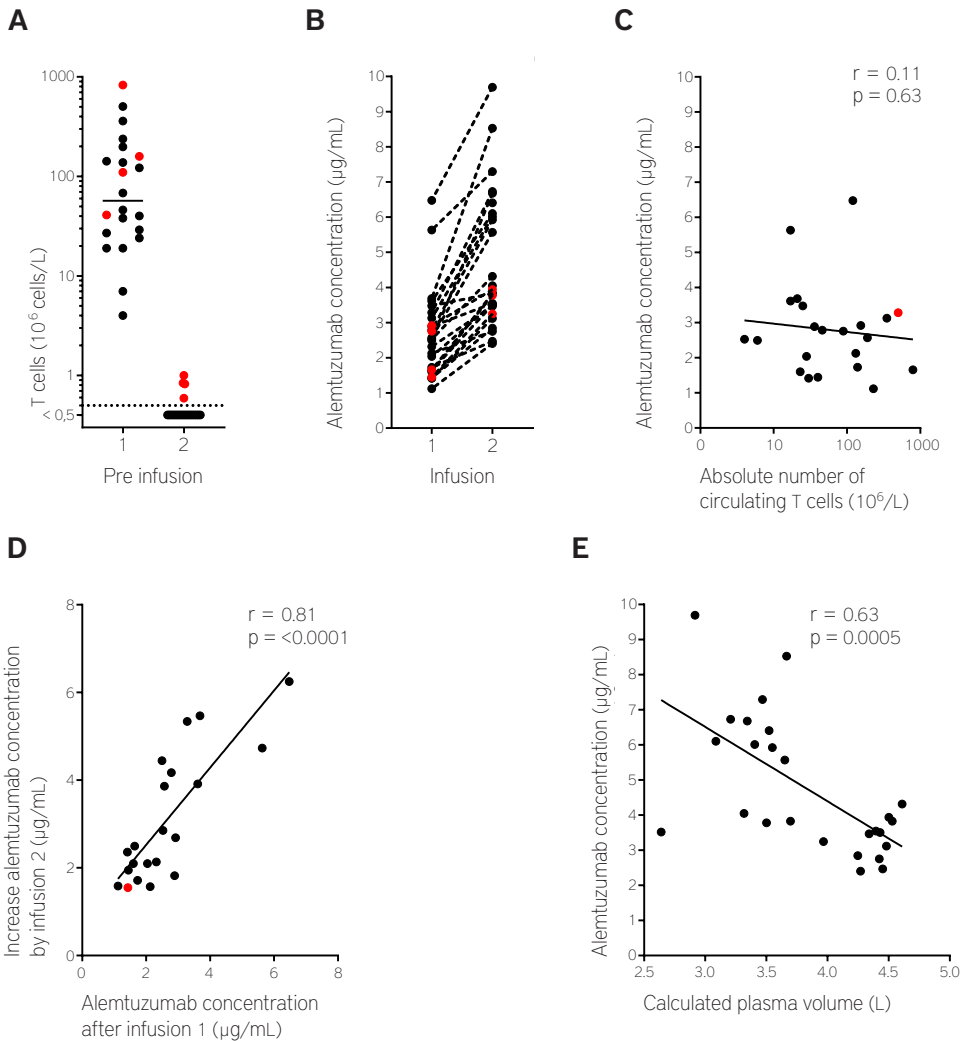
Figure 1B). No correlation was found between the alemtuzumab plasma levels and the numbers of circulating T cells (r = 0.11, p = 0.63, **Figure 1C**) or the total numbers of circulating lymphocytes (r = 0.13, p = 0.58, data not shown) before infusion. Alemtuzumab plasma levels were comparable between patients diagnosed with different malignancies (data not shown). The median alemtuzumab plasma level before the second infusion was 1.7 µg/mL (range 0.8–3.4 µg/mL, n = 23, data not shown) and increased to 3.9 µg/mL (range 2.4–9.7 µg/mL, n = 26, **Figure 1B**) after the second infusion. In patients with detectable T cells after the two alemtuzumab infusions (**Figure 1A** red symbols), alemtuzumab plasma levels were within the normal range (**Figure 1B** red symbols). The increase in the alemtuzumab plasma levels by infusion 2 correlated with the alemtuzumab plasma levels that had been reached in individual patients after infusion 1 (p < 0.0001, both samples available for 22 patients, **Figure 1D**). Because therapeutic antibodies are initially distributed in the blood plasma volume,[32] we analyzed whether the alemtuzumab plasma levels in individual patients correlated with their calculated plasma volumes. A strong negative correlation was found between the calculated plasma volumes and the alemtuzumab plasma levels measured after infusion 1 (r = 0.58, p = 0.002, data not shown) and infusion 2 (r = 0.63, p = 0.0005, **Figure 1E**). Weaker or no significant correlation was found between body surface area and weight and alemtuzumab plasma levels after infusion 2 (r = 0.48, p = 0.01 and r = 0.31, p = 0.13, respectively; **Figure S1**). In conclusion, the plasma volumes and not the numbers of circulating lymphocytes correlated with the alemtuzumab plasma levels in patients after IV alemtuzumab infusions.

Alemtuzumab-induced lysis of donor T cells

To prevent acute GvHD, 20 mg alemtuzumab was added to the stem cell grafts. Due to the limited graft volumes (median 360 mL, range 115–730 mL), high alemtuzumab concentrations were reached in the bags (estimated median 55 µg/mL, range 27–177 µg/mL), thereby promoting efficient coating of target cells. Since grafts are only incubated with alemtuzumab for 30 minutes before infusion, we expected partial lysis of donor T cells "in the bag" followed by ongoing in-vivo lysis after infusion of the stem cell grafts into the patients. To estimate the magnitude of in-vitro T-cell depletion, absolute numbers of T cells before and after 30 minutes alemtuzumab incubation were determined in five grafts. The median T-cell count before alemtuzumab infusion was 14.6×10^9 T cells (range 8.3×10^9–17.3×10^9 T cells) and after incubation 0.5×10^9 T cells (range 0.2×10^9–1.3×10^9 T cells), indicating a 30 fold reduction (range 11–44 fold). After alemtuzumab incubation, the stem cell grafts including residual alemtuzumab-coated donor T cells and unbound alemtuzumab were infused into the patients. We determined the absolute numbers of circulating T cells in patient PB samples taken 30 min after graft infusion (available for 30

patients). In 22 patients, no circulating T cells were found. In the remaining 8 patients, low numbers of T cells (range $0.2x10^6$–$7x10^6$ cells/L) were detected at that time, but these were no longer found in subsequent samples (taken between days 1 and 7 after graft infusion) in 7 out of 8 patients (data not shown). The remaining patient continued to have low numbers of circulating T cells with the lowest number ($1.04x10^6$ cells/L) at day 14 after graft infusion. Insufficient cells were available to determine whether these cells were of patient or donor origin. These data show that in the majority of patients no circulating T cells are found after the infusion of a stem cell graft to which 20 mg alemtuzumab is added.

To evaluate the effect of alemtuzumab infused with the graft on the alemtuzumab plasma levels in the patients, we analyzed the alemtuzumab plasma levels in samples taken before (maximum 8h) and 30 min after graft infusion. In MA-conditioned patients with a sibling donor who had only received
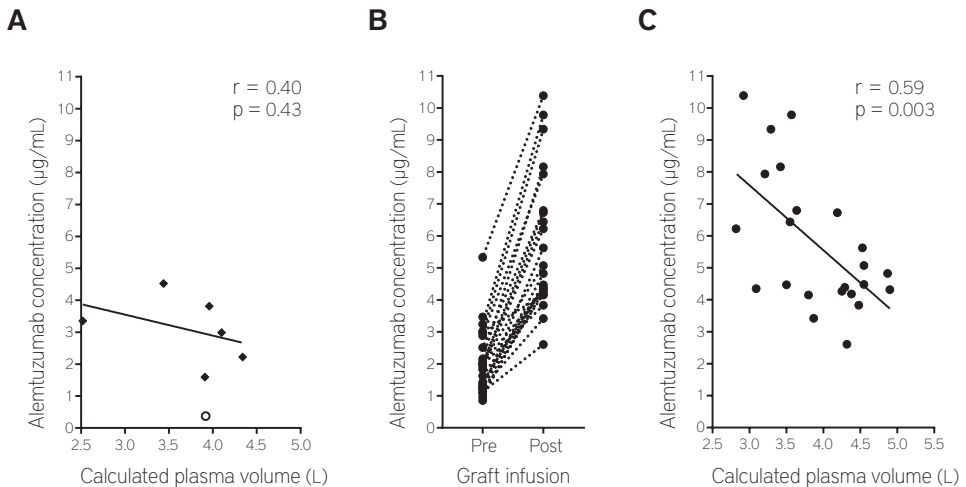
Figure 2. Increase in patients alemtuzumab plasma levels following graft infusion
(A) Relation between the alemtuzumab plasma levels directly after graft infusion and the patients' plasma volumes in patients who had not received alemtuzumab as part of the patient conditioning regimen. **(B)** Alemtuzumab plasma levels directly before and after graft infusion in patients who had already received alemtuzumab as part of the patients conditioning regimen. Dotted lines connect measurement from the same patient. **(C)** Correlation between the alemtuzumab plasma levels directly after graft infusion and the patients' plasma volumes in patients who had already received alemtuzumab as part of the patients conditioning regimen. The solid line depicts a non-linear regression analysis and P values were generated by F test.

alemtuzumab "in the bag", alemtuzumab plasma levels reached a median of 3.0 μg/mL (range 0.4–4.5 μg/mL, samples were available for 7 out of 8 patients). Since in these patients alemtuzumab was not part of the patient conditioning regimen, residual circulating patient T cells were present before graft infusion (range 1×10^6–64×10^6 cells/L), but these did not correlate with alemtuzumab plasma levels after graft infusion (r = 0.30, p = 0.51, data not shown). A trend was observed between higher calculated plasma volumes and lower alemtuzumab plasma levels (r = 0.40, p = 0.43, **Figure 2A**). In one patient, alemtuzumab levels were particularly low (0.4 μg/mL, **Figure 2C** open circle). This patient had a history of hairy cell leukemia and splenomegaly at the time of transplantation, which may have contributed to absorption of alemtuzumab. For patients who had already received alemtuzumab as part of the patient conditioning regimen, pre and post graft infusion samples were available for 23 out of 28 patients. Before graft infusion, a median alemtuzumab concentration of 2.0 μg/mL (range 1.0–5.3 μg/mL, **Figure 2B**) was present. After graft infusion, alemtuzumab plasma levels increased to a median of 4.8 μg/mL (range 2.6–10.4 μg/mL, **Figure 2B**). Similar alemtuzumab plasma levels were found between NMA-conditioned patient who had (median 4.8 μg/mL, range 3.4-10.4 μg/mL) or had not (median 4.6 μg/mL, range 2.6-9.8 μg/mL) received additional ATG during in-vivo conditioning. A strong negative correlation was found between the calculated patients' plasma volumes and the alemtuzumab plasma levels before (r = 0.67, p = 0.0001, data not shown) and after graft infusion (r = 0.59, p = 0.003, **Figure 2C**). Together these data show that the increase in alemtuzumab levels by graft infusion was independent of pre-treatment with alemtuzumab during patient conditioning. The increase in alemtuzumab levels were in line with an increase expected from direct IV injection, indicating presence of an excess amount of alemtuzumab "in the bag" whereby the bulk of alemtuzumab remained unbound.

Influence of circulating alemtuzumab on reconstitution of T cells

After transplantation, neutrophil repopulation indicated engraftment in all patients. To study the influence of alemtuzumab on T-cell reconstitution, we determined the absolute numbers of circulating CD4 and CD8 T cells starting at three weeks after the transplantation. At week three after graft infusion (data were available for 33 out of 36 patients), 23 patients had already reconstituted with CD4 T cells (range 0.9×10^6–106×10^6 cells/L) and 21 patients with CD8 T cells (range 0.7×10^6–848×10^6 cells/L). At week nine after graft infusion (data were available for 31 patients), 30 patients had circulating CD4 T cells (range 1.1×10^6–864×10^6 cells/L) and 29 patients had circulating CD8 T cells (range 4×10^6–3367×10^6 cells/L). Persistence of circulating alemtuzumab after graft infusion was modelled by population pharmacokinetics analysis with non-linear mixed effects modeling using alemtuzumab plasma

concentration-time data. Alemtuzumab pharmacokinetics was best described by a two-compartment intravenous model with first-order elimination. Random effect parameters for inter-individual variability in clearance, distribution volume of the central compartment and the peripheral compartment were identified (model parameters in **Table 2**; pcVPC and goodness of fit plots in **Figure S2** and **S3**, respectively). The mean half-life of alemtuzumab in the elimination phase was 8.7 days (range 2.4-19.1). No direct correlations were found between the number of CD4 or CD8 T cells and modelled alemtuzumab plasma levels at 3 weeks (r = 0.23 and r = 0.14, respectively) or 9 weeks (r = 0.06 and r = 0.16, respectively) post-transplantation. These data show no direct correlation between T-cell reconstitution and residual circulating alemtuzumab.

Table 2. Model parameter estimates

Clearance (L/day)	0.9 (0.2 – 14.0)
Half-life distribution phase (hours)	10 (4 – 23)
Half-life elimination phase (days)	8.7 (2.4 – 19.1)
Volume central compartment (L)	2.8 (1.1 – 29.2)
Inter-compartmental clearance (L/day)	2.9
Volume peripheral compartment (L)	6.3 (3.1 – 12.2)
Peak alemtuzumab concentration (µg/mL)	8.4 (0.7 – 22.2)
Total alemtuzumab exposure* (µg.day/mL)	25.2 (1.4 – 54.1)

After graft infusion
Median values (range) are given unless stated otherwise.

2

We and others have previously shown that after alemtuzumab-based T-cell-depleted alloSCT, reconstituting T cells have frequently lost CD52 membrane expression[18,33] making them resistant to alemtuzumab. We therefore evaluated the effect of residual alemtuzumab on reconstitution of CD52-positive and CD52-negative T cells. CD52 membrane expression was analyzed by flow cytometry and combined with the absolute numbers of circulating CD4 and CD8 T cells determined in samples taken at the same time point. Complete absence of CD52-positive CD4 and CD8 T cells was observed at week 3 when alemtuzumab plasma levels were above 0.7 µg/mL (**Figure 3A** and **3B**, respectively). In contrast, no association was found between alemtuzumab plasma levels and the numbers of CD52-negative CD4 and CD8 T cells (**Figure 3C** and **3D**, respectively). At week nine, all patients had alemtuzumab plasma levels <0.34 µg/mL and no effect of alemtuzumab plasma levels was observed on either CD52-negative of CD52-positive T-cell reconstitution (data not shown).
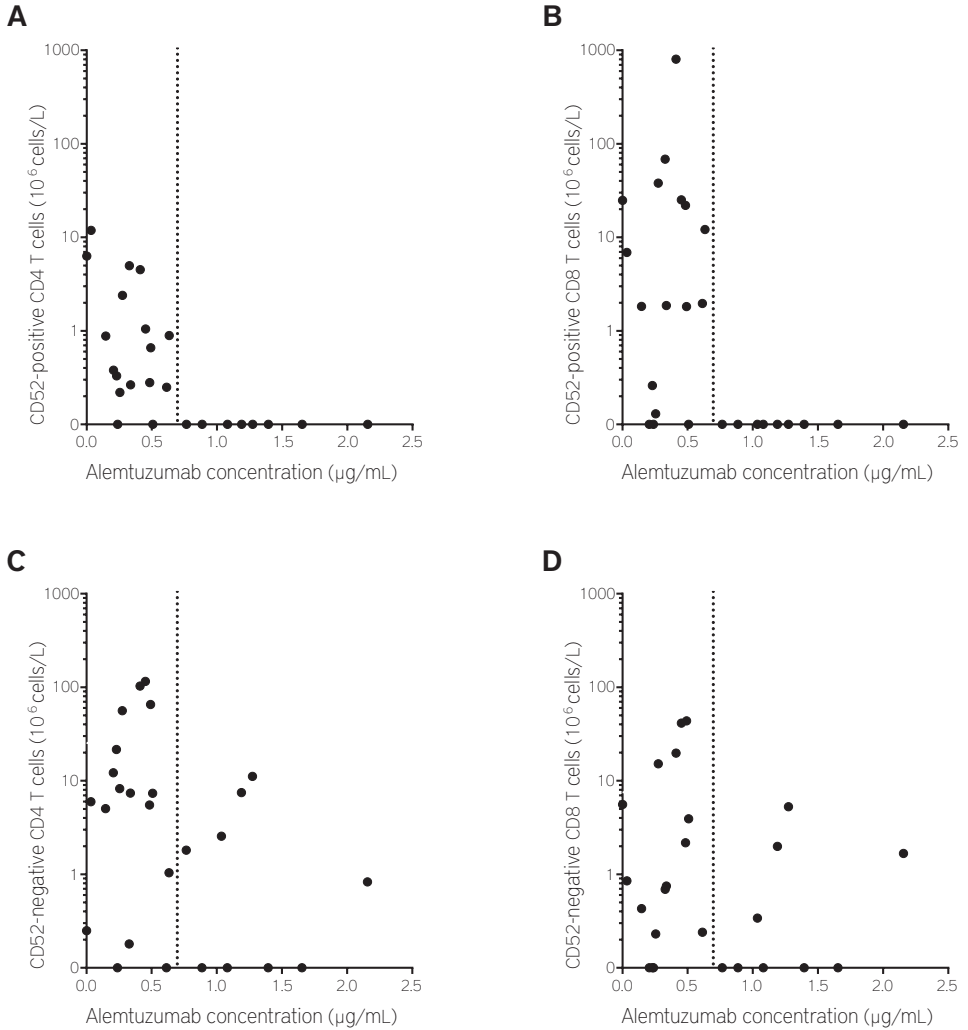
Figure 3. Reconstitution of CD52-positive T cells is blocked by persistence of lytic alemtuzumab plasma levels
Absolute number of circulating CD52-positive **(A)** CD4 and **(B)** CD8 and CD52-negative **(C)** CD4 and **(D)** CD8 T cells at week 3 after graft infusion. Each dot represents the analysis for one patient. The dotted lines indicate the alemtuzumab concentration of 0.7 µg/mL.

These data show that in-vivo alemtuzumab levels above 0.7 μg/mL prevented reconstitution of CD52-positive T cells.

Absence of GvHD in the presence of high alemtuzumab levels

Because acute GvHD is mediated by naïve donor T cells infused with the graft,[34] we investigated whether modelled alemtuzumab peak concentrations directly after graft infusion correlated with the incidence of GvHD. Two patients who had developed an early relapse (weeks 6 and 7 post graft infusion) and received additional chemotherapy were not included in the analysis. Three patients (one MA- and one NMA-conditioned patient with sibling donors and one MA-conditioned patient with an UD) had developed GvHD grade II or III within the first 10 weeks following graft infusion. All three patients had low peak alemtuzumab plasma concentrations (**Figure 4**). No GvHD was observed in patients with peak alemtuzumab levels above 6.5 μg/mL.

Effect of alemtuzumab exposure on viral complications

Because persistence of alemtuzumab was shown to affect CD52-positive T-cell reconstitution, we analyzed whether differences in alemtuzumab exposure after graft infusion had affected the incidence of viral complications. Alemtuzumab exposure was estimated for each patient using population pharmacokinetics and related to reactivations of EBV and CMV occurring within the first 10 weeks after graft infusion. 5 out of 36 patients were excluded from this analysis as they had developed an early relapse (n = 2) or GvHD (n = 3) and received additional chemotherapy or steroid treatment. No EBV-reactivation was observed in patients that were EBV-seronegative before transplantation (n = 3). From the 28 pre-transplant EBV-seropositive patients, 7 had an EBV-reactivation (of whom 2 had an EBV-seronegative donor). None of these patients required treatment for the EBV-reactivation and alemtuzumab exposure was comparable to patients without EBV-reactivation (mean area under the curve 28.4 ± 11.9 μg.day/mL compared to mean 31.2 ± 10.4 μg.day/mL, p = 0.63). For CMV, no reactivation was observed in the patients who were CMV-seronegative before transplantation (n = 14). From the 17 pre-transplant CMV-seropositive patients, all had detectable CMV-reactivations within the first 10 weeks after graft infusion and 14 patients were consequently treated with antiviral drugs. None of the patients developed CMV-disease. There was a weak correlation between alemtuzumab exposure and the duration of CMV viremia (**Figure 5**). Although circulating alemtuzumab levels in this cohort were sufficient to prevent the development of acute GvHD in the majority of patients, no patient developed viral disease in this period.
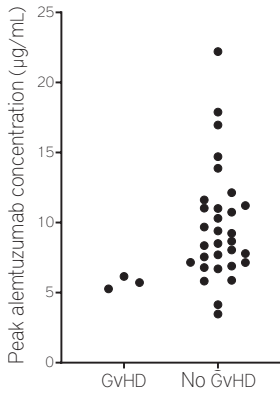
Figure 4. Absence of GvHD in the presence of high alemtuzumab levels

Peak alemtuzumab plasma levels and the occurrence of GvHD within the first 10 weeks after graft infusion. Alemtuzumab peak levels were estimated for each patient using pharmacokinetics modelling. Each dot represents the analysis for one patient.
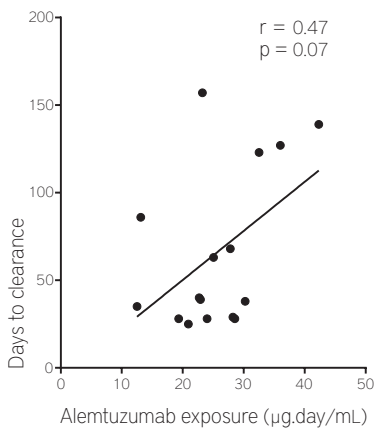
Figure 5. Effect of alemtuzumab exposure on CMV-clearance

Relation between alemtuzumab exposure and time to clear a CMV-reactivation. Alemtuzumab exposure was estimated for each patient using population pharmacokinetics modelling. Each dot represents the analysis for one patient. The solid line depicts a non-linear regression analysis and P values were generated by F test.

DISCUSSION

This study confirms that the combination of in-vivo and in-vitro alemtuzumab effectively prevents acute GvHD after alloSCT without compromising engraftment.[35,36] Our data demonstrate that plasma volume rather than the number of circulating lymphocytes determines inter-individual variation in alemtuzumab plasma peak. Patients with a plasma peak level after transplantation above 6.5 µg/mL did not develop acute GvHD. Although the post-transplantation T-cell suppression in this cohort was sufficient to prevent acute GvHD in the majority of patients, no cases of EBV-PTLD or CMV-disease were seen. Antiviral immune protection results from an early outgrowth of CD52-negative T cells. Whereas circulating CD52-positive T cells were absent when residual alemtuzumab level were above 0.7 µg/mL, the reconstitution of CD52-negative T cells was not affected by alemtuzumab.

One of the aims of adding of alemtuzumab to the conditioning regimen of a patient before alloSCT is the eradication of patient T cells to avoid graft rejection. We showed that virtually all circulating T cells were efficiently depleted in patients who had received infusion of 30 mg alemtuzumab IV. In contrast, in MA-conditioned patients with a sibling donor who had not received alemtuzumab IV, circulating T cells were found up to the moment of graft infusion. Alemtuzumab plasma levels in our cohort correlated with the patients' plasma volumes. In patients with CLL treated with alemtuzumab, alemtuzumab plasma levels were found to be highly affected by the tumor burden due to target-cell-mediated alemtuzumab absorbtion[37-39]. In our cohort, alemtuzumab plasma levels did not correlate with the numbers of circulating T cells present at time of alemtuzumab infusion, likely because patients in our cohort were in remission for the primary disease when receiving the alloSCT and had received TBI and/or chemotherapy before alemtuzumab, together resulting in low numbers of circulating lymphocytes. One patient had particularly low alemtuzumab plasma levels. This patient had a history of hairy cell leukemia and had splenomegaly at the start of the alloSCT, which was given to treat a therapy related acute myeloid leukemia. We hypothesize that the spleen effectively absorbed alemtuzumab and therefore we suggest that patients with residual bulky disease require higher alemtuzumab dosing to overcome alemtuzumab absorption, as previously suggested by Chakraverty et al.[40]

Alemtuzumab is added to the graft to eradicate donor-derived T cells thereby preventing GvHD. We showed that pre-incubation of the graft with 20 mg alemtuzumab reduced donor T-cell numbers on average by a factor of 30. After infusion of the graft with remaining donor T cells with bound and

unbound alemtuzumab, circulating alemtuzumab led to ongoing lysis of circulating T lymphocytes. In order to correlate alemtuzumab pharmacokinetics with clinical outcomes like the occurrence of acute GvHD, viral reactivation, and T cell reconstitution after alloSCT, alemtuzumab peak concentrations and alemtuzumab exposure were estimated for each patient using population pharmacokinetics analysis with non-linear mixed effects modeling. Three patients in our cohort developed limited GvHD after alloSCT, suggesting that some donor T cells had escaped alemtuzumab treatment. Because GvHD is predominantly mediated by naïve donor T cells infused with the graft,[34] which express high levels of CD52 and as a consequence are highly sensitive to alemtuzumab-mediated cell lysis,[41] acute GvHD would be expected to occur because of inadequate peak alemtuzumab levels. Indeed, low alemtuzumab peak concentrations were found in all three patients who developed GvHD. Furthermore, no GvHD was observed in patients with alemtuzumab peak levels above 6.5 µg/mL, illustrating that adequate alemtuzumab peak levels indeed effectively prevent GvHD. These plasma peak levels were the product of alemtuzumab added to the graft and alemtuzumab applied IV as part of the conditioning. Since the plasma peak levels correlated with the patients' plasma volume, modifying the alemtuzumab dose based on this parameter could be considered as a way to dictate the plasma peak level post-transplant. Indeed, the three patients in our cohort who developed GvHD coinciding with low alemtuzumab peak levels had relatively high plasma volumes. However, we are somewhat reluctant to suggest patient-specific adjustment of the alemtuzumab dose based on plasma volume only, due to the low patient numbers and the likelihood that proper prediction of the peak levels post-transplant most likely requires inclusion of additional parameters such as pre-transplant alemtuzumab serum measurements, and factors like splenomegaly. The incidence of GvHD in our cohort was comparable to previous studies in which patients received in-vivo alemtuzumab in combination with post-transplant immune suppression with cyclosporin.[40,42]

Persistence of high levels of residual alemtuzumab can also delay reconstitution of protective virus-specific T cells. Here we established an in-vivo lytic alemtuzumab plasma level of 0.7 µg/mL as the lower threshold for reconstitution with CD52-positive CD4 and CD8 T cells. This level is substantially higher than the previously suggested lytic alemtuzumab level of 0.1 µg/mL, which was based on the anticipated combined effect of ADCC and CDC as effector mechanisms.[42,43] Low numbers of effectors cells early after alloSCT may decrease the contribution of ADCC to in-vivo cell lysis. CDC, which is known from in-vitro tests to be efficient only at higher alemtuzumab concentrations starting at levels identical to the minimal lytic alemtuzumab level we found,[44] may be the main mechanism causing T-cell depletion

after transplantation. Although a correlation between alemtuzumab levels and outgrowth of CD52-positive T cells was found, there was no correlation between total numbers of T cells and alemtuzumab exposure. This discrepancy resulted from rapid outgrowth of large populations of CD52-negative alemtuzumab-resistant T cells early after transplantation. Previously we have reported that these CD52-negative T-cell populations are mainly of a memory phenotype and contain functional virus-specific CD8 T cells, including CMV-specific T cells. These CD52-negaive memory T cells appeared to be mainly of donor origin, but also profound outgrowth of CD52-negative memory T cells of recipient origin was observed in some patients, especially associated with viral clearance shortly after the transplantation.[18] The protective effect of these cells likely explains why no correlation was found between the level of alemtuzumab exposure and the incidence of EBV- or CMV-reactivation, or on EBV-clearance, and only a minimal effect on CMV-clearance. Of note, unlike naïve T cells, these CD52-negative memory T cells are not expected to contribute to GvHD.

We conclude that after alloSCT using in-vitro with or without prior in-vivo T-cell depletion with alemtuzumab, plasma alemtuzumab peak levels above 6.5 μg/mL prevent the development of acute GvHD. After alloSCT, circulating CD52-positive T cells are absent as long as the circulating alemtuzumab level is above 0.7 μg/mL. The reconstitution of CD52-negative cells is not influenced by alemtuzumab level and contributes to the prevention of viral disease after alloSCT.

Acknowledgement

REFERENCE LIST

1.   Miller JS, Warren E, van den Brink M, et al. NCI First International Workshop on The Biology, Prevention, and Treatment of Relapse After Allogeneic Hematopoietic Stem Cell Transplantation: Report from the Committee on the Biology Underlying Recurrence of Malignant Disease following Allogeneic HSCT: Graft-versus-Tumor/Leukemia Reaction. *Biol Blood Marrow Transplant*. 2010;16(5):565-586.

2.   Deol A, Lum LG. Role of donor lymphocyte infusions in relapsed hematological malignances after stem cell transplantation revisited. *Cancer Treat Rev*. 2010;36(7):528-538.

3.   Roddie C, Peggs KS. Donor lymphocyte infusion following allogeneic hematopoietic stem cell transplantation. *Expert Opin Biol Ther*. 2011;11(4):473-487.

4.   Eefting M, von dem Borne PA, de Wreede LC, et al. Intentional donor lymphocyte-induced limited acute graft-versus-host disease is essential for long-term survival of relapsed acute myeloid leukemia after allogeneic stem cell transplantation. *Haematologica*. 2014;99(4):751-758.

5.   Eefting M, Halkes CJ, de Wreede LC, et al. Myeloablative T cell-depleted alloSCT with early sequential prophylactic donor lymphocyte infusion is an efficient and safe post-remission treatment for adult ALL. *Bone Marrow Transplant*. 2014;49(2):287-291.

6.   Hale G, Bright S, Chumbley G, et al. Removal of T cells from bone marrow for transplantation: a monoclonal antilymphocyte antibody that fixes human complement. *Blood*. 1983;62(4):873-882.

7.   Novitzky N, Davison G, Abdulla R, Mowla S. Definition of the variables affecting efficacy of immunodepletion ex vivo of peripheral blood progenitor cell grafts by alemtuzumab (Campath in the bag). *Biol Blood Marrow Transplant*. 2013;19(12):1753-1759.

8.   Perez-Simon JA, Kottaridis PD, Martino R, et al. Nonmyeloablative transplantation with or without alemtuzumab: comparison between 2 prospective studies in patients with lymphoproliferative disorders. *Blood*. 2002;100(9):3121-3127.

9.   Kottaridis PD, Milligan DW, Chopra R, et al. In vivo CAMPATH-1H prevents GvHD following nonmyeloablative stem-cell transplantation. *Cytotherapy*. 2001;3(3):197-201.

10.   Chakraverty R, Peggs K, Chopra R, et al. Limiting transplantation-related mortality following unrelated donor stem cell transplantation by using a nonmyeloablative conditioning regimen. *Blood*. 2002;99(3):1071-1078.

11.   Mead AJ, Thomson KJ, Morris EC, et al. HLA-mismatched unrelated donors are a viable alternate graft source for allogeneic transplantation following alemtuzumab-based reduced-intensity conditioning. *Blood*. 2010;115(25):5147-5153.

12.   Eefting M, de Wreede LC, Halkes CJ, et al. Multi-state analysis illustrates treatment success after stem cell transplantation for acute myeloid leukemia followed by donor lymphocyte infusion. *Haematologica*. 2016;101(4):506-514.

13.   Novitzky N, Thomas V, Hale G, Waldmann H. Myeloablative conditioning is well tolerated by older

patients receiving T-cell-depleted grafts. *Bone Marrow Transplant*. 2005;36(8):675-682.

14. Lee SJ, Vogelsang G, Flowers ME. Chronic graft-versus-host disease. *Biol Blood Marrow Transplant*. 2003;9(4):215-233.

15. Goker H, Haznedaroglu IC, Chao NJ. Acute graft-vs-host disease: pathobiology and management. *Exp Hematol*. 2001;29(3):259-277.

16. Chakrabarti S, Mautner V, Osman H, et al. Adenovirus infections following allogeneic stem cell transplantation: incidence and outcome in relation to graft manipulation, immunosuppression, and immune recovery. *Blood*. 2002;100(5):1619-1627.

17. Chakrabarti S, Mackinnon S, Chopra R, et al. High incidence of cytomegalovirus infection after nonmyeloablative stem cell transplantation: potential role of Campath-1H in delaying immune reconstitution. *Blood*. 2002;99(12):4357-4363.

18. Loeff FC, Falkenburg JHF, Hageman L, et al. High Mutation Frequency of the PIGA Gene in T Cells Results in Reconstitution of GPI Anchor(-)/CD52(-) T Cells That Can Give Early Immune Protection after Alemtuzumab-Based T Cell-Depleted Allogeneic Stem Cell Transplantation. J *Immunol*. 2018.

19. Spyridonidis A, Liga M, Triantafyllou E, et al. Pharmacokinetics and clinical activity of very low-dose alemtuzumab in transplantation for acute leukemia. *Bone Marrow Transplant*. 2011;46(10):1363-1368.

20. Tholouli E, Liakopoulou E, Greenfield HM, et al. Outcomes following 50 mg versus 100 mg alemtuzumab in reduced-intensity conditioning stem cell transplants for acute myeloid leukaemia and poor risk myelodysplasia. *Br J Haematol*. 2008;142(2):318-320.

21. Bertz H, Spyridonidis A, Wasch R, Grullich C, Egger M, Finke J. A novel GVHD-prophylaxis with low-dose alemtuzumab in allogeneic sibling or unrelated donor hematopoetic cell transplantation: the feasibility of deescalation. *Biol Blood Marrow Transplant*. 2009;15(12):1563-1570.

22. von dem Borne PA, Beaumont F, Starrenburg CW, et al. Outcomes after myeloablative unrelated donor stem cell transplantation using both in vitro and in vivo T-cell depletion with alemtuzumab. *Haematologica*. 2006;91(11):1559-1562.

23. Glucksberg H, Storb R, Fefer A, et al. Clinical manifestations of graft-versus-host disease in human recipients of marrow from HL-A-matched sibling donors. *Transplantation*. 1974;18(4):295-304.

24. Rebello P, Hale G. Pharmacokinetics of CAMPATH-1H: assay development and validation. *J Immunol Methods*. 2002;260(1-2):285-302.

25. Nijmeijer BA, Szuhai K, Goselink HM, et al. Long-term culture of primary human lymphoblastic leukemia cells in the absence of serum or hematopoietic growth factors. *Exp Hematol*. 2009;37(3):376-385.

26. Loeff FC, van Egmond HME, Nijmeijer BA, Falkenburg JHF, Halkes CJ, Jedema I. Complement-dependent cytotoxicity induced by therapeutic antibodies in B-cell acute lymphoblastic leukemia is dictated by target antigen expression levels and augmented by loss of membrane-bound complement inhibitors. *Leuk Lymphoma*. 2017;58(9):1-14.

2

27. Lindbom L, Pihlgren P, Jonsson EN. PsN-Toolkit--a collection of computer intensive statistical methods for non-linear mixed effect modeling using NONMEM. *Comput Methods Programs Biomed*. 2005;79(3):241-257.

28. Keizer RJ, van Benten M, Beijnen JH, Schellens JH, Huitema AD. Pirana and PCluster: a modeling environment and cluster infrastructure for NONMEM. *Comput Methods Programs Biomed*. 2011;101(1):72-79.

29. Nadler SB, Hidalgo JH, Bloch T. Prediction of blood volume in normal human adults. Surgery. 1962;51(2):224-232.

30. Bergstrand M, Hooker AC, Wallin JE, Karlsson MO. Prediction-corrected visual predictive checks for diagnosing nonlinear mixed-effects models. *Aaps j*. 2011;13(2):143-151.

31. Kalpoe JS, Kroes AC, de Jong MD, et al. Validation of clinical application of cytomegalovirus plasma DNA load measurement and definition of treatment criteria by analysis of correlation to antigen detection. *J Clin Microbiol*. 2004;42(4):1498-1504.

32. Tabrizi M, Bornstein GG, Suria H. Biodistribution mechanisms of therapeutic monoclonal antibodies in health and disease. *Aaps j*. 2010;12(1):33-43.

33. Garland RJ, Groves SJ, Diamanti P, et al. Early emergence of PNH-like T cells after allogeneic stem cell transplants utilising CAMPATH-1H for T cell depletion. *Bone Marrow Transplant*. 2005;36(3):237-244.

34. Falkenburg JHF, Jedema I. Graft versus tumor effects and why people relapse. *Hematology Am Soc Hematol Educ Program*. 2017;2017(1):693-698.

35. von dem Borne PA, Starrenburg CW, Halkes SJ, et al. Reduced-intensity conditioning allogeneic stem cell transplantation with donor T-cell depletion using alemtuzumab added to the graft ('Campath in the bag'). Curr Opin Oncol. 2009;21 Suppl 1:S27-29.

36. Barge RM, Starrenburg CW, Falkenburg JH, Fibbe WE, Marijt EW, Willemze R. Long-term follow-up of myeloablative allogeneic stem cell transplantation using Campath "in the bag" as T-cell depletion: the Leiden experience. *Bone Marrow Transplant*. 2006;37(12):1129-1134.

37. Ishizawa K, Fukuhara N, Nakaseko C, et al. Safety, efficacy and pharmacokinetics of humanized anti-CD52 monoclonal antibody alemtuzumab in Japanese patients with relapsed or refractory B-cell chronic lymphocytic leukemia. *Jpn J Clin Oncol*. 2017;47(1):54-60.

38. Mould DR, Baumann A, Kuhlmann J, et al. Population pharmacokinetics-pharmacodynamics of alemtuzumab (Campath) in patients with chronic lymphocytic leukaemia and its link to treatment response. *Br J Clin Pharmacol*. 2007;64(3):278-291.

39. Hale G, Rebello P, Brettman LR, et al. Blood concentrations of alemtuzumab and antiglobulin responses in patients with chronic lymphocytic leukemia following intravenous or subcutaneous routes of administration. *Blood*. 2004;104(4):948-955.

40. Chakraverty R, Orti G, Roughton M, et al. Impact of in vivo alemtuzumab dose before reduced intensity conditioning and HLA-identical sibling stem cell transplantation: pharmacokinetics, GVHD, and immune

reconstitution. *Blood*. 2010;116(16):3080-3088.

41. Rao SP, Sancho J, Campos-Rivera J, et al. Human peripheral blood mononuclear cells exhibit heterogeneous CD52 expression levels and show differential sensitivity to alemtuzumab mediated cytolysis. *PLoS One*. 2012;7(6):e39416.

42. Rebello P, Cwynarski K, Varughese M, Eades A, Apperley JF, Hale G. Pharmacokinetics of CAMPATH-1H in BMT patients. *Cytotherapy*. 2001;3(4):261-267.

43. Morris EC, Rebello P, Thomson KJ, et al. Pharmacokinetics of alemtuzumab used for in vivo and in vitro T-cell depletion in allogeneic transplantations: relevance for early adoptive immunotherapy and infectious complications. *Blood*. 2003;102(1):404-406.

44. Riechmann L, Clark M, Waldmann H, Winter G. Reshaping human antibodies for therapy. *Nature*. 1988;332(6162):323-327.

2

SUPPLEMENTAL DATA

Table S1. Demographic formulas

Body surface area	BSA (m²)	=	$\sqrt{\dfrac{\text{Height (cm) x Weight (kg)}}{3600}}$
Body mass index	BMI $\left(\dfrac{kg}{m^2}\right)$	=	$\dfrac{\text{Weight (kg)}}{[\text{Height (m)}]^2}$
Blood volume (male)	BV (L)		= [Length (m)]³ x 0.367 + Weight (kg)x 0.032+0.604
Blood volume (female)	BV (L)		= [Length (m)]³ x 0.356 + Weight (kg)x 0.033+0.183
Plasma volume corrected for hematocrit	PV (L)		= BV (L) x $\left(1\text{-ht}\left(\dfrac{L}{L}\right)\right)$

S1. A

r = 0.48
p = 0.01

B

r = 0.31
p = 0.13
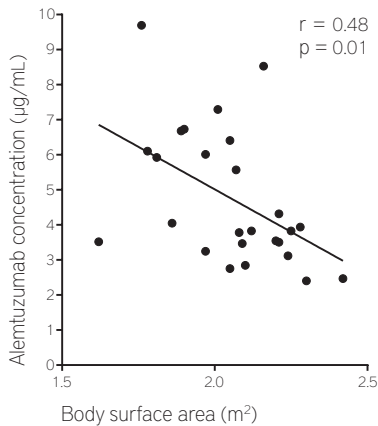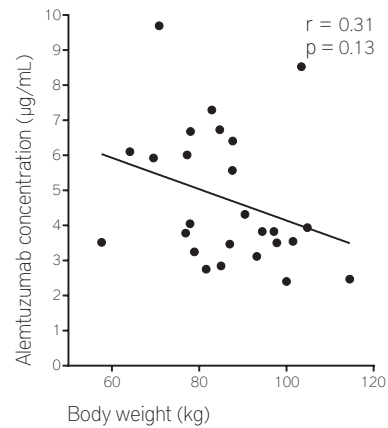
S2.
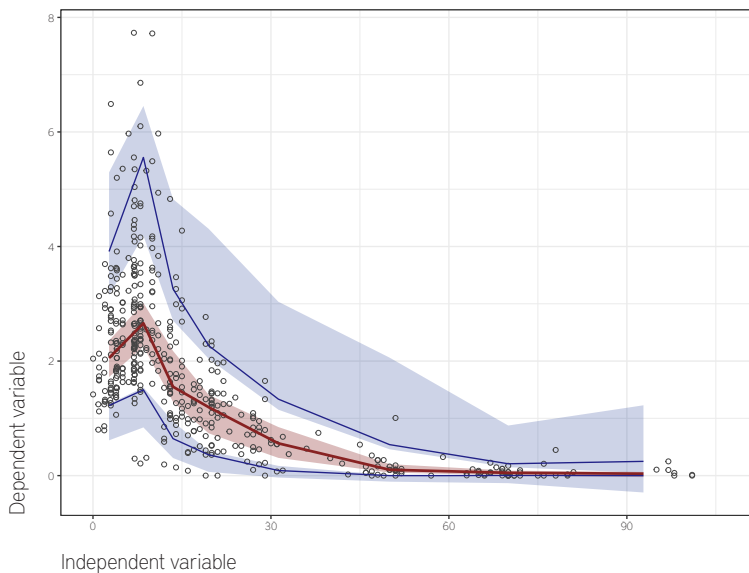
Figure S1. (A) Correlation between the alemtuzumab plasma levels directly after IV alemtuzumab infusion 2 and the calculated patients' body surface area. **(B)** Correlation between the alemtuzumab plasma levels directly after IV alemtuzumab infusion 2 and the patients' body weight. The solid lines depicts linear regression analyses and P values were generated by F test.

Figure S2. Prediction corrected visual predictive check with median, 10th and 90th observation percentile. The observed alemtuzumab plasma concentrations are shown as open circles. The red and blue lines represent the observed median and 10th and 90th percentile. The shaded areas represent the 95% confidence interval around each of the prediction percentiles.

Figure S3. Representative examples of goodness of fit plots of individuals receiving MA-conditioning and a sibling donor graft **(A)** or an UD graft **(B)**, or receiving NMA-conditioning and a sibling donor graft **(C)** or an UD graft **(D)**. Blue circles indicate the measured concentration, the red line is the individual prediction of the model. The moment of graft infusion is modeled to occur at day 7 in all plots.
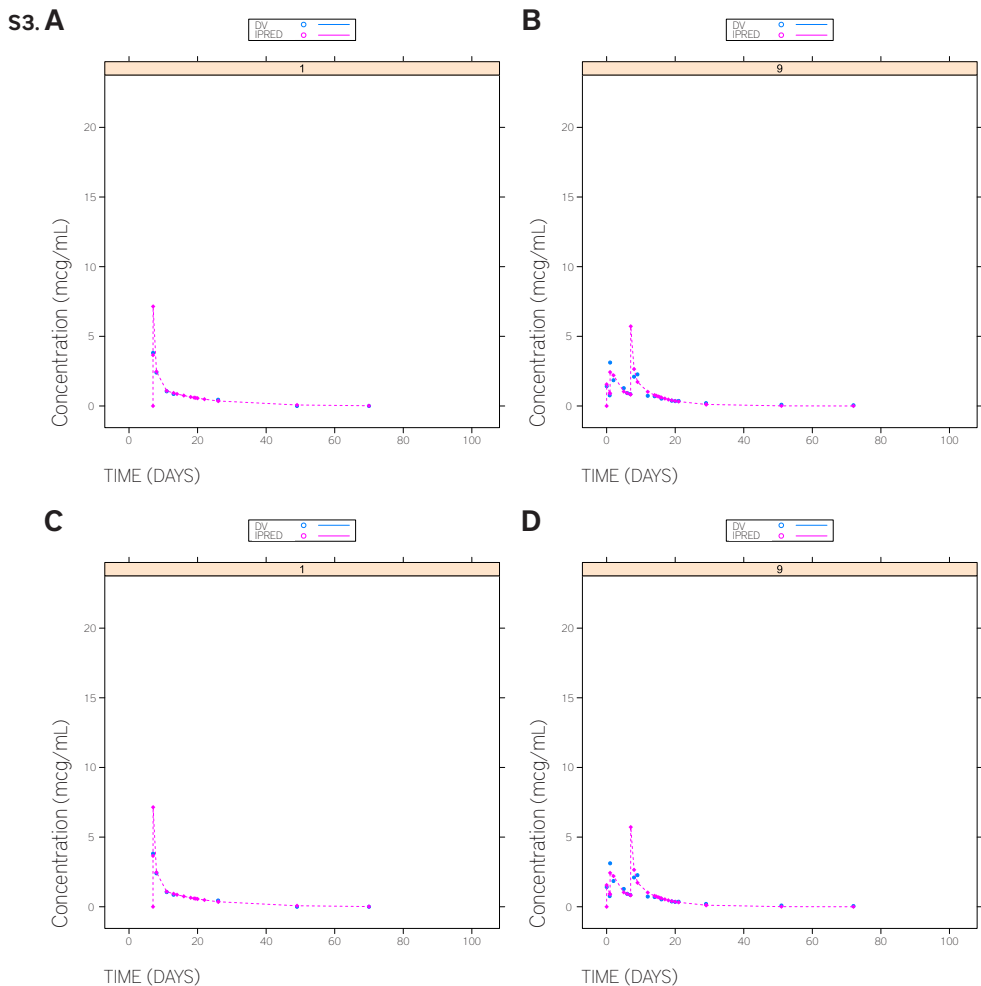
Floris C. Loeff[1]
H.M. Esther van Egmond[1]
Bart A. Nijmeijer[1]
J.H. Frederik Falkenburg[1]
Constantijn J. Halkes[1]*
Inge Jedema[1]*

CHAPTER 3

Complement-dependent cytotoxicity induced by therapeutic antibodies in B-cell acute lymphoblastic leukemia is dictated by target antigen expression levels and augmented by loss of membrane-bound complement inhibitors

[1] Department of Hematology - Leiden University Medical Center - Leiden - the Netherlands
* C.J.H. and I.J. share senior authorship

ABSTRACT

To optimally utilize therapeutic monoclonal antibodies in the treatment of B-cell acute lymphoblastic leukemia (B-ALL) understanding their mechanisms of action and the factors influencing these mechanisms is required. We show strong correlations between target antigen expression levels and sensitivity to complement-dependent cytotoxicity (CDC) induced by rituximab, ofatumumab, or alemtuzumab in a panel of cell lines derived from primary B-ALL cells and in primary B-ALL samples. Simultaneous loss of expression of membrane-bound complement regulatory proteins (mCRP) CD55 and CD59 due to glycophosphatidylinositol-anchor deficiency, significantly increased sensitivity to CDC. Accordingly, induced increase in CD55 or CD59 expression protected cells against CDC. The extent of protection co-depended on antigen expression and antibody concentration. In contrast, natural variation in mCRP expression could not be used as a single factor to predict sensitivity to CDC. In conclusion, sensitivity of B-ALL cells to CDC was predominantly determined by antibody concentration and target antigen expression.

INTRODUCTION

Incorporation of chimeric and humanized monoclonal antibodies in the management of B-cell derived hematologic malignancies improved treatment outcome in recent years. Successes in treatment of chronic lymphocytic leukemia (CLL) and B-cell lymphoma by targeting surface antigens CD20 using rituximab (RTX) or ofatumumab (OFA) and CD52 using alemtuzumab (ALM),[1] has initiated the interest of using these antibodies in the treatment of B-cell acute lymphoblastic leukemia (B-ALL). Although results from initial single-agent approaches were disappointing,[2] single-arm and comparative studies using CD20 targeting antibodies in combination with chemotherapeutics have shown safety and efficacy.[3,4] These results were underlined by results from the randomized Group for Research on Adult Acute Lymphoblastic Leukemia 2005 trial, in which addition of RTX to standard therapy improved event free survival.[5]

To optimally exploit the potential of therapeutic antibodies it is essential to understand their mechanisms of action and the factors that influence these mechanisms. The primary mechanisms of action include antibody-dependent cellular cytotoxicity (ADCC), antibody-dependent cellular phagocytosis (ADCP), and complement-dependent cytotoxicity (CDC).[6-9] Although their relative contribution in-vivo is not fully clarified, experiments in C1q knock-out mice and in mice pretreated with cobra venom factor indicate a dominant role for CDC.[10,11] This is supported by the observation of complement consumption in patients treated with RTX, OFA, or ALM,[12-14] longer time to progression in RTX-treated follicular lymphoma (FL) patients carrying a specific C1q phenotype,[15] and superior correlation between clinical outcome and in-vitro CDC compared with ADCC experiments in patients with B-cell malignancies.[16]

Several factors contribute to successful eradication of tumor cells by CDC. For instance, higher antigen expression levels are associated with higher levels of complement activation by the therapeutic antibodies, increased CDC in-vitro,[17,18] and improved clinical outcome.[19] In contrast, expression of membrane-bound complement regulatory proteins (mCRP) decay accelerating factor (DAF, CD55) and membrane inhibitor of reactive lysis (MIRL, CD59), which normally protect cells from the effect of spontaneous and bystander complement pathway activation, have been suggested as down-regulators of CDC.[20-23] However, whether these mechanisms are relevant in B-ALL which is characterized by a particular heterogeneous level of antigen expression is not known.

3

In this study, we analyzed the relation between effectiveness of CDC induction by therapeutic antibodies and antibody concentration, the level of target antigen expression, and expression of mCRPs CD55 and CD59 in B-ALL. We hypothesized that the down-modulating effect of mCRPs CD55 and CD59 on the level of CDC is co-dependent on the level of target antigen expression, with the most prominent effect in samples that display intermediate target antigen expression levels. Our results showed that full, simultaneous loss of CD55 and CD59 expression, due to glycophosphatidylinositol (GPI)-anchor deficiency, greatly enhanced the sensitivity to antibody-induced CDC of B-ALL cells with intermediate levels of target antigen expression. By retrovirally inducing increased CD55 or CD59 expression we showed that both mCRPs were individually able to convey protection against antibody-induced CDC and that this protection co-depended on antibody concentration and target antigen expression level. In contrast, we showed that natural variation in expression of these mCRPs could not be used as a single factor to predict sensitivity of B-ALL cells to CDC. In conclusion, sensitivity of B-ALL cells to antibody-induced CDC is dictated by antibody concentration and target antigen expression and is increased in cells displaying complete loss of mCRP expression.

MATERIAL AND METHODS

Patient samples and cell culture

After informed consent, mononuclear cells (MNC) isolated by Ficoll-Isopaque separation from bone marrow (BM) or peripheral blood (PB) taken for the purpose of diagnosis from patients with B-ALL were stored anonymously for future research by cryopreservation in Iscove's modified Dulbecco's media (IMDM, Lonza, Verviers, Belgium) supplemented with 25% fetal calf serum (FCS, Lonza) and 10% dimethyl sulfoxide (DMSO, Sigma-Aldrich, Zwijdrecht, the Netherlands). Before each experiment cells were thawed, washed twice with IMDM to remove DMSO, and maintained on ice in IMDM with 10% FCS. B-ALL cell lines used in this study were generated in our laboratory from primary B-ALL cells and maintained as described before[24] in an IMDM-based serum-free medium.

Immunofluorescence

Target antigen and mCRP expression was measured by staining samples with RTX (MabThera, Roche Diagnostics, Woerden, the Netherlands) or ALM (MabCampath, Sanofi Genzyme, Naarden, the Netherlands) conjugated to fluorescein isothiocyanate (FITC, Sigma-Aldrich) as described,[25]

or phycoerythrin (PE)-conjugated anti-CD55 (IA10, BD, Becton Dickinson, San Jose, CA, USA), or allophycocyanin (APC)-conjugated anti-CD59 (OV9A2, eBioscience, Vienna, Austria). Primary samples were additionally stained with PE or APC-conjugated anti-CD19 (HIB19, BD). GPI-anchor expression was analyzed by staining cells with Alexa Fluor 488 labeled inactivated toxin pro-aerolysin (FLAER, Sanbio, Uden, the Netherlands) and anti-CD52-APC (HI186, ITK diagnostics BV, Uithoorn, the Netherlands). Fluorescence was analyzed by flow cytometric analysis.

CDC-assay

$2.5x10^4$ B-ALL cells suspended in 40 µL medium were seeded per well in 96-well round bottom plates and incubated with serial dilutions of clinical grade monoclonal antibodies RTX, OFA (Arzerra, GlaxoSmithKline, Zeist, the Netherlands), or ALM in 10 µL PBS for 30 min at 4°C. Incubation with PBS only served as reference condition. Next, blood serum from healthy volunteers (normal human serum, NHS) was added at 50% (v/v) as a source of complement. Heat inactivated serum or medium were used as controls. After 4 h (primary B-ALL samples) or 18 h (B-ALL cell lines) incubation at 37°C and 5% CO_2, samples were stained with anti-CD19-APC for 30 min at 4°C followed by incubation with propidium iodide (PI, Millipore, Amsterdam-Zuidoost, the Netherlands) to exclude dead cells. Cells were kept on ice until analysis. Target cell death was determined using quantitative flow cytometry as described before.[26] Briefly, a fixed number (10,000) of CytoCount™ (DAKO, Glostrup, Denmark) or Accucount (Spherotech, Lake Forest, IL, USA) fluorescent beads was supplemented to each sample as an internal reference directly before sample acquisition. Per sample, 2000 beads were acquired. The number of viable cells (PI-negative, CD19-positive) per sample was calculated using the following formula:

$$\text{Total \# viable cells per sample} = \frac{\text{\# PI-negative, CD19-positive cells}}{\text{\# Beads}} * 10,000$$

The magnitude of cell loss (% CDC) was calculated using the formula:

$$\text{\% CDC} = \frac{\text{\# Cells reference condition} - \text{\# Cells experimental condition}}{\text{\# Cells reference condition}} * 100\%$$

Retroviral transduction of B-ALL cells with CD55 and CD59

B-ALL cell lines were stably transduced using retroviral particles encoding CD55 or CD59 as described before.[27,28] Briefly, CD55 and CD59[(ref. 29)] were individually subcloned into the bicistronic LZRS vector containing a truncated form of the nerve growth factor receptor (tNGFR), which served as marker gene.

Retroviral particles were generated using the φ-NX-A packaging cell line and supplemented to wells of a flat bottom non-tissue treated 96-well plate pre-coated with human fibronectin fragments (Retronectin, TaKaRa Biotec). 1.5×10^5 B-ALL cells were incubated per well for 24 h at 37°C, then transferred to tissue culture-treated plates and allowed to expand. Transduced cells were purified by magnetic activated cell sorting (MACS) based on marker gene expression using anti-tNGFR-APC (ME20.4, Sanbio, Uden, the Netherlands) and anti-APC MicroBeads (Miltenyi Biotec, Bergisch Gladbach, Germany), following manufacturer's instructions. Cells were kept in culture until used in CDC-assays.

RESULTS

Sensitivity to antibody-induced CDC is strongly influenced by target antigen expression levels

To test the effect of antigen expression on the sensitivity to CDC induced by the therapeutic antibodies RTX and OFA (targeting CD20), and ALM (targeting CD52), we used a panel of B-ALL cell lines (n = 11) that resemble the primary malignancy both in terms of phenotype and karyotype.[24] A wide distribution of antigen expression levels (median fluorescence intensity; MFI) was observed on these B-ALL cells by flow cytometry (range 44-5898 for CD20 and 100-2033 for CD52) (**Table 1**). Sensitivity to antibody-induced CDC was analyzed by incubating the B-ALL cells with concentrations of RTX, OFA, or ALM ranging from 3.3 μg/mL to 100 μg/mL, using NHS as a source of complement. Strong positive correlations were

Table 1. Cell lines characteristics, antigen and complement inhibitor expression

Cell line	CD20 (MFI)	CD52 (MFI)	CD55 (MFI)	CD59 (MFI)	Cytogenetic abnormalities#
Leiden-ALL-CM	5898	1912	405	4427	t(9;22)
Leiden-ALL-PH	2540	2033	344	4570	t(9;22)
Leiden-ALL-VG	845	633	203	3315	etv6-abl
Leiden-ALL-CR	718	180	387	4996	
Leiden-ALL-BV	704	659	247	2068	t(9;22)
Leiden-ALL-HP	367	760	522	3269	
Leiden-ALL-VB	143	564	304	2736	t(9;22)
Leiden-ALL-RL	103	236	248	3723	t(1;19)
Leiden-ALL-KW	68	174	242	1459	t(9;22)
Leiden-ALL-BL	47	538	191	1828	t(9;22)
Leiden-ALL-SK	44	100	587	3053	t(11;19)

Membrane expression of target antigens CD20 and CD52, and complement inhibitors CD55 and CD59 is displayed as average calculated from three independent measurements by flow cytometric analysis. MFI: median fluorescence intensity; #: Only typical are shown

found between the level of CDC induced by RTX (R = 0.93 or higher), OFA (R = 0.96 or higher), and ALM (R = 0.78 or higher) and target antigen expression in a non-linear regression analysis (**Figure 1**). No lysis was observed when antibody-coated cells were incubated with heat inactivated NHS (**Figure S1**), confirming the complement-dependence of lysis induction.
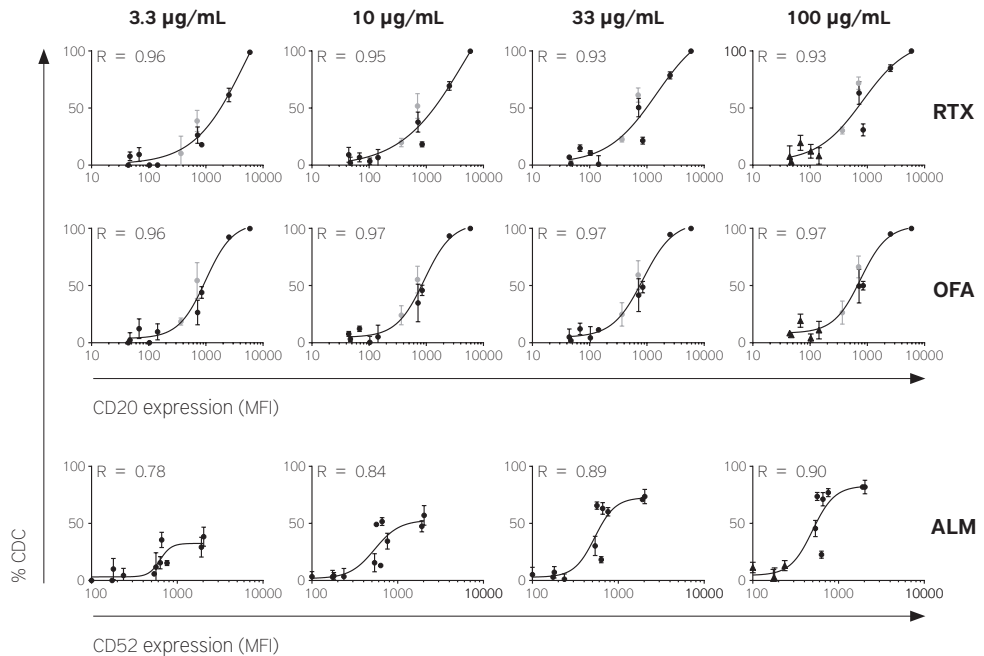
Figure 1. Effects of antibody concentration and the level of target antigen expression on sensitivity to antibody-induced CDC in B-ALL cells

Association between target antigen expression and CDC was analyzed by incubation of individual B-ALL cell lines (n = 11) with RTX, OFA, or ALM at indicated concentrations for 30 min at 4°C followed by addition of 50% NHS as a source of complement. After 18 h incubation at 37°C, the absolute number of surviving cells was measured using a quantitative flow cytometry-based cytotoxicity assay. Percentage CDC was determined by calculating the percentage cell loss compared to the reference condition without antibody. Each dot represents the average percentage of CDC induced in one cell line in three separate experiments and whiskers represent the standard deviation. Correlations between target antigen expression and the induced CDC percentage were calculated using a four parameter logistic regression analysis and are depicted by solid lines and the R-values are presented in the upper left corner of each graph. Cell lines Leiden-ALL-BV and Leiden-ALL-HP contained small populations of GPI-anchor negative cells (9.9% and 0.3%, respectively) and are highlighted in gray. Cell lines that were not prone to CDC induction despite the addition of saturating antibody concentrations (100 µg/mL) are indicated with triangels in the right panels.

Complete absence of mCRP expression increases the sensitivity to antibody-induced CDC

Since B-ALL cells with intermediate antigen density (MFI 250-1500) reached a maximum level of CDC below 100% despite saturating antibody concentrations (**Figure 1**, 100 µg/mL), we tested whether expression of mCRPs CD55 and CD59 affected the maximum level of lysis. Two B-ALL cell lines that displayed intermediate levels of antigen expression contained small populations of GPI-anchor negative cells as determined by FLAER staining (Leiden-ALL-BV 9.9%, Leiden-ALL-HP 0.3%; **Figure 1**, highlighted in gray). As a result, these cell populations lacked membrane expression of the GPI-anchored proteins CD55 and CD59. Purified GPI-anchor negative and GPI-anchor positive B-ALL subcultures were generated from Leiden-ALL-BV and Leiden-ALL-HP using flow cytometric cell sorting. Loss of CD55 and CD59 expression in the GPI-anchor negative cells was confirmed using flow cytometric analysis (**Figure 2A**). CD20 expression levels were identical between the GPI-anchor negative and GPI-anchor positive subcultures (**Figure 2B**). Sensitivity of these subcultures to antibody-induced CDC was evaluated by incubation with concentrations of RTX or OFA ranging between 3.3 µg/mL and 100 µg/mL. Considering that the CD52 antigen is also GPI-anchored and therefore not expressed on the GPI-anchor negative cells, ALM-induced CDC was not examined. Higher levels of antibody-induced CDC were observed in GPI-anchor negative B-ALL cells compared with their GPI-anchor positive counterparts, with up to 2.3 fold (Leiden-ALL-BV) and 6.3 fold (Leiden-ALL-HP) increase when induced by RTX and up to 1.7 fold (Leiden-ALL-BV) and 4.1 fold (Leiden-ALL-HP) increase when induced by OFA (**Figure 2C**). This resulted in almost complete eradication of GPI-anchor negative B-ALL cells.

Level of expression of either CD55 or CD59 can individually influence sensitivity to antibody-induced CDC

Since loss of GPI-anchor expression resulted in complete loss of both CD55 and CD59 expression, we next examined to which extent CD55 and CD59 individually contribute to a protective effect against CDC. Since it is impossible to induce re-expression of CD55 or CD59 in GPI-anchor negative cell lines, we selected several B-ALL cell lines with various target antigen expression levels from our B-ALL panel and transduced them with a construct encoding CD55 (Leiden-ALL-CM, Leiden-ALL-VG, Leiden-ALL-VB, Leiden-ALL-RL, Leiden-ALL-BL) or CD59 (Leiden-ALL-CM, Leiden-ALL-PH, Leiden-ALL-VG, Leiden-ALL-VB, Leiden-ALL-BL), or with empty vector (mock) as a control. Transduced cells were purified and expanded resulting in B-ALL subcultures with homogeneous expression of at least 3.3 fold increase for CD55 and at least 1.8 fold increase for CD59 compared to their mock transduced counterparts (**Figures 3A** and **4A**).
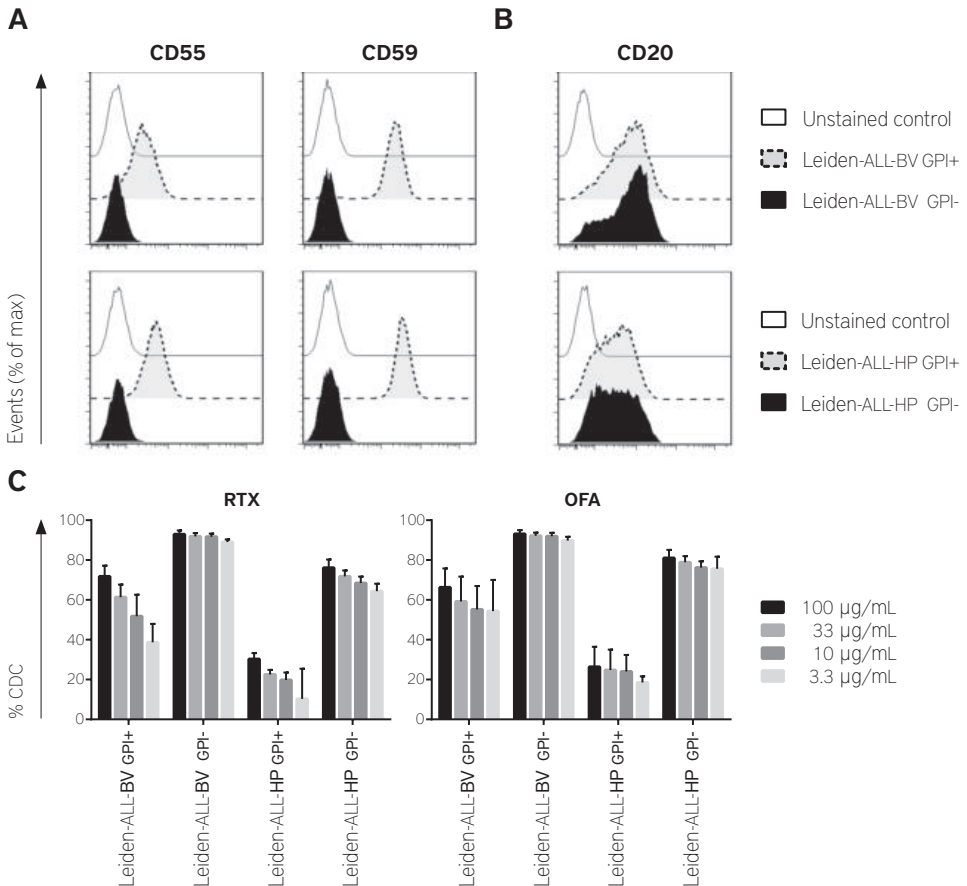
Figure 2. Complete absence of expression of mCRPs CD55 and CD59 due to GPI-anchor deficiency results in increased sensitivity to antibody-induced CDC
Representative example of CD55, CD59 **(A)**, and CD20 **(B)** expression patterns of GPI-anchor negative (black-filled curves) and GPI-anchor positive (gray-filed curve) subcultures of cell lines Leiden-ALL-BV and Leiden-ALL-HP as measured by flow cytometric analysis. Unstained cells were used as reference (open curves). **(C)** Sensitivity to antibody-induced CDC of GPI-anchor positive versus GPI-anchor negative subcultures of cell lines Leiden-ALL-BV and Leiden-ALL-HP. CDC was induced by RTX or OFA at 100 μg/mL, 33 μg/mL, 10 μg/mL, or 3.3 μg/mL and analyzed as described before. Bars represent average percentage of CDC induced in three separate experiments and whiskers represent the standard deviation.

To measure the effect of the induced CD55 and CD59 expression, CDC experiments were performed with RTX, OFA, or ALM at concentrations of 100 μg/mL, 10 μg/mL, and 1.0 μg/mL. In Leiden-ALL-CM, which displayed a high CD20 expression level, the protective effect of CD55 and CD59 transduction was only minimal when CDC was induced at high RTX or OFA concentrations (100 μg/mL), while at lower RTX and OFA concentrations (10 μg/mL and 1.0 μg/mL), CDC decreased by up to 25% and 16% upon CD55

transduction (**Figure 3B**) and 20% and 22% upon CD59 transduction (**Figure 4B**), respectively, compared with the mock transduced counterpart. In B-ALL cells with intermediate levels of CD20 expression (CD55 transduced: Leiden-ALL-VG, Leiden-ALL-RL, and Leiden-ALL-BL; CD59 transduced: Leiden-ALL-PH and Leiden-ALL-VG), levels of CDC were already substantially decreased when induced at high RTX or OFA antibody concentrations (100 μg/mL) with up to 48% and 34% decrease upon CD55 (**Figure 3B**) and 20% and 47% upon CD59 (**Figure 4B**) transduction, respectively. At lower RTX and OFA concentrations (10 μg/mL, 1.0 μg/mL), CDC was decreased up to 31% and 35% in CD55 (**Figure 3B**) and up to 13% and 49% in CD59 (**Figure 4B**) transduced B-ALL cells, respectively. When CDC was induced by ALM, again minimal effect of CD55 and CD59 transduction was observed in Leiden-ALL-CM, which displayed a high CD52 expression level, when CDC was induced at high antibody concentrations (100 μg/mL), while at lower ALM concentrations (10 μg/mL and 1.0 μg/mL) CDC decreased up to 30% upon CD55 (**Figure 3B**) and 27% upon CD59 transduction (**Figure 4B**). In Leiden-ALL-PH, which also displayed a high CD52 expression level, CDC was decreased by 34% when induced at high ALM concentrations (100 μg/mL)

Figure 3. Induction of increased CD55 expression increases the sensitivity to antibody-induced CDC of B-ALL cells **(A)** Bar graph depicts the fold increase in CD55 expression of 5 B-ALL cell lines retrovirally transduced with a construct encoding CD55 (CD55) relative to their empty vector (Mock) transduced controls. Fold increase was calculated using the mean CD55 MFI as determined from three separate flow cytometric analyses. **(B)** Sensitivity to antibody-CDC induced of Mock (gray) versus CD55 (black) transduced cell lines. CDC was induced as described before by RTX, OFA, or ALM at indicated concentrations. Bars represent the average percentage of CDC induced in three separate experiments and whiskers represent the standard deviation. The statistical significance is shown by asterisks, * P < 0.05; ** P < 0.01; *** P < 0.001 (one-sided paired T-test).
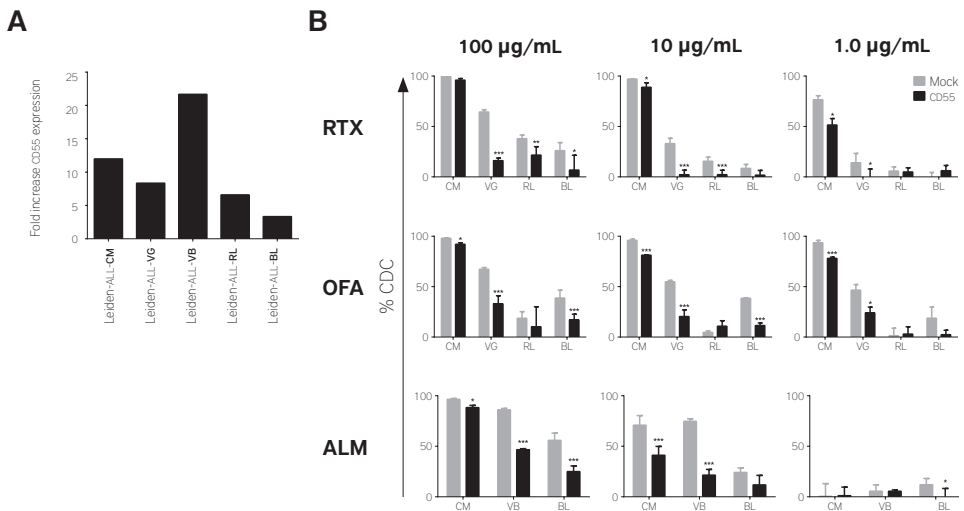
and by up to 52% at lower ALM concentrations (10 µg/mL and 1.0 µg/mL) upon CD59 transduction. In B-ALL cells with intermediate CD52 antigen expression levels (Leiden-ALL-VB and Leiden-ALL-BL), CDC induced at high ALM concentrations (100 µg/mL) decreased with up to 40% in CD55 (**Figure 3B**) and 23% in CD59 (**Figure 4B**) transduced B-ALL cells and when induced at lower ALM concentrations (10 µg/mL, 1.0 µg/mL) with up to 53% upon CD55 (**Figure 3B**) and up to 36% in CD59 (**Figure 4B**) upon transduction.

Together these data illustrate that induced CD55 and CD59 expression can individually supply a level of protection against antibody-induced CDC, especially in cells displaying intermediate target antigen expression levels. However, this protective effect was overpowered when CDC was induced at high antibody concentrations in B-ALL cells that display high target antigen expression levels. Furthermore, despite substantial increase of CD55 and CD59 expression upon transduction, complete abrogation of CDC induction was not accomplished. These results indicate that the protective effect of complement inhibitors is present but not dominant.

Figure 4. Induction of increased CD59 expression increases the sensitivity to antibody-induced CDC of B-ALL cells **(A)** Bar graph depicts the fold increase in CD59 expression of 5 B-ALL cell lines retrovirally transduced with a construct encoding CD59 (CD59) relative to their empty vector (Mock) transduced controls. Fold increase was calculated using the mean CD59 MFI as determined from three separate flow cytometric analyses. **(B)** Sensitivity to antibody-CDC induced of Mock (gray) versus CD59 (black) transduced cell lines. CDC was induced as described before by RTX, OFA, or ALM at indicated concentrations. Bars represent the average percentage of CDC induced in three separate experiments and whiskers represent the standard deviation. The statistical significance is shown by asterisks, * P < 0.05; ** P < 0.01; *** P < 0.001 (one-sided paired T-test).
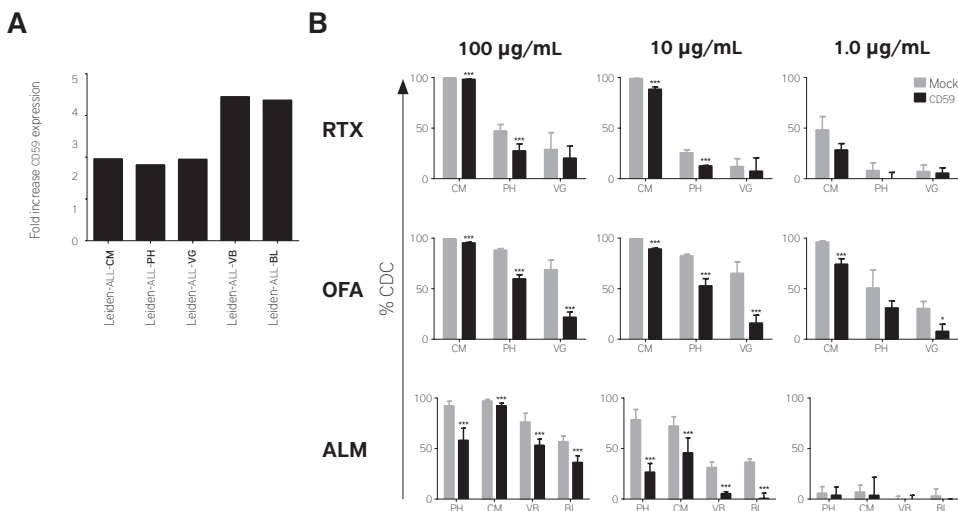
Natural variation of CD55 and CD59 expression cannot be used as a single marker to predict sensitivity of B-ALL cells to antibody-induced CDC

To assess whether natural variation in CD55 or CD59 expression can be used as a marker to predict the sensitivity of B-ALL cells to antibody-induced CDC, we analyzed their expression levels in our panel of B-ALL cell lines (**Table 1**). The level of expression within individual cell lines was homogeneous, but varied largely between cell lines (range MFI 191-587 for CD55 and 1459-4996 for CD59) and was always clearly positive. No correlation was found between the levels of CD55 (**Figure 5**, left panels) or CD59 (**Figure 5**, right panels) expression on B-ALL cell lines and their sensitivity to CDC induced by RTX, OFA, or ALM at 10 µg/mL. Identical results were obtained at higher (100 µg/mL) and lower (3.3 µg/mL) antibody concentrations (data not shown).

Next, we evaluated whether similar results would be obtained using primary B-ALL cells. For this, CD20, CD52, CD55 and CD59 expression levels were measured on CD19+ B-cells within MNC samples (n = 7) derived from B-ALL patients (**Table 2**). The CD20 antigen expression was too low to analyze RTX and OFA induced CDC. CD52 antigen expression was substantial and ranged from MFI 120 to 1662. Clear correlations were present between CD52 expression and ALM-induced CDC in a non-linear regression analysis (maximum R = 0.98, **Figure 6A**). In contrast, in accordance with the observations in the B-ALL cell lines, no correlations were found between levels of CD55 or CD59 expression and the level of ALM-induced CDC at 10 µg/mL (**Figure 6B**), or at 0.1 µg/mL, 1.0 µg/mL, or 100 µg/mL (data not shown).

Together these data show that the natural level of CD55 or CD59 expression on the B-ALL cells had no predictive value as single markers for the sensitivity of B-ALL cells to antibody-induced CDC.

Table 2. Primary sample characteristics, antigen and complement inhibitor expression

Sample	CD20 (MFI)	CD52 (MFI)	CD55 (MFI)	CD59 (MFI)	Source	% CD19+*
ALL-1	89	1662	416	2377	BM	90.8
ALL-2	87	1370	752	4486	PB	65.0
ALL-3	64	1406	1012	2122	BM	82.3
ALL-4	44	986	873	1850	BM	85.8
ALL-5	35	608	400	2393	PB	73.7
ALL-6	25	1230	230	590	BM	95.7
ALL-7	21	120	511	4505	BM	92.1

*Membrane expression of target antigens CD20 and CD52, and complement inhibitors CD55 and CD59 was measured on CD19+ cells within primary B-ALL patient samples by flow cytometric analysis; MFI: median fluorescence intensity; PB: peripheral blood; BM: bone marrow; *: percentage of CD19+ cells within the MNC samples*

A

B
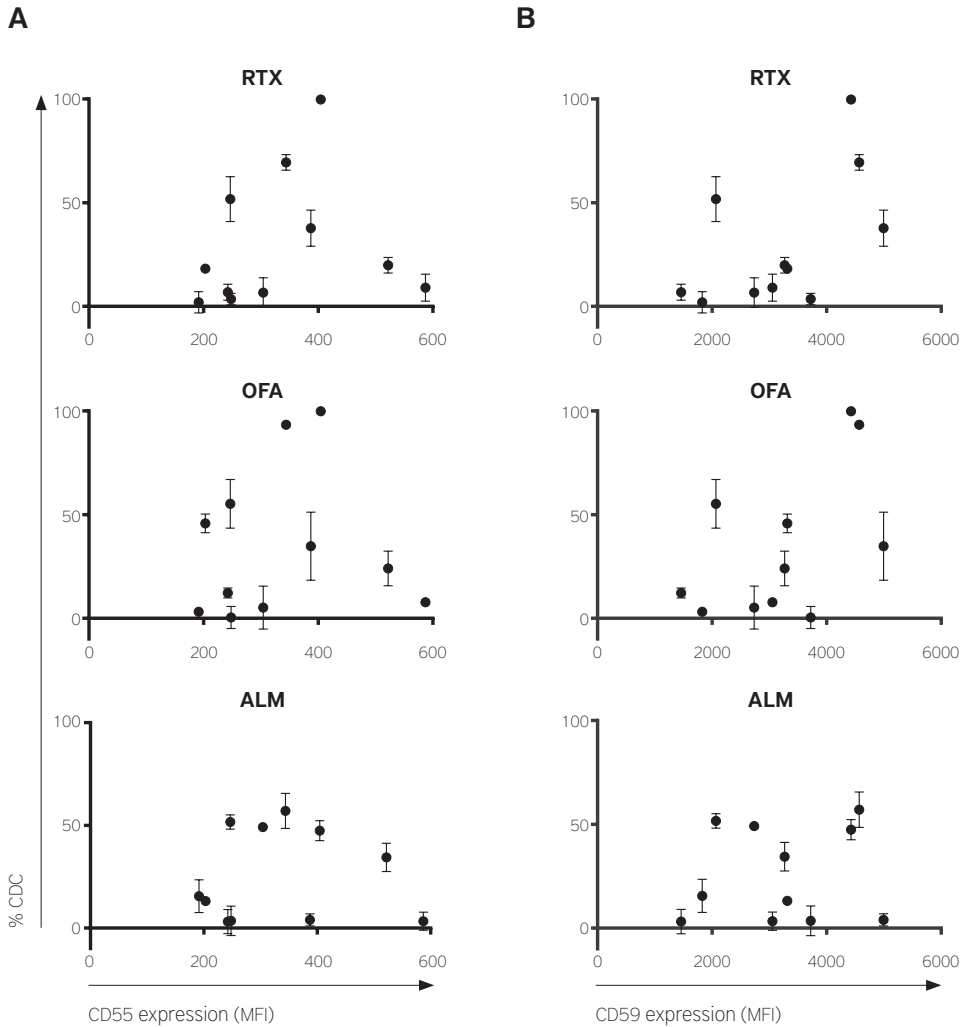
Figure 5. Relation between natural variation in the level of complement inhibitors CD55 and CD59 expression and sensitivity of B-ALL cells for antibody-induced CDC

CD55 (left panels) and CD59 (right panels) expression (MFI) as determined by flow cytometry is plotted against the level of CDC induced by RTX, OFA, or ALM at 10 µg/mL. Dots represent average percentage of CDC induced in three separate experiments and whiskers represent the standard deviation.
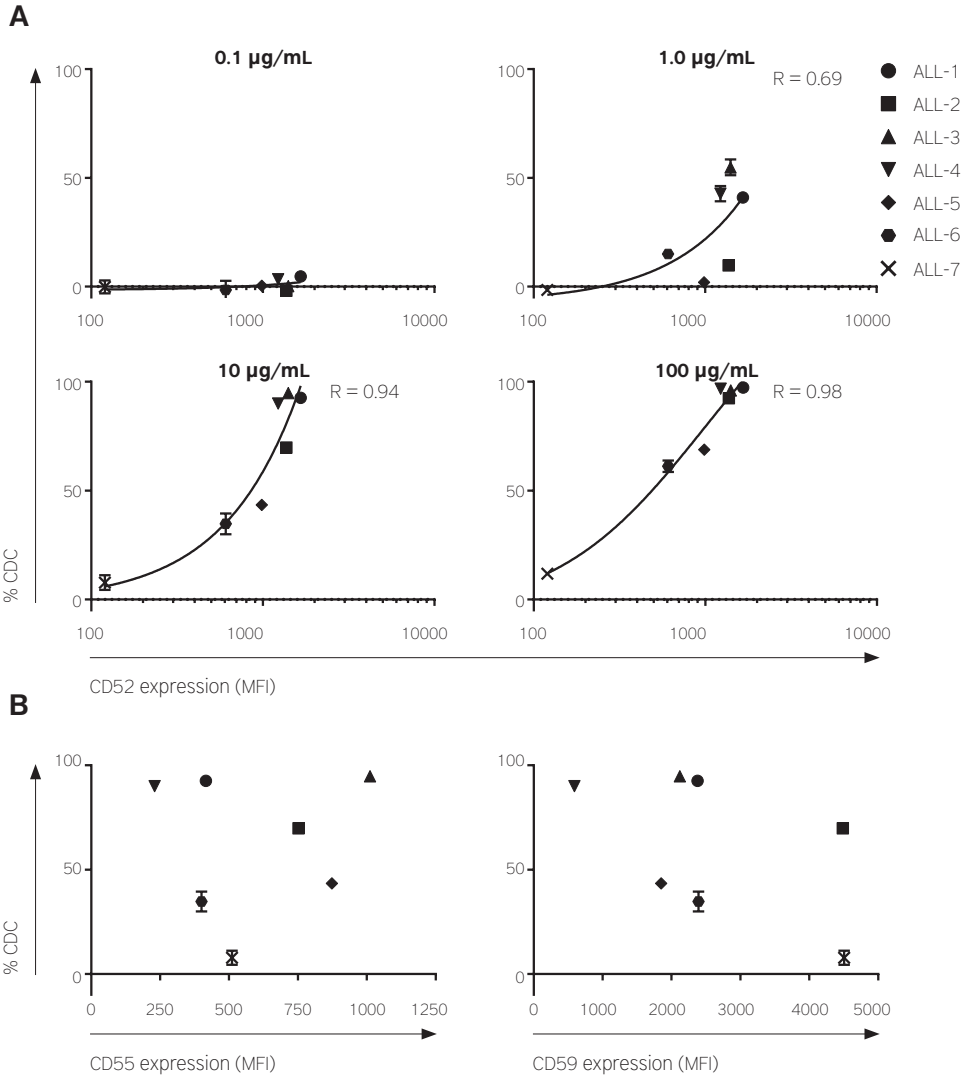
Figure 6. Relation between natural variation in the level of antigen expression or complement inhibitors CD55 or CD59 and sensitivity of primary malignant B-cells for antibody-induced CDC

(A) Association between CD52 target antigen expression and CDC was analyzed by incubation of primary B-ALL samples with ALM at indicated concentrations and 50% NHS. Each dot represents the average percentage of CDC per sample in a duplicate measurement and whiskers represent the range. The correlations between CD52 target antigen expression and the level of ALM-induced CDC were calculated using a three parameter logistic regression analysis and are depicted by solid lines and the R-values of these correlations are presented in the upper left corner of each graph. **(B)** Relation between complement inhibitor expression and sensitivity of primary B-ALL patient samples for ALM-induced CDC. CD55 (left panel) and CD59 (right panel) expression as determined by flow cytometry on primary B-ALL samples is plotted against the level of CDC induced by ALM at 10 µg/mL.

DISCUSSION

Recent advances in use of monoclonal therapeutic antibodies against B-ALL required a comprehensive analysis of the factors that determine the sensitivity of B-ALL cells to antibody-induced CDC. We investigated the role of antibody concentration, target antigen expression, and expression of mCRPs CD55 and CD59 on the sensitivity of B-ALL cells to CDC induced by RTX, OFA, and ALM in a panel of 11 cell lines generated from primary B-ALL cells and in primary B-ALL samples. Strong positive correlations were found between target antigen expression levels and the sensitivity to antibody-induced CDC. Manipulation of individual B-ALL cell lines allowed us to study to what extent mCRP expression affected the sensitivity of B-ALL cells to antibody-induced CDC at distinct target antigen expression levels. In B-ALL cells expressing intermediate levels of target antigen, the sensitivity to antibody-induced CDC was significantly increased upon simultaneous loss of CD55 and CD59 membrane expression which resulted from GPI-anchor deficiency. In accordance, induction of increased membrane expression of CD55 and CD59 individually by retroviral transduction decreased the sensitivity to antibody-induced CDC of the B-ALL cell lines, illustrating that both molecules were able to convey relative protection against antibody-induced CDC. The extent of the protective effect by mCRPs was co-dependent on target antigen expression and the concentration of the therapeutic antibody. Nonetheless, natural variation in CD55 and CD59 expression within our panel of B-ALL cell lines and within primary B-ALL samples could not be used as a single factor to predict the sensitivity of these cells to antibody-induced CDC, indicating that these mCRPs do not dominantly affect the sensitivity of B-ALL cells to CDC induced by therapeutic antibodies.

Since expression levels of CD20 and CD52 on malignant cells of different patients with B-ALL are highly variable,[6,19,30] we analyzed the relation between target antigen expression and sensitivity of B-ALL cells to CDC induced by CD20 or CD52 targeting therapeutic antibodies. We found strong correlations between higher levels of CD20 and CD52 antigen expression and higher levels of CDC induced by RTX and OFA, or ALM. This confirms results from several studies that suggested the presence of these correlations based on experiments using samples from patients with various B-cell malignancies.[19,31,32] However, in contrast with these studies, and analogous to what has been shown by van Meerten et al. in a study of RTX-induced CDC in T-cell clones with induced CD20 expression,[18] correlations in our model were defined by sigmoidal instead of linear functions. This type of correlation suggests a threshold of minimal target antigen expression required to initiate antibody-induced CDC. Indeed, we found that even at saturating antibody concentrations no substantial CDC was induced in the B-ALL cells displaying the

lowest levels of target antigen expression. Although we cannot exclude that in-vivo these cells might still be sensitive to other mechanisms such as ADCC or ADCP, which are reported to induce lysis even if target cells display low target antigen expression levels,[16,18] it may explain the disappointing outcome using these antibodies as single-agent treatment in patients with B-ALL, which is particularly characterized by low and heterogeneous target antigen expression within and between patients. Addition of antibody treatment to standard therapy may overcome this problem as malignant cells with low target antigen expression may still be sensitive to chemotherapeutics, resulting in additive or even synergistic effects.[33]

An alternative approach that may improve the effectiveness of antibody therapy is removing the brake for CDC induction by elimination of the protective effect of mCRPs. We showed that simultaneous loss of CD55 and CD59, which resulted from GPI-anchor deficiency, significantly increased the sensitivity of B-ALL cells to antibody-induced CDC. Several strategies have been developed aimed at eliminating the protective effect of mCRPs in-vitro, including pretreatment of target cells with specific mCRP blocking antibodies or with small interfering RNA (siRNA) aimed to decrease mCRP expression. Thus far, these strategies have shown only modest effects on the sensitivity of cells to antibody-induced CDC.[19,32,34] We hypothesized that this may in part result from the fact that these studies did not account for the effect of differential target antigen levels expressed by target cells. The relevance of this additional level of detail was demonstrated in experiments where we showed by artificially increasing expression of CD55 and CD59 on target cells that their protective effect against antibody-induced CDC was co-dependent on the level of target antigen expression. The most prominent protective effect was observed in B-ALL cells with intermediate target antigen expression levels, whereas only minimal effect was seen in B-ALL cells with high target antigen expression levels. Consequently, these results suggest that only malignant cells displaying intermediate levels of target antigen expression will be prone to the effect of mCRP targeting antibodies or siRNAs. In the clinical setting, this may imply that only a subpopulation of patients will benefit from implementing methods to eliminate the protective effect of mCRPs. This hypothesis may be tested by studying the clinical results from patients that received a combination of RTX and fludarabine, which showed a strong synergistic cytotoxic effect in FL and CLL cells likely resulting from fludarabine-induced down-regulation of CD55 expression,[35] and relate this to target antigen and mCRP expression.

Lack of effectiveness of strategies to eliminate the protective effect of complement inhibitors may also in part result from the inability of blocking antibodies and siRNAs to completely abrogate expression of CD55 and CD59.[34,36] We showed that relative variation in the naturally occurring levels expression of

CD55 and CD59 in B-ALL cells did not dominantly affect the sensitivity to antibody-induced CDC, unless they were completely absent as seen in the GPI-anchor deficient B-ALL cells.

In conclusion, our data showed that the concentration of the therapeutic antibody and the level of target antigen expression are the dominant factors determining the sensitivity to antibody-induced CDC in B-ALL cells. Expression of the mCRPs CD55 and CD59 was shown to affect antibody-induced CDC, but their level of expression could not be used as a single factor to predict the sensitivity of B-ALL cells to antibody-induced CDC.

3

REFERENCE LIST

1. Weiner LM, Surana R, Wang S. Monoclonal antibodies: versatile platforms for cancer immunotherapy. *Nat Rev Immunol*. 2010;10(5):317-327.

2. Tibes R, Keating MJ, Ferrajoli A, et al. Activity of alemtuzumab in patients with CD52-positive acute leukemia. *Cancer*. 2006;106(12):2645-2651.

3. Thomas DA, O'Brien S, Faderl S, et al. Chemoimmunotherapy with a modified hyper-CVAD and rituximab regimen improves outcome in de novo Philadelphia chromosome-negative precursor B-lineage acute lymphoblastic leukemia. *JCO*. 2010;28(24):3880-3889.

4. Sasaki K, Koller PB, Kantarjian HM, et al. Phase II Study of the Frontline Hyper-CVAD in Combination with Ofatumumab for Adult Patients (pts) with CD-20 Positive Acute Lymphoblastic Leukemia (ALL). *Blood*. 2015;126(23):1295-1295.

5. Maury S, Chevret S, Thomas X, et al. Rituximab in B-Lineage Adult Acute Lymphoblastic Leukemia. *N Engl J Med*. 2016;375(11):1044-1053.

6. Nijmeijer BA, van Schie M, Halkes C, Griffioen M, Willemze R, Falkenburg JHF. A mechanistic rationale for combining alemtuzumab and rituximab in the treatment of ALL. *Blood*. 2010;116(26):5930-5940.

7. Glennie MJ, French R, Cragg M, Taylor RP. Mechanisms of killing by anti-CD20 monoclonal antibodies. *Mol immunol*. 2007;44(16):3823-3837.

8. Zent CS, Chen J, Kurten R, Kaushal G, Lacy H, Schichman SA. Alemtuzumab (CAMPATH 1H) does not kill chronic lymphocytic leukemia cells in serum free medium. *Leuk Res*. 2004;28(5):495-507.

9. Seidel UJ, Schlegel P, Lang P. Natural killer cell mediated antibody-dependent cellular cytotoxicity in tumor immunotherapy with therapeutic antibodies. *Front Immunol*. 2013;4(76).

10. Di Gaetano N, Cittera E, Nota R, et al. Complement activation determines the therapeutic activity of rituximab in vivo. *J Immunol*. 2003;171(3):1581-1587.

11. Cragg MS, Glennie MJ. Antibody specificity controls in vivo effector mechanisms of anti-CD20 reagents. *Blood*. 2004;103(7):2738-2743.

12. Winkler U, Jensen M, Manzke O, Schulz H, Diehl V, Engert A. Cytokine-release syndrome in patients with B-cell chronic lymphocytic leukemia and high lymphocyte counts after treatment with an anti-CD20 monoclonal antibody (rituximab, IDEC-C2B8). *Blood*. 1999;94(7):2217-2224.

13. Kennedy AD, Beum P, Solga M, et al. Rituximab infusion promotes rapid complement depletion and acute CD20 loss in chronic lymphocytic leukemia. *J Immunol*. 2004;172(5):3280-3288.

14. Beurskens FJ, Lindorfer M, Farooqui M, et al. Exhaustion of cytotoxic effector systems may limit monoclonal antibody-based immunotherapy in cancer patients. *J Immunol*. 2012;188(7):3532-3541.

15. Racila E, Link B, Weng W, et al. A polymorphism in the complement component C1qA correlates with

prolonged response following rituximab therapy of follicular lymphoma. *Clin Cancer Res*. 2008;14(20):6697-6703.

16. Manches O, Lui G, Chaperot L, et al. In vitro mechanisms of action of rituximab on primary non-Hodgkin lymphomas. *Blood*. 2003;101(3):949-954.

17. Ratzinger G, Reagan J, Heller G, Busam K, Young J. Differential CD52 expression by distinct myeloid dendritic cell subsets: implications for alemtuzumab activity at the level of antigen presentation in allogeneic graft-host interactions in transplantation. *Blood*. 2003;101(4):1422-1429.

18. van Meerten T, van Rijn R, Hol S, Hagenbeek A, Ebeling S. Complement-induced cell death by rituximab depends on CD20 expression level and acts complementary to antibody-dependent cellular cytotoxicity. *Clin Cancer Res*. 2006;12(13):4027-4035.

19. Golay J, Cortiana C, Manganini M, et al. The sensitivity of acute lymphoblastic leukemia cells carrying the t(12;21) translocation to campath-1H-mediated cell lysis. *Haematologica*. 2006;91(3):322-330.

20. Gao LJ, Ding L, Guo S, et al. Role of decay-accelerating factor in regulating survival of human cervical cancer cells. *J Cancer Res Clin Oncol*. 2011;137(1):81-87.

21. Golay J, Zaffaroni L, Vaccari T, et al. Biologic response of B lymphoma cells to anti-CD20 monoclonal antibody rituximab in vitro: CD55 and CD59 regulate complement-mediated cell lysis. *Blood*. 2000;95(12):3900-3908.

22. Hu W, Ge X, You T, et al. Human CD59 inhibitor sensitizes rituximab-resistant lymphoma cells to complement-mediated cytolysis. *Cancer Res*. 2011;71(6):2298-2307.

23. Macor P, Tripodo C, Zorzet S, et al. In vivo targeting of human neutralizing antibodies against CD55 and CD59 to lymphoma cells increases the antitumor activity of rituximab. *Cancer Res*. 2007;67(21):10556-10563.

24. Nijmeijer B, Szuhai K, Goselink H, et al. Long-term culture of primary human lymphoblastic leukemia cells in the absence of serum or hematopoietic growth factors. *Exp Hematol*. 2009;37(3):376-385.

25. The T, Feltkamp TE. Conjugation of fluorescein isothiocyanate to antibodies. I. Experiments on the conditions of conjugation. *Immunology*. 1970;18(6):865-873.

26. Jedema I, van der Werff N, Barge R, Willemze R, Falkenburg JH. New CFSE-based assay to determine susceptibility to lysis by cytotoxic T cells of leukemic precursor cells within a heterogeneous target cell population. *Blood*. 2004;103(7):2677-2682.

27. Heemskerk MH, Hoogeboom M, de Paus R, et al. Redirection of antileukemic reactivity of peripheral T lymphocytes using gene transfer of minor histocompatibility antigen HA-2-specific T-cell receptor complexes expressing a conserved alpha joining region. *Blood*. 2003;102(10):3530-3540.

28. Alford SE, Kothari A, Loeff FC, et al. BH3 Inhibitor Sensitivity and Bcl-2 Dependence in Primary Acute Lymphoblastic Leukemia Cells. *Cancer Res*. 2015;75(7):1366-1375.

29. Charreau B, Cassard A, Tesson L, et al. Protection of rat endothelial cells from primate complement-mediated lysis by expression of human CD59 and/or decay-accelerating factor. *Transplantation*. 1994;58(11):1222-1229.

3

30. Thomas DA, O'Brien S, Jorgensen J, et al. Prognostic significance of CD20 expression in adults with de novo precursor B-lineage acute lymphoblastic leukemia. *Blood*. 2009;113(25):6330-6337.

31. Bellosillo B, Villamor N, Lopez-Guillermo A, et al. Complement-mediated cell death induced by rituximab in B-cell lymphoproliferative disorders is mediated in vitro by a caspase-independent mechanism involving the generation of reactive oxygen species. *Blood*. 2001;98(9):2771-2777.

32. Golay J, Lazzari M, Facchinetti V, et al. CD20 levels determine the in vitro susceptibility to rituximab and complement of B-cell chronic lymphocytic leukemia: further regulation by CD55 and CD59. *Blood*. 2001;98(12):3383-3389.

33. Bologna L, Gotti E, Da RF, et al. Ofatumumab is more efficient than rituximab in lysing B chronic lymphocytic leukemia cells in whole blood and in combination with chemotherapy. *J Immunol*. 2013;190(1):231-239.

34. Mamidi S, Hone S, Teufel C, Sellner L, Zenz T, Kirschfink M. Neutralization of membrane complement regulators improves complement-dependent effector functions of therapeutic anticancer antibodies targeting leukemic cells. *Oncoimmunology*. 2015;4(3):e979688.

35. Di Gaetano N, Xiao Y, Erba E, et al. Synergism between fludarabine and rituximab revealed in a follicular lymphoma cell line resistant to the cytotoxic activity of either drug alone. *Br J Haematol*. 2001;114(4):800-809.

36. Coyne KE, Hall SE, Thompson S, et al. Mapping of epitopes, glycosylation sites, and complement regulatory domains in human decay accelerating factor. *J Immunol*. 1992;149(9):2906-2913.

SUPPLEMENTAL DATA
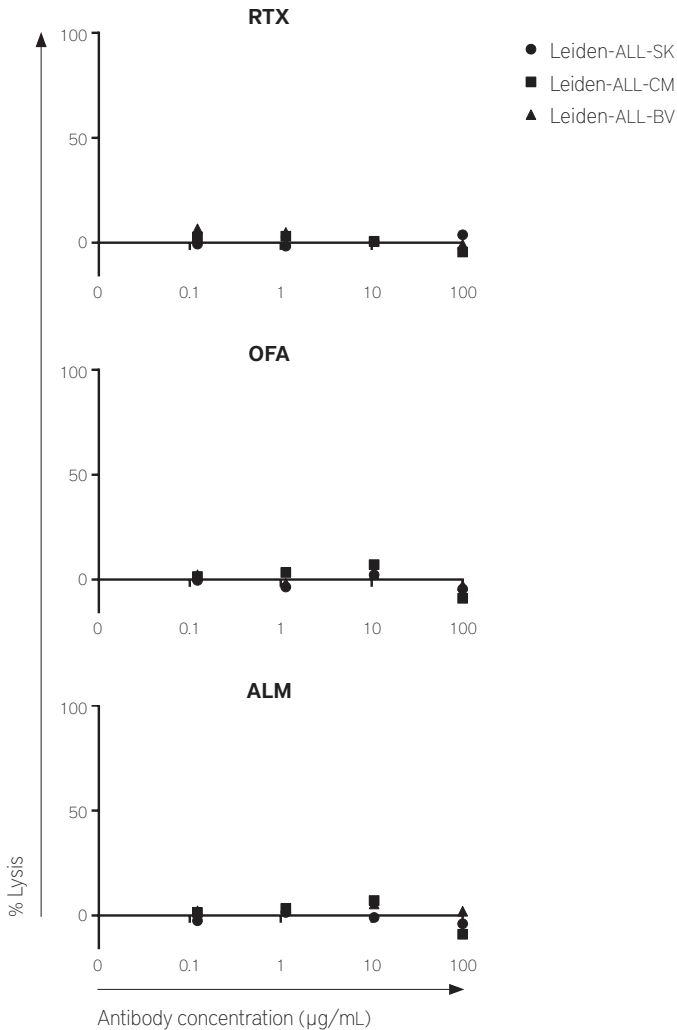
Figure S1. No antibody induced lysis in B-ALL cell lines when incubated with heat inactivated NHS
Relation between antibody concentration and lysis induced by heat inactivated NHS. Lysis was induced by incubation of cell lines Leiden-ALL-CM, Leiden-ALL-BV, and Leiden-ALL-SK with serial dilutions of RTX, OFA, or ALM for 30 min at 4°C followed by addition of 50% heat inactivated NHS. After 18 h incubation at 37°C, the absolute number of surviving cells was measured using a quantitative flow cytometry-based cytotoxicity assay. Percentage lysis was determined by calculating the percentage cell loss compared to reference conditions without antibody. Each dot represents the average lysis from three separate experiments and whiskers represent the standard deviation.

Floris C. Loeff[1]

J.H. Frederik Falkenburg[1]

Lois Hageman[1]

Wesley Huisman[1,2]

Sabrina A.J. Veld[1]

H.M. Esther van Egmond[1]

Marian van de Meent[1]

Peter A. von dem Borne[1]

Hendrik Veelken[1]

Constantijn J.M. Halkes[1]*

Inge Jedema[1]*

CHAPTER 4

High mutation frequency of the *PIGA* gene in T cells results in reconstitution of GPI-anchor/CD52-negative T cells that can give early immune protection after alemtuzumab-based T-cell depleted allogeneic stem cell transplantation

[1] Department of Hematology - Leiden University Medical Center - Leiden - the Netherlands
[2] Department of Hematopoiesis - Sanquin Research - Amsterdam - the Netherlands
* C.J.H. and I.J. share senior authorship

ABSTRACT

Alemtuzumab (ALM) is used for T-cell depletion in the context of allogeneic hematopoietic stem cell transplantation (alloSCT) to prevent acute graft versus host disease and graft rejection. Following ALM-based T-cell depleted alloSCT, relatively rapid recovery of circulating T cells has been described, including T cells that lack membrane expression of the glycophosphatidylinositol (GPI)-anchored ALM target antigen CD52. We show in a cohort of 89 human recipients of an ALM-based T-cell depleted alloSCT graft that early lymphocyte reconstitution always coincided with the presence of large populations of T cells lacking CD52 membrane expression. In contrast, loss of CD52 expression was not overt within B cells or NK cells. We show that loss of CD52 expression from the T-cell membrane resulted from loss of GPI-anchor expression caused by a highly polyclonal mutational landscape in the *PIGA* gene. This polyclonal mutational landscape in the *PIGA* gene was also found in CD52-negative T cells present at a low frequency in peripheral blood of healthy donors. Finally, we demonstrate that the GPI/CD52-negative T-cell populations that arise after ALM-based T-cell depleted alloSCT contain functional T cells directed against multiple viral targets that can play an important role in immune protection early after ALM-based T-cell depleted transplantation.

INTRODUCTION

Allogeneic hematopoietic stem cell transplantation (alloSCT) is being used in the treatment of patients with a variety of malignant and non-malignant hematological diseases. The goal of alloSCT is to replace a patient's hematopoiesis (including the malignancy) with cells derived from a healthy donor by administration of a hematopoietic stem cell graft. T cells derived from patient and donor play a major role in the effectiveness and toxicity of this treatment. Although recognition of residual malignant cells by donor T cells can induce a therapeutic graft-versus-tumor effect (GvT),[1] recognition of non-hematopoietic healthy tissue by these donor T cells can result in detrimental graft-versus-host disease (GvHD).[2,3] In contrast, recognition of donor hematopoiesis by residual patient T cells may induce graft rejection. Depletion strategies for patient and donor T cells before transplantation, have been developed to reduce the risk for graft rejection and GvHD. Postponed application of donor lymphocyte infusions is used to induce therapeutic GvT and conversion to full donor chimerism.[4,5]

Alemtuzumab (ALM, Campath-1H), a humanized therapeutic IgG1 antibody, has been successfully used for in vivo and in-vitro T-cell depletion in the alloSCT setting for several decades.[6,7] ALM targets the glycophosphatidylinositol (GPI)-anchored protein CD52 that is expressed on all mature lymphocytes, but not (or only marginally) on hematopoietic stem cells.[8] Although ALM induces profound depletion of lymphocytes, relatively rapid recovery of circulating T cells can be observed after ALM-based in-vitro T-cell depleted alloSCT. Moreover, reconstitution of populations of T cells completely lacking CD52 membrane expression has been described.[9,10] The mechanism underlying this lack of CD52 expression and the effect on the functionality of these T cells are not known.

The aims of this study were to comprehensively analyze to what extent CD52-negative lymphocytes contribute to early lymphocyte reconstitution in recipients of an ALM-based T-cell depleted alloSCT and to unravel the mechanism underlying the loss of CD52 membrane expression. We show in a cohort of 89 patients with hematological diseases treated with an ALM-based T-cell depleted alloSCT that reconstitution of CD52-negative cells is common within the CD4 and the CD8 T-cell compartments, but not within the B-cell and NK-cell compartments. We demonstrate that loss of CD52 expression from the membrane of these cells did not result from loss of *CD52* gene expression, but, instead, from loss of GPI-anchor expression. In turn, loss of GPI-anchor expression resulted from a highly polyclonal mutational landscape in the *PIGA* gene, one of the genes essential for GPI-anchor biosynthesis. We show

that GPI/CD52-negative *PIGA* mutant T cells are also present at low frequencies in peripheral blood (PB) of healthy donors. Finally, we show that GPI/CD52-negative T-cell populations contain functional T cells specific against multiple viral targets that can contribute to early immune protection after alloSCT.

MATERIAL AND METHODS

Patient and samples

A consecutive cohort of 89 adult patients who underwent alloSCT with ALM-based T-cell depleted grafts at Leiden University Medical Center was included in this retrospective study. Study protocols were approved by the Leiden University Medical Center Research Ethics Committee, and patients had given informed consent for treatment and scientific evaluation. Patients received a myeloablative (MA) or a non-myeloablative (NMA) conditioning regimen (**Table S1**). MA conditioning consisted of cyclophosphamide combined with total body irradiation or i.v. busulfan. In the case of an unrelated donor (UD), patients received 15 mg of ALM (MabCampath, Sanofi Genzyme, Naarden, the Netherlands) i.v. at days -6 and -5. NMA conditioning consisted of 15 mg of ALM i.v. at days -4 and -3, fludarabine, and i.v. busulfan. Nine NMA-conditioned patients with a UD also received antithymocyte globulin (thymoglobulin, 1 or 2 mg/kg at day -2, **Table S1**). Patients received an allogeneic G-CSF-mobilized peripheral stem cell graft (n = 86) or a bone marrow graft (n = 3). All grafts were subjected to T-cell depletion by the addition of 20 mg of ALM "to the bag".[11] Cyclosporin, as posttransplantation immune suppression, was only given to MA-conditioned patients with a UD, starting at day -1 and tapered off from day 30 onward. PB was collected for direct routine clinical evaluation, and PB mononuclear cells (PBMC) were isolated by Ficoll-isopaque separation and cryopreserved for later scientific evaluation.

CD52 and GPI-anchor expression analysis

PBMC were thawed, and CD52 membrane expression was analyzed on CD4 and CD8 T cells (gating on CD3+CD4+ or CD3+CD8+ cells, respectively), NK cells (gating on CD3-CD56+ cells), and B cells (gating on CD3-CD19+ cells) by counterstaining with ALM conjugated to fluorescein isothiocyanate (FITC, Sigma-Aldrich, Zwijndrecht, the Netherlands), as described previously,[12] combined with allophycocyanin (APC)-conjugated anti-CD3, phycoerythrin (PE)-conjugated anti-CD4, and peridinin chlorophyll (PerCP)- or pacific blue (PacBlue)-conjugated anti-CD8 or anti-CD3-APC, anti-CD8-PerCP, and anti-CD56-PE or anti-CD3-PerCP and anti-CD19-APC antibodies (BD, Becton Dickinson, Breda, the Netherlands).

GPI-anchor expression was analyzed on CD4 and CD8 T cells (gating on CD3+CD4+ or CD3+CD4+ cells, respectively) by staining with the GPI-anchor specific inactivated toxin proaerolysin coupled to Alexa Fluor 488 (FLAER-AF488; Sanbio, Uden, the Netherlands), anti-CD3-PE-Texas Red (PETxR; Invitrogen, Thermo Fisher Scientific, Bleiswijk, the Netherlands), anti-CD4-PerCP (BD), anti-CD8-PacBlue (BD), and anti-CD52-APC (HI186; ITK diagnostics BV, Uithoorn, the Netherlands). Fluorescence was measured by flow cytometry on a FACSCalibur or LSRII analyzer (both from BD).

Analysis of absolute numbers of circulating cells

Absolute numbers of circulating CD4 T cells (gating on CD45+CD3+CD4+ cells), CD8 T cells (gating on CD45+CD3+CD8+ cells), B cells (gating on CD45+CD3-CD19+ cells), and NK cells (gating on CD45+CD3-CD16/CD56+ cells) were determined as part of routine clinical evaluations on fresh venous blood using BD Trucount tubes, following the manufacturer's instructions. Samples were stained with anti-CD3-APC, anti-CD4-FITC, anti-CD8-PE, and anti-CD45-PerCP, or with anti-CD3-FITC, anti-CD16-PE, anti-CD19-APC, anti-CD45-PerCP, and anti-CD56-PE (BD). Fluorescence was measured on a FACSCalibur.

Chimerism analysis

Donor-patient chimerism analysis was performed on FACS-purified CD4 and CD8 T cells using a short tandem repeat PCR-based protocol, as described previously.[13]

CD52 and GPI-anchor synthesis pathway gene expression analysis

GPI/CD52-negative and GPI/CD52-positive CD4 and CD8 T-cell populations were purified from thawed PBMC using FACS after staining with FLAER-AF488, anti-CD3-PETxR, anti-CD8-PacBlue, anti-CD4-PerCP, and anti-CD52-APC. mRNA was isolated from 2.5×10^4 cells using an RNAqueous-Micro Total RNA Isolation Kit (Thermo Fisher Scientific) and completely converted to cDNA using Moloney murine leukemia virus reverse transcriptase (Invitrogen) and oligo-dT primers. *CD52* mRNA was amplified by PCR using specific primers (**Table S2**) and Phusion Flash High-Fidelity PCR Master Mix (Thermo Fisher Scientific). As a control *GAPDH* was amplified. mRNA coding for the 28 GPI-anchor synthesis pathway genes was amplified by individual PCRs using specific primers (**Table S2**) and Pwo SuperYield DNA Polymerase (Roche, Woerden, the Netherlands). Resulting products were analyzed by gel electrophoresis.

Isolation and culture of T-cell clones

GPI/CD52-negative and GPI/CD52-positive CD4 and CD8 T-cell clones were generated by single-cell FACS from thawed PBMC collected at 3 months after transplantation. PBMC were stained with FLAER-AF488, anti-CD4-PacBlue, anti-CD8-PacBlue, anti-CD45-PerCP, and anti-CD52-APC. Isolated T cells were stimulated with irradiated PBMC as feeder cells, phytohaemagglutinin, and IL-2, as described.[14] Proliferating T-cell clones were restimulated every 14 days. The phenotype of individual clones was analyzed by staining with FLAER-AF488, anti-CD4-PE, anti-CD8-PerCP, and anti-CD52-APC.

GPI/CD52-negative T cells from a healthy donor were pre-enriched by MACS before single-cell FACS. T cells were isolated from 100×10^6 PBMC using a MACS Pan T Cell Isolation Kit (Miltenyi Biotec, Bergisch Gladbach, Germany). Subsequently, CD52-positive cells were depleted by MACS using anti-CD52-APC and anti-APC Microbeads (Miltenyi), following the manufacturer's instructions.

PIGA mutational analysis

mRNA was isolated from 5×10^5 cells from each T-cell clone and converted to cDNA as described. *PIGA* mRNA was amplified using primer set 1 (**Table S2**) and Phusion Flash High-Fidelity PCR Master Mix. The resulting product was directly cleaned using the Wizard SV Gel and PCR Clean-Up System (Promega, Leiden, the Netherlands). Nested PCRs were performed using primer sets 2a and 2b (**Table S2**) for which the forward or reverse primer nested in the terminal region of exon 2, thereby amplifying only *PIGA* transcription variant 1 (NM_002641.3). The resulting products were directly cleaned and analyzed by Sanger sequencing using the four primers from sets 2a and 2b.

Retroviral transduction

A construct encoding wild-type (wt)*PIGA* coupled via a GSG linker and a self-cleaving T2A peptide sequence to a truncated form of the nerve growth factor receptor (t*NGFR*), which served as a marker gene, was cloned into the LZRS plasmid. As control (mock), wt*PIGA* was removed from the plasmid by restriction enzyme digestion, followed by religation. Retroviral transduction was performed as described previously.[15] In brief, for each T-cell clone 2.5×10^4 cells were restimulated. After 3 or 4 days, T-cell clones were transferred to wells containing retroviral particles, generated using the φ-NX-A packaging cell line, and incubated for 24 h at 37°C. T-cell clones were subsequently transferred to new plates and expanded for 7 days before analysis by flow cytometry, counterstaining with FLAER-AF488, anti-CD52-APC, anti-CD3-PETxR, and anti-NGFR-PE (BD).

Functional analysis

Virus antigen-specific T-cell populations were identified, using flow cytometry, by staining with PE-conjugated peptide/MHC complexes [16] (tetramers) (**Table S3**), for 15 min at 37°C, followed by counterstaining with anti-CD8-PerCP for 15 min at 4°C. Tetramer-positive CD8 T cells were isolated by FACS and expanded as described for the T-cell clones. After 2 weeks, reactivity of isolated T cells was assessed. A total of 4×10^3 (HLA-B*08:01/CMV-IE1-QIKVRVDMV) or 5×10^3 (HLA-B*35:01/CMV-pp65-IPSINVHHY, HLA-A*02:01/CMV-IE1-VLEETSVML, and HLA-B*08:01/EBV-BZLF1-RAKFKQLL) virus antigen-specific T cells was cocultured for 24 h at 37°C with Epstein-Barr virus-transformed lymphoblastoid cells (EBV-LCLs) (E:T ratio of 1:5) exogenously loaded with a serial dilution (10 pM to 1 μM) of the relevant peptide. IFN-γ secretion was analyzed in the supernatant by ELISA (PeliKine compact human IFN-γ; Sanquin, Amsterdam, the Netherlands), following the manufacturer's instructions.

4

RESULTS

Reconstitution of CD52-negative T cells after ALM-based T-cell depleted alloSCT is a common phenomenon

To evaluate whether reconstitution of CD52-negative lymphocytes is a common phenomenon after ALM-based T-cell depleted alloSCT, we retrospectively analyzed PBMC samples taken from 89 alloSCT recipients at a median of 42 days after transplantation (range 35 - 98 days). CD52 expression on CD4 and CD8 T cells, B cells, and NK cells was determined by multicolor flow cytometry (results are summarized in **Table S1**). CD52-negative T cells were found in all recipients that displayed T-cell reconstitution and accounted for a median of 81% of circulating CD4 T cells (range 0.0 - 98.2%) and for a median of 32% of circulating CD8 T cells (range 0.0 - 97.5%). In contrast, CD52-negative B cells were not common, with populations observed in only three recipients (5.7, 7.7, and 88.2% of the circulating B cells). Within NK cells, no CD52-negative cell populations were detected in 59 recipients, whereas in the remaining 30 recipients, potential CD52-negative NK cells could not be discriminated from the bulk of cells that displayed low CD52 expression. Combining these results with the absolute number of circulating lymphocytes, which was determined for individual lymphocyte subsets as part of routine clinical evaluation at the same time point (**Table S1**), showed that sizeable populations of CD52-negative CD4 T cells (median 65.5×10^6 cells/L, range $0.0 \times 10^6 - 608.8 \times 10^6$ cells/L, **Figure 1A**) and CD52-negative CD8 T cells (median 6.1×10^6 cells/L, range $0.0 \times 10^6 - 1718.9 \times 10^6$ cells/L, **Figure 1B**) were present within recipients early after ALM-based T-cell depleted alloSCT. These CD52-negative T cells remained detectable in some patients years after transplantation (data not shown).

These data show that CD52-negative T cells form a mayor contribution to T-cell reconstitution after ALM-based T-cell depleted alloSCT.

Reconstituted CD52-negative T cells are primarily of donor origin

Because donor cells (20 mg of ALM "to the bag" containing the stem cell graft) and patient cells (by ALM in the conditioning and/or residual ALM infused with the graft) are exposed to ALM, we investigated whether CD52-negative T cells found in recipients after alloSCT were of donor or patient hematopoietic origin. Donor-patient chimerism analysis was performed on purified CD4 (n = 52) and CD8 (n = 46) T-cell subsets derived from 53 of the 89 patients (for whom sufficient sample was available) and plotted against the percentages of CD52-negative T cells present in these respective subsets (**Figure 2**). In
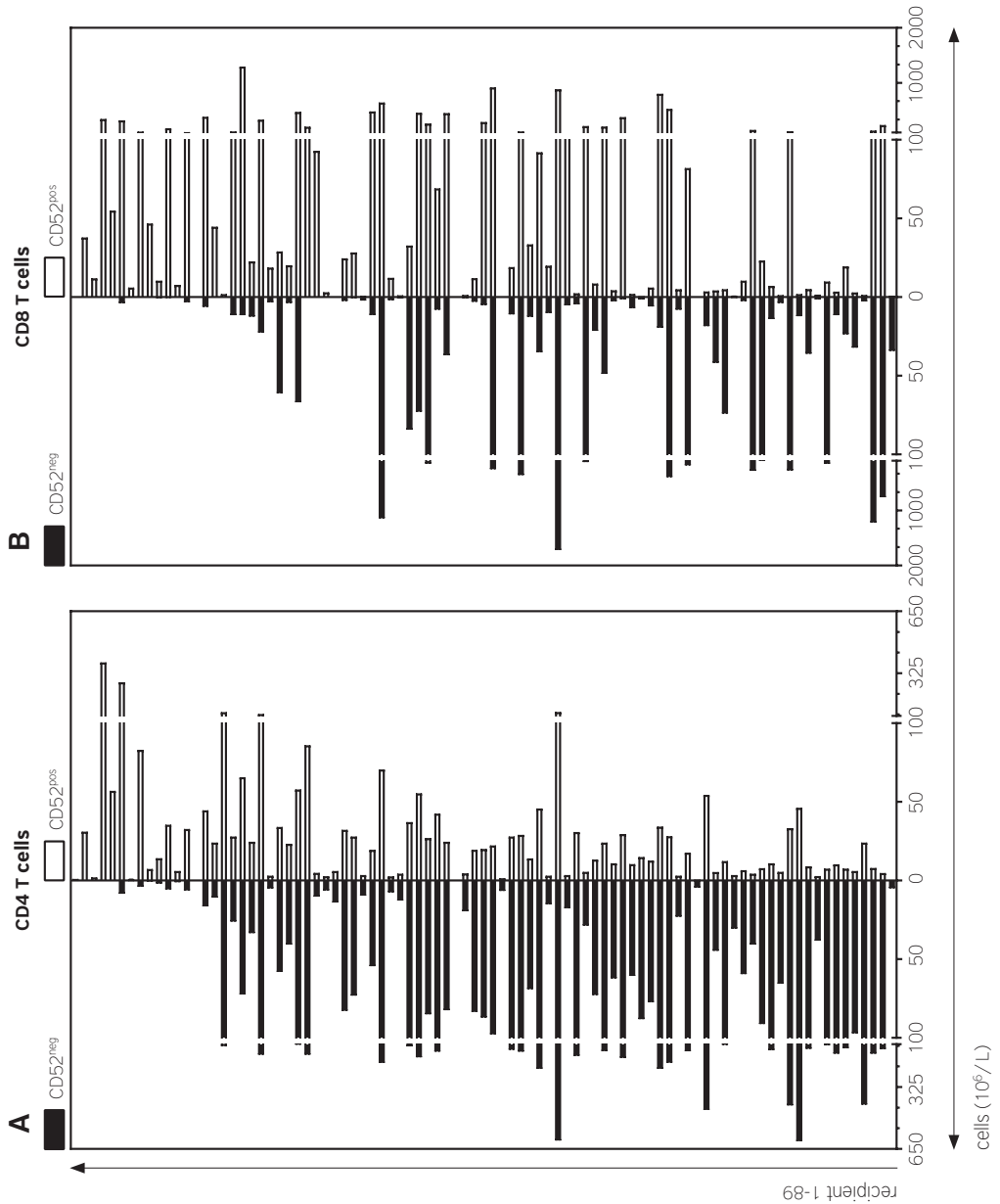
Figure 1. Presence of CD52-negative T-cell populations in alloSCT recipients early after transplantation

Absolute numbers of circulating CD52-negative (filled bars) and CD52-positive (open bars) within the CD4 **(A)** and CD8 **(B)** T-cell compartment were calculated for 89 alloSCT recipients by multiplying the absolute T cell counts, which were obtained for routine transplantation monitoring, with the portion of CD52-negative cells determined by flow cytometry on cryopreserved PBMC samples obtained from recipients at the same day. Results from individual recipients are arranged horizontally. Recipients were ordered based on the percentage of GPI-anchor negative cells within the CD4 T-cell compartment (**Table S1**).

general, for each recipient equal or higher percentages of donor chimerism were found compared with the percentages of CD52-negative T cells within the CD4 and CD8 T cell subsets, indicating a marked contribution of donor T cells to the observed CD52-negative T-cell populations. Notable exceptions were recipients 6, 19, 38, and 57, who displayed high percentages of CD52-negative T cells coinciding with high levels of patient chimerism, indicating that, in some patients, the observed CD52-negative T-cell populations were dominated by T cells of recipient origin. These four patients had received NMA conditioning; in addition, recipient 19 had received high doses of ALM shortly before transplantation to treat the primary disease, and recipient 38 was transplanted for severe aplastic anemia and might have possessed GPI-negative paroxysmal nocturnal hemoglobinuria (PNH)-like cells pretransplantation (not tested because of the absence of sample material).

These data show that the majority of CD52-negative T cells reconstituting following ALM-based T cell depleted alloSCT are of donor origin.

CD52-negative T cells lack expression of the GPI anchor

To unravel the mechanism underlying the loss of CD52 membrane expression on a portion of the circulating T cells in recipients of an ALM-based T-cell depleted alloSCT, we analyzed *CD52* mRNA expression in these cells. CD52-negative and CD52-positive CD4 and CD8 T-cell populations were purified
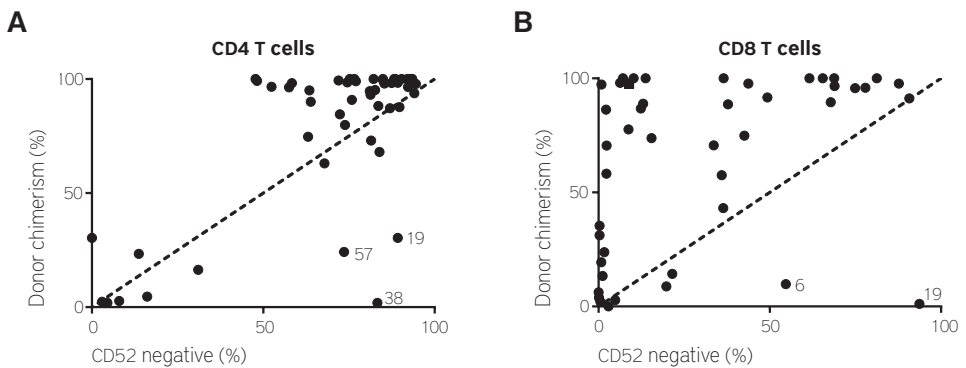
Figure 2. Reconstituted CD52-negative T cells are mainly from donor origin
Relation between the percentages of CD52-negative CD4 **(A)** and CD8 **(B)** T cells and the levels of donor-patient chimerism in these respective subsets. Each dot represents the analysis for a single recipient. Analysis of recipient 6, 19, 38, and 57 are indicated with their respective recipient number. A 45 degree dotted line is depicted as reference. Donor-patient chimerism analysis was performed on samples that had been taken from the recipients at the same day as the samples used for CD52 membrane expression analysis.

by FACS from PBMC of recipients 2, 28, and 37. Normal *CD52* mRNA expression was observed in CD4 and CD8 T cells without CD52 membrane expression and in their CD52-positive counterparts (**Figure S1A**), showing that loss of CD52 membrane expression was not caused by loss of *CD52* gene expression.

A

B
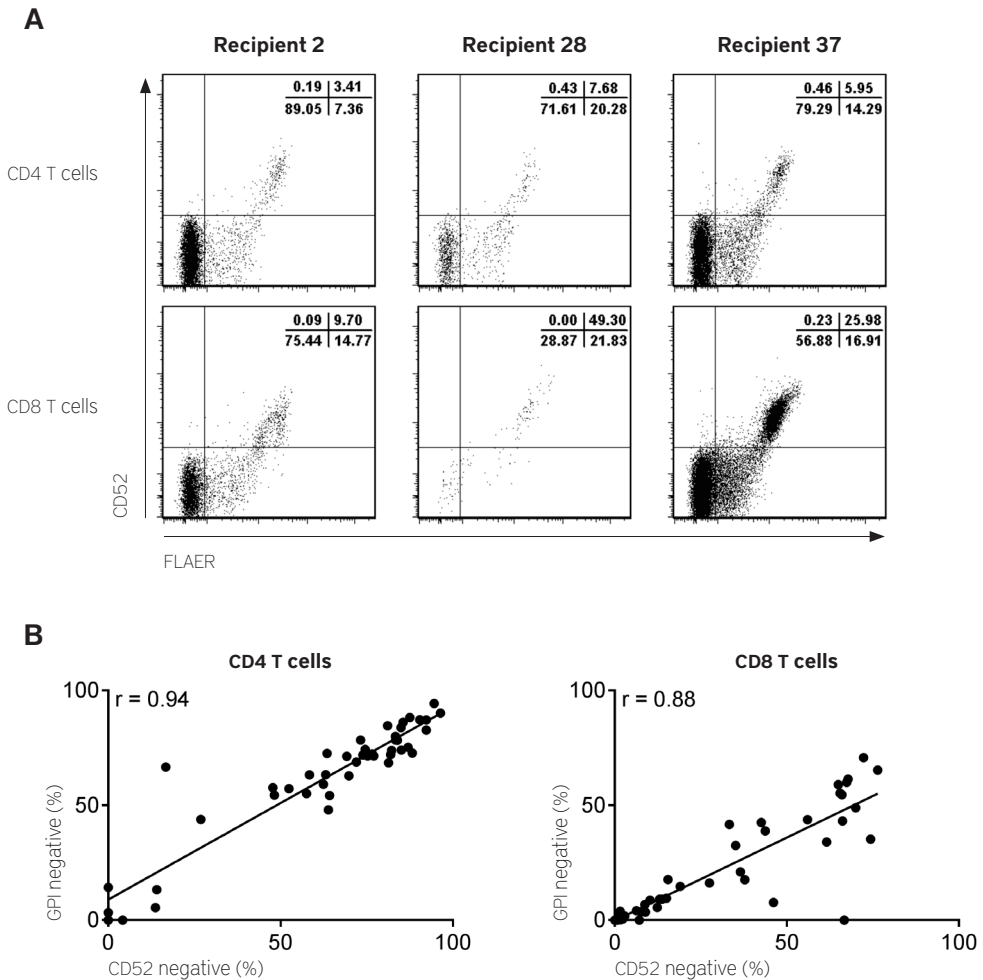
Figure 3. Loss of CD52 membrane expression directly results from loss of GPI-anchor expression
(A) Representative examples of flow cytometric analysis of CD52 and GPI-anchor (FLAER) expression within CD4 and CD8 T cells from recipients 2, 28, and 37. Numbers represent the percentage of cells within the quartiles.
(B) Correlation between the percentage of CD52-negative CD4 (left panel) and CD8 (right panel) T cells and the percentage of GPI-anchor negative CD4 and CD8 T cells within recipients. Each dot represents one recipient (n = 46). Linear regression analysis was performed and depicted as solid lines and the r-value of the curve is presented in the upper left corner of each graph.

Because CD52 membrane expression depends on expression of the GPI anchor, we evaluated whether loss of CD52 membrane expression resulted from loss of GPI-anchor expression. We examined GPI-anchor (by direct FLAER staining) and CD52 membrane expression on CD4 and CD8 T cells in PBMC from 46 recipients using flow cytometry. **Figure 3A** shows in three representative examples that loss of CD52 membrane expression coincided with the absence of GPI-anchor expression in the majority of CD52-negative CD4 T cells and CD8 T cells (lower left quadrant), whereas the remaining CD52-negative T cells expressed significantly lower levels of the GPI anchor (lower right quadrant) compared with CD52-positive T cells (upper right quadrant). Aggregated results from all 46 recipients showed strong correlations between the percentages of CD52-negative and GPI-anchor negative cells (CD4 r = +0.94, p < 0.0001; CD8 r = +0.88, p < 0.0001; **Figure 3B**). These data illustrate that loss of CD52 membrane expression is due to defective GPI-anchor expression.

Mutations in *PIGA* lead to loss of GPI-anchor expression

To study whether loss of GPI-anchor expression in the T cells lacking CD52 membrane expression occurs by active genetic downregulation of one of the 28 genes that make up the GPI-anchor biosynthesis pathway, we performed mRNA expression analysis for these genes in purified GPI/CD52-negative and GPI/CD52-positive CD4 and CD8 T-cell populations from recipients 2, 28, and 37. Normal mRNA expression was observed for all 28 GPI-anchor genes within the GPI/CD52-negative CD4 and CD8 T-cell populations of all three recipients (**Figure S1B**, representative example), indicating that loss of GPI-anchor expression was not caused by loss of expression of one of the GPI-anchor biosynthesis pathway genes.

Because loss of GPI-anchor expression in bone marrow disorders, such as PNH and aplastic anemia, was reported to result from mutations in the *PIGA* gene,[17,18] one of the 28 GPI-anchor biosynthesis genes and unique for its location on the X-chromosome, we analyzed whether the GPI/CD52-negative phenotype of T cells found in recipients after ALM-based T-cell depleted alloSCT also resulted from mutations in the *PIGA* gene. Initial analysis of bulk isolated GPI/CD52-negative T-cell populations indicated that they were polyclonal and carried multiple mutations in the *PIGA* gene. To perform detailed analyses, we clonally isolated and expanded GPI/CD52-negative CD4 and CD8 T cells from recipients 2, 28, and 37. As controls, GPI/CD52-positive CD4 and CD8 T-cell clones were generated from the same individuals. For each clone, *PIGA* mRNA was amplified by PCR and analyzed by Sanger sequencing. In total, 61 GPI/CD52-negative CD4, 12 GPI/CD52-positive CD4, 12 GPI/CD52-negative CD8, and 6 GPI/CD52-

Table 1. Clonal analysis of *PIGA* mutations

Recipient	T cell subset	Clone	Mutation	Position	Codon	Exon	Consequence
2	CD4	1	A>T	312	66	2	Stop-codon
		2	Del 1 bp	456	114	2	Frameshift
		3	A>G	499	128	2	His>Arg
		4	A>G	499	128	2	His>Arg
		5	Del 2 bp	498-499	128	2	Frameshift
		6	T>G	583	156	2	Leu>Arg
		7	T>G	672	186	2	Tyr>Asp
		8	Del 1 bp	857	247	3	Frameshift
		9	Del 16 bp	920-935	268-274	3	Frameshift
		10	Loss exon 3	832-964	278-321	3	Frameshift
		11	Del 3 bp	1036-1038	307-308	4	Del Asn
		12	Del 3 bp, ATA	1036-1038	307-308	4	Del Asn
		13	Del 18 bp, CCCTTACTGAAGCATTCT	1042-1059	309-314	4	Del 6 aa, SLTEAF
		14	Del 6 bp, TTCTGC	1056-1061	314-315	4	Del 2 aa, FC
		15	Loss exon 5	1098-1304	328-396	5	Del 69 aa
		16	Loss exon 5	1098-1304	328-396	5	Del 69 aa
		17	Loss exon 5	1098-1304	328-396	5	Del 69 aa
		18	Ins 1 bp	1100	328	5	Frameshift
		19	Del 1 bp	1213	366	5	Frameshift
		20	G>A	1276	387	5	Stop-codon
	CD8	1	T>A	220	35	2	Ile>Lys
		2	G>A	259	48	2	Gly>Asp
28	CD4	1	Loss exon 2	53-831		2	Loss start site
		2	G>T	132	6	2	Stop-codon
		3	C>T	414	100	2	Stop-codon
		4	A>G	493	126	2	His>Arg
		5	Del 3 bp	626-628	170-171	2	Del Leu
		6	Del 153 bp	679-834	188-239	2	Del 51 AA
		7	Del 1 bp	688	191	2	Frameshift
		8	Del 5 bp, GTACT	693-697	193-194	2	Frameshift
		9	Del 5 bp, GTACT	693-697	193-194	2	Frameshift
		10	Del 2 bp	701-702	195-196	2	Frameshift
		11	Loss exon 3	832-964	278-321	3	Frameshift
		12	Loss exon 3	832-964	278-321	3	Frameshift
		13	Ins 1 bp	994	293	4	Frameshift
		14	Ins 1 bp	996	293	4	Frameshift
		15	Ins 2 bp	1012-1013	299	4	Frameshift
		16	Del 2 bp	1085-1086	323-324	4	Frameshift
		17	Ins 1 bp	1102	329	5	Frameshift
		18	Ins 7 bp, del 2 bp	1168	351	5	Frameshift
		19	Ins 5 bp	1180-1184	355	5	Frameshift
		20	Del 1 bp	1328	404	6	Frameshift
	CD8	1	C>T	288	58	2	Stop-codon
		2	C>T	345	77	2	Stop-codon
		3	Del 223 bp, retention intron 4	609-831, 1097	165-239	2 & 4	Frameshift
		4	Del 153 bp	679-834	188-239	2	Del 51 aa
		5	Loss exon 3	832-964	278-321	3	Frameshift
		6	Loss exon 3	832-964	278-321	3	Frameshift
		7	Loss exon 4	965-1097	283-327	4	Frameshift
		8	Ins 1 bp	1102	329	5	Frameshift
37	CD4	1	Del 1 bp	133	6	2	Frameshift
		2	Del 1 bp	427	104	2	Frameshift
		3	Del 1 bp	427	104	2	Frameshift
		4	Del 1 bp	427	104	2	Frameshift
		5	C>A	580	155	2	Ser>Tyr
		6	Del 5bp GTACT	693-697	193-194	2	Frameshift
		7	G>A	903	263	3	Gly>Arg
		8	Loss exon 4	965-1097	283-327	4	Frameshift
		9	Loss exon 4	965-1097	283-327	4	Frameshift
		10	Loss exon 4	965-1097	283-327	4	Frameshift
		11	Loss exon 5	1098-1304	328-396	5	Del 69 aa
		12	G>A	1117	334	5	Gly>Asp

Del indicates deletion; Ins insertions; aa amino acid

4

positive CD8 T-cell clones were screened. *PIGA* mutations were detected in 52 of 61 GPI/CD52-negative CD4 T-cell clones and in 10 of 12 GPI/CD52-negative CD8 T-cell clones (**Table 1**). Mutations included deletions (n = 24), substitution mutations (n = 16), exon skipping (n = 14), and insertions (n = 8). In 48 T-cell clones (all clones except those that displayed exon skipping), the exact nucleotide sequence resulting in the mutation was identified. Most mutations were detected only once, with the exception of one mutation (r.427del) that was found three times within CD4 T-cell clones from recipient 37, two mutations (r.1102_1103ins; r.679-834del) that were found within the CD4 and CD8 T-cell compartments of recipient 28, and one mutation (r.693-697del) that was found in recipients 28 and 37. No mutations in *PIGA* mRNA were found in the GPI/CD52-positive CD4 or CD8 T-cell clones from the same recipients.
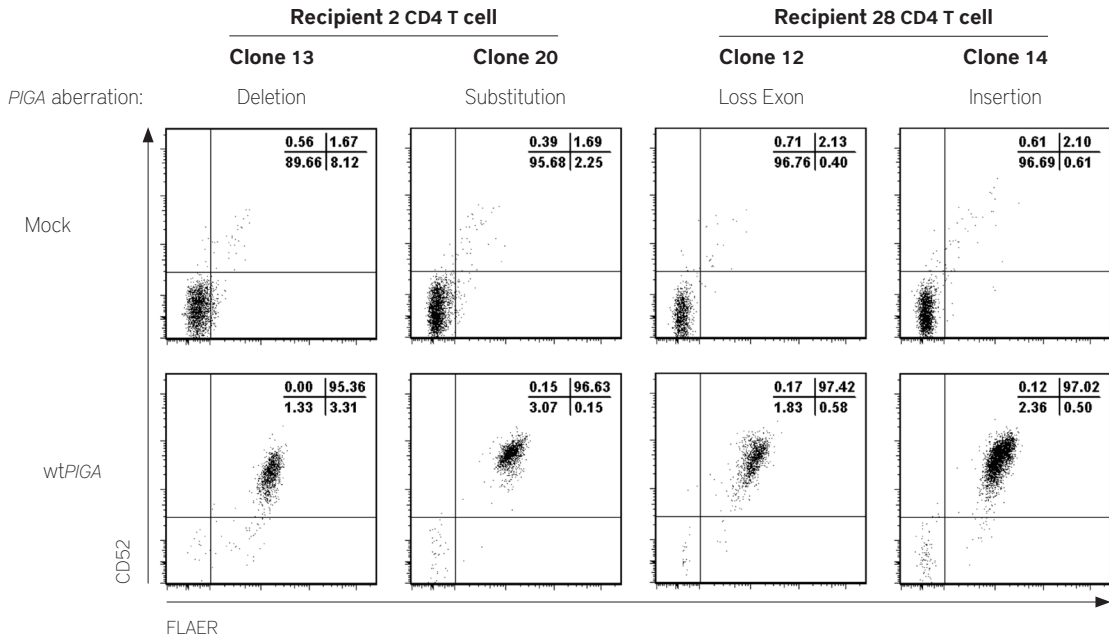
Figure 4. Retroviral transduction with wt*PIGA* restores CD52 and GPI-anchor expression in clonally expanded GPI/CD52-negative T cells

Flow cytometric analysis of CD52 and GPI-anchor (FLAER) expression on clonally expanded GPI/CD52-negative CD4 T-cell clones retrovirally transduced with a construct encoding wt*PIGA* coupled to the t*NGFR* marker gene or with a control construct encoding marker gene only (Mock). A representative clone is displayed for each type of mutation that was found in the *PIGA* gene by Sanger sequencing. The upper panels depict the mock transduced clones gated on t*NGFR* marker gene positive cells and the lower panels depict the clones transduced with wt*PIGA* gated on t*NGFR* marker gene positive cells. Numbers represent the percentage of cells within the quartiles.

These data show that GPI-anchor deficiency in the CD52-negative T cells reconstituting after ALM-based T-cell depleted alloSCT coincided with a highly polyclonal mutational landscape in the *PIGA* gene.

To confirm that mutations found in *PIGA* caused the GPI-anchor negative phenotype, we retrovirally transduced all GPI/CD52-negative T-cell clones (n = 73) with a construct encoding wt*PIGA*, or empty vector as a control. In 48 T-cell clones, marker gene expression indicated successful transduction (CD4 clones n = 46; CD8 clones n = 2; median transduction efficiency within these clones = 15%) which always coincided with restored GPI-anchor and CD52 membrane expression in the wt*PIGA* transduced cells, independent of the type of mutation found in the individual clones (**Figure 4**, representative examples). No restored expression was observed in the mock transduced controls. These data validate that the various mutations found in the *PIGA* gene in the individual T-cell clones were solely responsible for the GPI/CD52-negative phenotype.
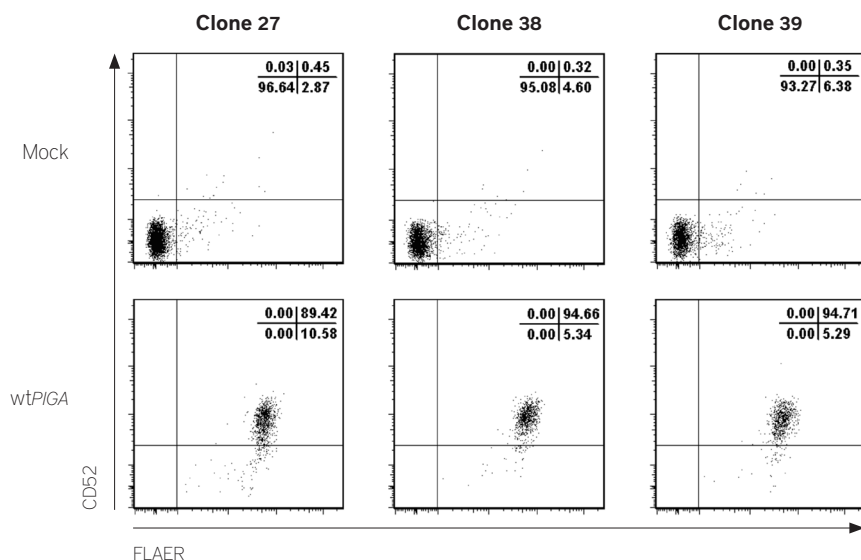
Figure 5. GPI/CD52-negative donor T-cell clones re-express CD52 and GPI-anchor expression upon retroviral transduction with wt*PIGA*

Three examples of GPI/CD52-negative CD4 T-cell clones from donor A retrovirally transduced with a construct encoding wt*PIGA* coupled to the t*NGFR* marker gene or with a control construct encoding the marker gene only (Mock). Depicted are flow cytometric analyses of CD52 and GPI-anchor (FLAER) expression. The upper panels depict the mock transduced clones gated on t*NGFR* marker gene positive cells and the lower panels depict the clones transduced with wt*PIGA* gated on t*NGFR* marker gene positive cells. Numbers represent the percentage of cells within the quartiles.

PIGA mutations found in GPI/CD52-negative donor T cells

Because it has been reported that low numbers of circulating GPI/CD52-negative T cells can be found in healthy individuals,[17] we explored whether GPI/CD52-negative T cells carrying *PIGA* mutations could be detected in donors. We screened PBMC from two donors for the presence of GPI/CD52-negative T cells by flow cytometry. GPI/CD52-negative T cells were detected at frequencies of 22 per 10^6 T cells for donor A (donor of recipient 2) and 27 per 10^6 T cells for donor B (donor of recipient 37). To explore whether the GPI/CD52-negative phenotype in these cells resulted from mutations in *PIGA*, we purified, clonally expanded, and screened GPI/CD52-negative T cells from donor A for *PIGA* mutations. A total of 40 GPI/CD52-negative CD4 and 3 GPI/CD52-negative CD8 T-cell clones was analyzed. The pattern of mutational diversity of the *PIGA* gene within this donor was similar to the one of the recipients (who showed full donor chimerism at the time of analysis) and included substitution mutations (n = 25), deletions (n = 16), and exon skipping (n = 2) (**Table 2**). One of these mutations (r.499a>g) was found twice; in donor A and in corresponding recipient 2. No mutations in *PIGA* mRNA were found in GPI/CD52-positive T-cell clones isolated from this donor (CD4 n = 9, CD8 n = 9; data not shown). Retroviral transduction was performed on the GPI/CD52-negative donor T-cell clones (n = 43), with a construct encoding wt*PIGA* or an empty vector as a control. Marker gene expression indicated successful transduction in 28 clones (only CD4 clones; median transduction efficiency within these clones = 16%) which always coincided with a restored GPI/CD52-positive phenotype in the wt*PIGA* transduced cells, but not in the control condition (**Figure 5**, 3 representative examples). These results confirmed that the mutations found in *PIGA* caused the GPI/CD52-negative phenotype in donor T cells.

Functional T cells specific against multiple viral targets are present within the GPI/CD52-negative T-cell population

Because loss of GPI-anchor expression results in the loss of membrane expression of a large number of GPI-anchored proteins, some of which are involved in T-cell activation,[19] we explored whether T cells that lost GPI-anchor expression remained functional. We screened PBMC from recipients 2, 28, and 37 to identify GPI/CD52-negative and/or GPI/CD52-positive CD8 T-cell populations specific against antigens from CMV or EBV by flow cytometry using fluorescently labeled HLA/peptide complexes (tetramers). In PBMC from recipient 37, an HLA-B*08:01/CMV-IE1-QIK positive CD8 T-cell population was identified that contained GPI/CD52-negative and GPI/CD52-positive T cells. These cells were purified and expanded. Comparable levels of IFN-γ were produced between GPI/CD52-negative HLA-B*08:01/CMV-IE1-QIK CD8 T cells and their GPI/CD52-positive counterparts upon stimulation with EBV-LCLs loaded with

Table 2. Clonal analysis of *PIGA* mutations in T cells from donor A

T cell subset	Clone	Mutation	Position	Codon	Exon	Consequence
CD4	1	Del 4 bp	168-171	18-19	2	Frameshift
	2	G>A	256	47	2	Gly>Glu
	3	Del 1 bp	276	54	2	Frameshift
	4	Del 2 bp	324-325	70	2	Frameshift
	5	C>G	362	82	2	Stop-codon
	6	A>G	378	88	2	Lys>Glu
	7	Del 32 bp	436-467	107-117	2	Frameshift
	8	A>G	493	126	2	His>Arg
	9	A>G	499	128	2	His>Arg
	10	A>G	499	128	2	His>Arg
	11	A>C	501	129	2	Ser>Arg
	12	C>T	558	148	2	Stop-codon
	13	Del 28 bp	571-598	152-161	2	Frameshift
	14	C>T	580	155	2	Ser>Phe
	15	C>T	607	164	2	Ser>Leu
	16	C>T	607	164	2	Ser>Leu
	17	G>T	664	183	2	Cys>Phe
	18	Del 153 bp	679-834	188-239	2	Del 51 AA
	19	T>G	689	191	2	Asn>Lys
	20	Del 5 bp , GTACT	693-697	193-194	2	Frameshift
	21	Del 1 bp	752	212	2	Frameshift
	22	T>G	817	234	2	Leu>Arg
	23	G>A	909	265	3	Gly>Arg
	24	G>A	909	265	3	Gly>Arg
	25	G>T	942	276	3	Stop-codon
	26	Loss exon 4	965-1097	283-327	4	Frameshift
	27	Loss exon 4	965-1097	283-327	4	Frameshift
	28	T>G	967	284	4	Val>Gly
	29	G>A	1021	302	4	Gly>Glu
	30	Del 1 bp	1044	310	4	Frameshift
	31	Del 1 bp	1101	329	5	Frameshift
	32	G>A	1117	334	5	Gly>Asp
	33	G>A	1128	338	5	Glu>Lys
	34	Del 16 bp	1139-1154	341-346	5	Frameshift
	35	Del 1 bp	1165	350	5	Frameshift
	36	A>T	1173	353	5	Stop-codon
	37	C>T	1209	365	5	Stop-codon
	38	Del 15 bp	1282-1296	389-393	5	Del 5aa, NVEAR
	39	G>A	1447	444	6	Stop-codon
	40	Del 2 bp	1455-1456	447	6	Frameshift
CD8	1	Del 1bp	792	226	2	Frameshift
	2	Del 10bp	1243-1252	376-379	5	Frameshift
	3	A>T	1197	361	5	Stop-codon

Del indicates deletion; Ins insertions

4

the relevant viral peptide (**Figure 6A**). In addition, similarly high levels of IFN-γ were observed when GPI/CD52-negative CD8 T cells positive for tetramers HLA-A*02:01/CMV-IE1-VLE (recipient 2) and HLA-B*35:01/CMV-pp65-IPS (recipient 28) were tested and compared with GPI/CD52-positive CD8 T cells positive for tetramer HLA-B*08:01/EBV-BZLF1-RAK (recipient 37) (**Figure 6B**). These data show that loss of GPI-anchor expression did not impair the functionality of virus-specific GPI/CD52-negative CD8 T cells.
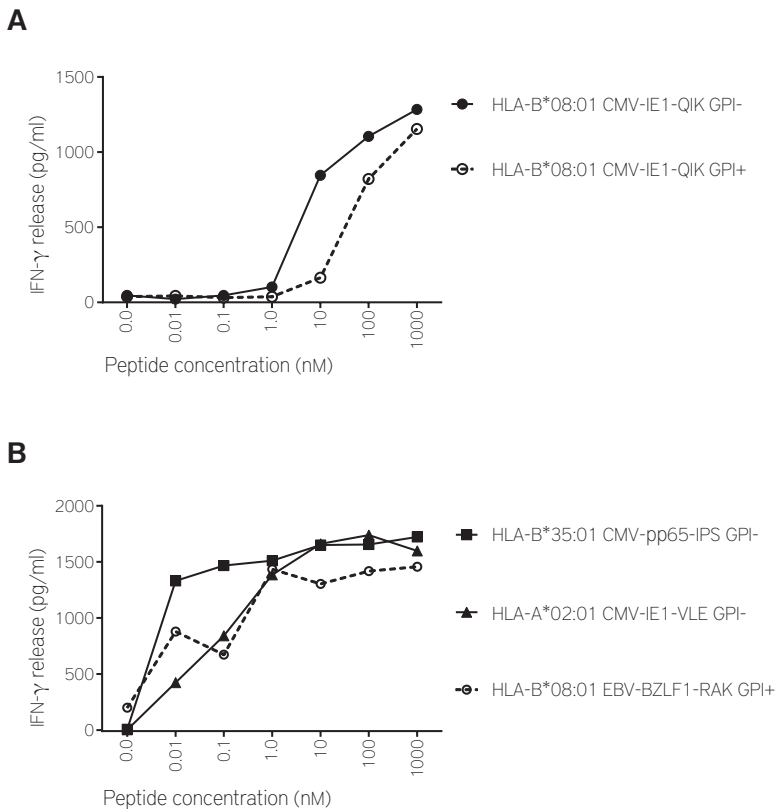
Figure 6. Functional T cells specific against multiple viral targets are present within GPI/CD52-negative T-cell populations

(A) Reactivity of GPI/CD52-negative and GPI/CD52-positive virus specific T cells (HLA-B*08:01/CMV-IE1-QIK) isolated and expanded from recipient 37 tested against third party EBV-LCLs loaded with a serial dilution of the relevant peptide in IFN-γ ELISA. Data are presented as concentration IFN-γ released in the supernatant after 24 h of co-incubation. **(B)** Reactivity of isolated and expanded GPI/CD52-negative virus specific T-cell populations (HLA-A*02:01/CMV-IE1-VLE GPI- and HLA-B*35:01/CMV-pp65-IPS GPI-) tested against EBV-LCLs loaded with a serial dilution of relevant viral peptides in IFN-γ ELISA. As a reference, reactivity of a GPI/CD52-positive T-cell population (HLA-B*08:01/EBV-BZLF1-RAK GPI+) was tested. Data are presented as concentration IFN-γ released in the supernatant after 24 h of co-incubation.

DISCUSSION

ALM-based T-cell depleted alloSCT protocols are used to prevent acute GvHD and graft rejection. In this study we show in a cohort of 89 ALM-based T-cell depleted alloSCT recipients that early lymphocyte reconstitution generally consists of reconstitution of large populations of T cells lacking membrane expression of the ALM target antigen CD52. In contrast, CD52-negative cells were found to be uncommon within B cells and NK cells, confirming earlier reports.[9,10] We and other investigators have shown previously that lack of CD52 expression from the membrane of T cells following ALM-based alloSCT results from the loss of GPI-anchor expression. However, the mechanism resulting in this loss remained unknown. In this article, we illustrate that a highly polyclonal mutational landscape in the *PIGA* gene results in the loss of GPI-anchor expression in CD52-negative T cells reconstituting following ALM-based T-cell depleted alloSCT. The patterns of *PIGA* mutations were highly diverse between recipients, as well as within T cell populations from single recipients. A similar diverse pattern of *PIGA* mutations was observed within the extremely low frequency of CD52-negative T cells isolated from PB of a healthy donor, indicating that the susceptibility for gaining mutations in the highly mutagenic *PIGA* gene of T cells is a general phenomenon and is not solely caused by exposure to ALM. In turn, this provides an explanation for the frequent presence of CD52/GPI-anchor negative T cell populations following ALM treatment, because this treatment allows the preferential outgrowth of CD52-negative cells. We show that, despite loss of GPI-anchor expression, GPI/CD52-negative T-cell populations contain functional T cells specific against multiple viral antigens.

CD52 is expressed on all mature lymphocyte subsets, but at different levels: CD4 T cells generally express higher levels of CD52 than CD8 T cells.[20] Subsets with higher CD52 expression levels are more sensitive to ALM-induced cell death resulting in more profound depletion.[8,20] We show that, upon lymphocyte reconstitution following ALM-based T-cell depleted alloSCT, ALM-resistant CD52-negative cells were more abundant in the CD4 T-cell compartment than in the CD8 T-cell compartment (median 81.3 and 32.0%, respectively). These fractions of CD52-negative T cells are inversely correlated with the normal level of CD52 expressed on these subsets in healthy individuals, suggesting that more profound ALM-induced selective pressure resulted in higher proportions of CD52-negative ALM-resistant cells. Higher selective pressure also likely explains why CD52-negative T cells are mainly from donor origin, because ALM concentrations present in the bag containing the graft are >5-fold higher compared with ALM plasma concentrations reached in the patient (F.C. Loeff, H.M. van Egmond, J.H.F. Falkenburg, C.J.M.

Halkes, and I. Jedema, unpublished observations). In concordance, in patients receiving transplantation without ALM treatment, CD52-negative T cell populations are detected at the same low frequencies as seen in PB of healthy donors.[9]

Many of the *PIGA* mutations found in this study have previously been reported to result in a GPI-anchor deficient phenotype in patients with PNH, aplastic anemia, or myelodysplastic syndrome.[21-24] In these patients, this phenotype results from clonal outgrowth of a progenitor cell carrying a single *PIGA* mutation that generally affects multiple hematopoietic cell lineages. In contrast, the GPI/CD52-negative cell populations found in ALM-based T-cell depleted alloSCT recipients were mainly restricted to the T-cell lineage. Furthermore, the GPI/CD52-negative phenotype in T-cell populations from individual alloSCT recipients resulted from a multitude of *PIGA* mutations. The mechanism resulting in *PIGA* mutations in GPI/CD52-negative T cells was not studied, but they are likely acquired spontaneously during cell division. This implies that cell populations that have experienced an (antigen driven) expansion phase are especially likely to have acquired these mutations, which is supported by the observation that T cells with a memory phenotype preferentially survive ALM-based T-cell depletion.[25,26] Although this study has focused on the presence of GPI/CD52-negative T cells early after transplantation, when few naive T cells are present in the circulation, we indeed observed, in a different cohort, that, at later time points, GPI/CD52-negative T cells are mainly observed in the effector and memory T cell populations (F.C. Loeff, H.M. van Egmond, J.H.F. Falkenburg, C.J.M. Halkes, and I. Jedema, unpublished observations).

We found GPI/CD52-negative T cells in donor PBMC at frequencies similar to those previously reported in healthy individuals.[17] In contrast to that article, which recorded only one or two *PIGA* mutations per individual as a result of limited testing, we show that the GPI-anchor negative phenotype in the donor T-cell population resulted from ≥41 different *PIGA* mutations within a single individual. Our data, in combination with the data published for patients with PNH, aplastic anemia, or myelodysplastic syndrome, show that hundreds of distinct mutations in *PIGA* can result in the GPI-deficient phenotype. This may explain why only one of the mutations that we detected in donor material correlated with a mutation in the corresponding recipient.

Based on the frequencies of GPI/CD52-negative T cells determined in the donors, the average composition of a G-CSF-mobilized PB graft (384×10^6 T cells/kg of recipients body weight)[27,28], and the assumption that GPI/CD52-negative T cells survive ALM treatment, an average of 1.0×10^4 GPI/CD52-negative donor

T cells per kg of recipients body weight are infused with the graft during alloSCT. Antigen-dependent and homeostatic proliferation of these pre-existing GPI/CD52-negative cell likely explains why GPI/CD52-negative T cells are abundantly present during the first months following alloSCT.[29] However, *de novo*-acquired loss-of-function *PIGA* mutations in rapidly proliferating GPI/CD52-positive T cells that survived ALM-based depletion may also contribute to the GPI/CD52-negative T-cell population. The long lifespan of T cells[30] results in the persistence of GPI/CD52-negative T cells for years before they are completely replaced by GPI/CD52-positive T cells derived from engrafted stem cells.[9]

We show that functionality of GPI/CD52-negative T cells is comparable to their GPI/CD52-positive counterparts, confirming previous reports using T cells derived from *PIGA* deficient mice.[31,32] The clinical relevance of these GPI/CD52-negative T cells in the setting of alloSCT remains largely unknown. They may be beneficial by promoting GvT or by eliciting early antiviral immune protection. Alternatively, they may result in toxicity by induction of GvHD. We show that GPI/CD52-negative T-cell populations contained functional T cells specific against multiple viral antigens implicating their involvement in early immune protection. Because GPI/CD52-negative T cells are likely of memory phenotype, they are less prone to induce GvHD[33-35] compared with unselected T cells. Together, this may explain the clinical success of the ALM-based T-cell depleted alloSCT protocol.

In conclusion, loss of CD52 membrane expression in T cells reconstituting early after ALM-based T-cell depleted alloSCT is the result of various mutations in the *PIGA* gene and consequential loss of GPI-anchor expression. These GPI/CD52-negative populations contain functional virus-specific T cells and may be essential in immune protection early after transplantation.

4

REFERENCE LIST

1.   Miller JS, Warren E, van den Brink M, et al. NCI First International Workshop on The Biology, Prevention, and Treatment of Relapse After Allogeneic Hematopoietic Stem Cell Transplantation: Report from the Committee on the Biology Underlying Recurrence of Malignant Disease following Allogeneic HSCT: Graft-versus-Tumor/Leukemia Reaction. *Biol Blood Marrow Transplant*. 2010;16(5):565-586.

2.   Goker H, Haznedaroglu I, Chao NJ. Acute graft-vs-host disease: pathobiology and management. *Exp Hematol*. 2001;29(3):259-277.

3.   Lee SJ, Vogelsang G, Flowers ME. Chronic graft-versus-host disease. Biol Blood Marrow Transplant. 2003;9(4):215-233.

4.   Roddie C, Peggs KS. Donor lymphocyte infusion following allogeneic hematopoietic stem cell transplantation. *Expert Opin Biol Ther*. 2011;11(4):473-487.

5.   Deol A, Lum LG. Role of donor lymphocyte infusions in relapsed hematological malignances after stem cell transplantation revisited. *Cancer Treat Rev*. 2010;36(7):528-538.

6.   Eefting M, de Wreede LC, Halkes CJ, et al. Multi-state analysis illustrates treatment success after stem cell transplantation for acute myeloid leukemia followed by donor lymphocyte infusion. *Haematologica*. 2016;101(4):506-514.

7.   Eefting M, Halkes CJ, de Wreede LC, et al. Myeloablative T cell-depleted alloSCT with early sequential prophylactic donor lymphocyte infusion is an efficient and safe post-remission treatment for adult ALL. *Bone Marrow Transplant*. 2014;49(2):287-291.

8.   Hale G, Bright S, Chumbley G, et al. Removal of T cells from bone marrow for transplantation: a monoclonal antilymphocyte antibody that fixes human complement. *Blood*. 1983;62(4):873-882.

9.   Garland RJ, Groves S, Diamanti P, et al. Early emergence of PNH-like T cells after allogeneic stem cell transplants utilising CAMPATH-1H for T cell depletion. *Bone Marrow Transplant*. 2005;36(3):237-244.

10. Meyer RG, Wagner E, Konur A, et al. Donor CD4 T cells convert mixed to full donor T-cell chimerism and replenish the CD52-positive T-cell pool after alemtuzumab-based T-cell-depleted allo-transplantation. *Bone Marrow Transplant*. 2010;45(4):668-674.

11. Barge RM, Starrenburg CW, Falkenburg JH, Fibbe WE, Marijt EW, Willemze R. Long-term follow-up of myeloablative allogeneic stem cell transplantation using Campath "in the bag" as T-cell depletion: the Leiden experience. *Bone Marrow Transplant*. 2006;37(12):1129-1134.

12. The T, Feltkamp TE. Conjugation of fluorescein isothiocyanate to antibodies. I. Experiments on the conditions of conjugation. *Immunology*. 1970;18(6):865-873.

13. Marijt WA, Heemskerk MH, Kloosterboer FM, et al. Hematopoiesis-restricted minor histocompatibility antigens HA-1- or HA-2-specific T cells can induce complete remissions of relapsed leukemia. *Proc Natl Acad Sci U S A*. 2003;100(5):2742-2747.

14. Van Bergen CA, Rutten CE, Van Der Meijden ED, et al. High-throughput characterization of 10 new minor histocompatibility antigens by whole genome association scanning. *Cancer Res*. 2010;70(22):9073-9083.

15. Heemskerk MH, Hoogeboom M, de Paus RA, et al. Redirection of antileukemic reactivity of peripheral T lymphocytes using gene transfer of minor histocompatibility antigen HA-2-specific T-cell receptor complexes expressing a conserved alpha joining region. *Blood*. 2003;102(10):3530-3540.

16. Hombrink P, Hadrup SR, Bakker A, et al. High-throughput identification of potential minor histocompatibility antigens by MHC tetramer-based screening: feasibility and limitations. *PLoS One*. 2011;6(8):e22523.

17. Ware RE, Pickens C, Castro C, Howard TA. Circulating PIG-A mutant T lymphocytes in healthy adults and patients with bone marrow failure syndromes. *Exp Hematol*. 2001;29(12):1403-1409.

18. Brodsky RA. Paroxysmal nocturnal hemoglobinuria. *Blood*. 2014;124(18):2804-2811.

19. Loertscher R, Lavery P. The role of glycosyl phosphatidyl inositol (GPI)-anchored cell surface proteins in T-cell activation. *Transpl Immunol*. 2002;9(2-4):93-96.

20. Rao SP, Sancho J, Campos-Rivera J, et al. Human peripheral blood mononuclear cells exhibit heterogeneous CD52 expression levels and show differential sensitivity to alemtuzumab mediated cytolysis. *PLoS One*. 2012;7(6):e39416.

21. Mortazavi Y, Merk B, McIntosh J, Marsh J, chrezenmeier H, utherford TR. The spectrum of PIG-A gene mutations in aplastic anemia/paroxysmal nocturnal hemoglobinuria (AA/PNH): a high incidence of multiple mutations and evidence of a mutational hot spot. *Blood*. 2003;101(7):2833-2841.

22. Shen W, Clemente M, Hosono N, et al. Deep sequencing reveals stepwise mutation acquisition in paroxysmal nocturnal hemoglobinuria. *J Clin Invest*. 2014;124(10):4529-4538.

23. Rosse WF. Paroxysmal nocturnal hemoglobinuria as a molecular disease. *Medicine*. 1997;76(2):63-93.

24. Nafa K, Bessler M, Castro-Malaspina H, Jhanwar S, Luzzatto L. The spectrum of somatic mutations in the PIG-A gene in paroxysmal nocturnal hemoglobinuria includes large deletions and small duplications. *Blood Cells Mol Dis*. 1998;24(3):370-384.

25. Grimaldi F, Potter V, Perez-Abellan P, et al. Mixed T-Cell Chimerism after Allogeneic Hematopoietic Stem Cell Transplantation for Severe Aplastic Anemia Using an Alemtuzumab-Containing Regimen is Shaped by Persistence of Recipient CD8 T Cells. *Biol Blood Marrow Transplant*. 2016.

26. Pearl JP, Parris J, Hale DA, et al. Immunocompetent T-cells with a memory-like phenotype are the dominant cell type following antibody-mediated T-cell depletion. *Am J Transplant*. 2005;5(3):465-474.

27. Bensinger WI, Clift RA, Anasetti C, et al. Transplantation of allogeneic peripheral blood stem cells mobilized by recombinant human granulocyte colony stimulating factor. *Stem Cells*. 1996;14(1):90-105.

28. Panse JP, Heimfeld S, Guthrie KA, et al. Allogeneic peripheral blood stem cell graft composition affects early T-cell chimaerism and later clinical outcomes after non-myeloablative conditioning. *Br J Haematol*. 2005;128(5):659-667.

29. Seggewiss R, Einsele H. Immune reconstitution after allogeneic transplantation and expanding options for

immunomodulation: an update. *Blood*. 2010;115(19):3861-3868.

30. Westera L, Drylewicz J, den B, I, et al. Closing the gap between T-cell life span estimates from stable isotope-labeling studies in mice and humans. *Blood*. 2013;122(13):2205-2212.

31. Takahama Y, Ohishi K, Tokoro Y, et al. Functional competence of T cells in the absence of glycosylphosphatidylinositol-anchored proteins caused by T cell-specific disruption of the Pig-a gene. *Eur J Immunol*. 1998;28(7):2159-2166.

32. Hazenbos WL, Murakami Y, Nishimura J, Takeda J, Kinoshita T. Enhanced responses of glycosylphosphatidylinositol anchor-deficient T lymphocytes. *J Immunol*. 2004;173(6):3810-3815.

33. Anderson BE, McNiff J, Yan J, et al. Memory CD4+ T cells do not induce graft-versus-host disease. *J Clin Invest*. 2003;112(1):101-108.

34. Teschner D, Distler E, Wehler D, et al. Depletion of naive T cells using clinical grade magnetic CD45RA beads: a new approach for GVHD prophylaxis. *Bone Marrow Transplant*. 2014;49(1):138-144.

35. Bleakley M, Heimfeld S, Loeb KR, et al. Outcomes of acute leukemia patients transplanted with naive T cell-depleted stem cell grafts. *J Clin Invest*. 2015;125(7):2677-2689.

SUPPLEMENTAL DATA

Table S1. Recipient and sample information

Recipient	Percentage of CD52-negative cells				Absolute number of circulating cells (10^6 cells/L)			
	CD3+CD4+	CD3+CD8+	CD19+	CD3-CD16+	CD3+CD4+	CD3+CD8+	CD19+	CD3-CD16+
1	98,15	97,48		ND	5	35	0	5
2	96,36	76,41		ND	130	995	16	1116
3	94,96	90,02			157	1352	246	383
4	94,54	67,39			441	4	4	12
5	94,18	91,68			103	35	3	87
6	94,09	54,72	88,20	ND	128	43	1	36
7	93,49	76,86		ND	159	15	5	113
8	93,29	93,97			112	164	85	555
9	93,22	49,30		ND	41	3	0	85
10	93,19	87,69	7,70		132	41	86	244
11	92,95	86,45		ND	655	14	1	686
12	92,66	68,79		ND	454	396	3	192
13	92,26	74,36		ND	71	5	6	45
14	92,23	66,21			141	21	141	816
15	92,09	81,24		ND	99	124	36	139
16	90,36	65,48		ND	45	431	5	337
17	90,09	19,61			66	13	66	176
18	89,77	32,00		ND	34	1	0	150
19	89,26	93,71			115	79	10	94
20	89,26	90,77		ND	50	46	0	85
21	89,10	83,83		ND	499	22	63	179
22	88,99	13,95		ND	5	0	0	27
23	88,51	68,94			154	264	6	287
24	88,20	61,61		ND	26	13	87	521
25	87,49	42,59			225	923	21	813
26	86,99	2,36			263	821	500	567
27	85,92	49,47		ND	90	12	113	575
28	85,54	70,00		ND	103	2	5	46
29	85,37	77,91		ND	71	9	34	247
30	85,29	0,35			201	381	0	275
31	85,04	37,78			73	7	74	141
32	84,94	19,03			160	256	39	498
33	84,53	71,43			86	30	18	398
34	83,92	35,95			34	339	93	454
35	83,86	64,95			191	7	91	56
36	83,60	4,86		ND	21	106	1	101
37	83,37	66,01			726	2604	340	1396
38	83,33	33,63		ND	18	30	4	107
39	83,28	27,51			274	127	61	229
40	83,06	27,11			83	46	15	240
41	82,66	74,91		ND	167	477	424	715
42	82,22	36,50			157	30	30	82
43	81,94	46,15		ND	8	0	42	80
44	81,45	21,53			120	1171	89	619
45	81,28	1,67			107	296	1	1193
46	81,10	19,79			103	15	0	394
47	81,04	33,33			24	2	1	29
48	79,82	1,52			0	0	0	0

Diagnosis	Conditioning	Thymoglobulin	Kinship donor	Graft source	Days post-transplantation
Angioimmunoblastic T-NHL	NMA	2mg/kg	UD	MPB	39
B-ALL	MA		UD	MPB	43
AML	NMA		SIB	MPB	42
Lymphoplasmacytic B-NHL	NMA		SIB	MPB	41
SAA	NMA		UD	MPB	40
MM	NMA		UD	MPB	41
MM	NMA		UD	MPB	35
AML	NMA		UD	MPB	42
AML	NMA		UD	MPB	41
MM	NMA		UD	MPB	37
Anaplastic diffuse large T-NHL	NMA		UD	MPB	44
Mycosis Fungoides	NMA		UD	MPB	42
AML	MA		UD	MPB	46
T-ALL	MA		SIB	MPB	72
AML	NMA		UD	MPB	45
B-ALL	MA		UD	MPB	42
AML	NMA		SIB	MPB	43
AML	NMA	2mg/kg	UD	MPB	45
Blastic Plasmacytoid dendritic cell neoplasm	NMA		UD	MPB	42
Follicular B-NHL	NMA		SIB	MPB	41
MM	NMA		UD	MPB	42
MM	NMA		UD	MPB	37
AML	NMA		UD	MPB	43
CML	MA		SIB	MPB	42
MM	NMA		UD	MPB	42
CML	MA		SIB	MPB	90
AML	NMA		UD	MPB	45
CML BC	MA		UD	MPB	38
AML	NMA		SIB	MPB	39
Mantle cell B-NHL	NMA		SIB	MPB	42
CML BC	MA		SIB	MPB	48
B-ALL	MA		UD	MPB	42
AML	NMA		UD	MPB	38
AML	NMA		SIB	MPB	40
CML BC	MA		UD	MPB	98
MM	NMA		SIB	MPB	41
Peripheral T-NHL NOS	MA		UD	MPB	91
SAA	NMA	2mg/kg	UD	MPB	39
Angioimmunoblastic T-NHL	MA		SIB	MPB	41
MM	NMA		SIB	MPB	40
AML	NMA		SIB	MPB	41
AML	MA		SIB	MPB	42
Hemophagocytic Lymphohistiocytosis	MA		UD	MPB	45
AML	NMA		SIB	MPB	42
MDS RAEB-2	MA		SIB	MPB	43
Follicular B-NHL	NMA		SIB	MPB	57
AML	NMA	1mg/kg	UD	MPB	43
AML	NMA		UD	MPB	47

49	77,01	7,54			107	490	10	450
50	76,56	10,27		ND	181	77	105	261
51	75,88	36,41	5,70		112	415	57	212
52	75,25	13,74			224	530	81	722
53	74,92	72,00			148	117	7	124
54	74,51	43,75			17	2	0	82
55	73,84	13,03		ND	10	14	46	138
56	73,68	63,87			268	1787	0	441
57	73,60	2,29			74	495	32	95
58	73,18	72,30			13	3	46	45
59	72,38	2,17			101	29	2	105
60	71,95	8,89			115	27	62	369
61	69,83	56,00			20	0	0	36
62	69,20	0,00		ND	9	3	1	162
63	67,86	0,00			15	93	19	235
64	64,19	0,15		ND	240	207	8	185
65	63,87	12,37			160	540	184	734
66	63,47	15,49			64	24	191	275
67	63,07	67,81			92	90	6	252
68	62,42	15,01		ND	8	22	240	249
69	58,38	6,32			265	355	21	503
70	57,50	35,12		ND	58	35	0	52
71	52,42	0,88			138	1308	124	392
72	48,18	8,75			54	131	126	125
73	47,74	7,14		ND	229	2	16	96
74	31,03	0,54			35	45	74	193
75	26,85	1,56			61	392	20643	510
76	16,67	66,67			0	0	2	38
77	16,14	2,91			39	112	53	166
78	14,08	2,93			7	8	1	0
79	13,68	0,30			41	178	109	100
80	11,36	5,49			16	11	23	41
81	7,99	0,47			8	47	358	231
82	4,54	0,14			87	118	58	106
83	4,17	0,00		ND	1	6	2	23
84	2,95	1,17			285	324	201	204
85	0,08	0,04			57	55	52	26
86	0,05	0,00			381	345	0	118
87	0,00	0,83			2	12	209	236
88	0,00	0,33			31	38	165	141
89	0,00	0,00			1	0	45	159

ND indicates not detectable; AML, acute myeloid leukemia; BC, blast crisis; B-ALL, B cell acute lymphoblastic leukemia; B-NHL, B cell non-Hodgkin lymphoma; CLL, chronic lymphocytic leukemia; CML, chronic myeloid leukemia; CMML, chronic myelomonocytic leukemia; MCL, mantle cell lymphoma; MDS REAB-2, myelodysplastic syndrome refractory anemia with excess blasts-2; MM, multiple myeloma; NOS, not otherwise specified; SAA, severe aplastic anemia; T-ALL, T cell acute lymphoblastic leukemia; T-NHL, T cell non-Hodgkin lymphoma; NMA, non-myeloablative; MA, myeloablative; SIB, sibling; UD, unrelated donor; MPB, mobilized peripheral blood; BM, bone marrow.

B-CLL	MA		UD	MPB	51
T-ALL	MA		UD	MPB	69
MM	NMA		SIB	MPB	39
AML	MA		UD	MPB	94
B-CLL	NMA		UD	MPB	59
Double hit B-NHL	MA		UD	MPB	41
CMML	NMA		SIB	MPB	41
Follicular B-NHL	NMA		UD	MPB	44
Lymphoplasmacytic B-NHL	NMA		SIB	MPB	38
AML	MA		SIB	BM	44
AML	NMA		SIB	MPB	41
AML	MA		SIB	MPB	40
AML	MA		UD	MPB	40
AML	MA		SIB	MPB	37
Primary Myelofibrosis	NMA		SIB	MPB	40
B-ALL	MA		SIB	BM	43
AML	MA		SIB	MPB	44
CML BC	MA		SIB	BM	43
AML	NMA		SIB	MPB	40
MM	NMA		SIB	MPB	49
AML	MA		UD	MPB	41
MM	NMA		SIB	MPB	41
Hodgkin Lymphoma	MA		SIB	MPB	48
T-ALL	MA		SIB	MPB	43
MDS RAEB-2	MA		UD	MPB	45
AML	NMA		SIB	MPB	36
CLL	MA		UD	MPB	39
Mycosis Fungoides	NMA	2mg/kg	UD	MPB	37
B-CLL	NMA		UD	MPB	41
CML	NMA		UD	MPB	43
Mantle cell B-NHL	NMA		SIB	MPB	49
B-CLL	NMA		SIB	MPB	40
B-ALL	NMA		SIB	MPB	40
B-CLL	NMA		UD	MPB	43
B-ALL	NMA	1mg/kg	UD	MPB	43
B-CLL	NMA		SIB	MPB	57
B-CLL	NMA	2mg/kg	UD	MPB	37
NK T cell NHL, nasal type	MA		SIB	MPB	39
MM	NMA	2mg/kg	UD	MPB	43
AML	NMA		UD	MPB	43
AML	NMA	2mg/kg	UD	MPB	44

4

Table S2. Primer sequences used for mRNA expression analysis and mutation analysis

Set 1	GCCATGGAACTCACCGGTAATA	AAAACGTTTGGCCCTTCAG
Set 2a	CTCACCGGTAATAGAGGACAC	GCTTGTTTGTAAGCACCGAGC
Set 2b	GTTCGGGAGAGAGTCACGATA	TTCAGCACCCAAAGCTCTC
CD52	AGACAGCCCTGAGATCACCTA	GCCCCTACATCATTACCCCC
GAPDH	ATGTTCGTCATGGGTGTGAACCA	TGGCAGGTTTTTCTAGACGGCAG
PIGA	GTTCGGGAGAGAGTCACGATA	GCTTGTTTGTAAGCACCGAGC
PIGB	CTTACCCTTCTTTATTCATGGCTG	GGTTAATGAGTATCCACAGAACAC
PIGC	CTGCGCAACCCTAGGAACTC	GAAGAAGCCAGACCAGTCCC
PIGF	GTAGTTCCCCGCTTCCCTTC	CTCCAAGCCATGCTCCTACA
PIGH	GCCATTTACATGCAGAAGGT	GACTGTGTCCACCTGATGGT
PIGK	GGGAAGTCTGAAGCCGGTAA	CTAGGTGGGATCCTCCCAGT
PIGL	TACCTAAAGGGTGCTCTGTG	CCGGGAGAAGATAATGTAGAGG
PIGM	TCACCGCTTTCCTCTTATACC	TGGGAAGGATGTAAGTCACTG
PIGN	AGAAGTGAAGAAACCAAGCC	TCAACACTGATACAACAAGGTC
PIGO	TCGTTGCCCTGAAGAGACAC	ATGCCAATGGATGGCTGGAA
PIGP	GGTGGAAAATTCACCGTCGC	TGGATGGAGTCGAGTGGAGA
PIGQ	CTGTGGATCAGCTACATCCA	CCAGGTCATAGGAACAGGAG
PIGS	GCGGCTACACACCTAGAGG	CTGGGAGTAAGGCAACGAGG
PIGT	GCGGGAGGAACTTGTCATCA	CAAGAGCTTCTTCCAGGGGG
PIGU	TTCATTTCCGAGCGGGTGG	TGCGGGGATGAAATCCCAAG
PIGV	CATGTTCAGGTTCTCACCAG	GCCTAGAATGTATCGTGTGAC
PIGW	AGCCATCTCCTGTTTCCGTG	TGCACACCAGCCATGTGTAT
PIGX	CATAACAGAGGCAGTGATGG	CATTCTCCAAAGCACAAGGGG
PIGY	TGTTCTACTCAGCCTCTGTGG	CCCATCCAAGTCCAAAGGTG
PIGZ	GCCCTGGGAGTTTTACCCC	GAAGGTGGAACCAGAGATCAGC
DPM1	ACAGAATTCTTCTAAGACCACG	CTCCATTTCCTTTGTAGCGA
DPM2	TTAGCCTGATCATCTTCACCT	ATGAACAGTCCCACAAACAG
DPM3	ATGACGAAATTAGCGCAGTGG	TTAGGCTGTCAGAAGCGCAG
GPAA1	CCACGAGCGCTATATGGTGT	ATTGATGCCACGCAGGGTTA
PGAP1	TTCTATGTGCCTGCAAGGGG	ACCTCGTACCGACAGTCTGA
PGAP2	TCCCACTACCACTGGATCGG	GTGTGCTTCTTGGTCAACCG
PGAP3	ACCTGTCGGGACGACTGTAA	AAGAGCGGTGGGAAGTCAAG
SL15	CGTTCAGTGGGACTTGCTTC	GTGTGCCCGTTGTGGTAGTT

Table S3. Tetramers for detection of virus specific T cells

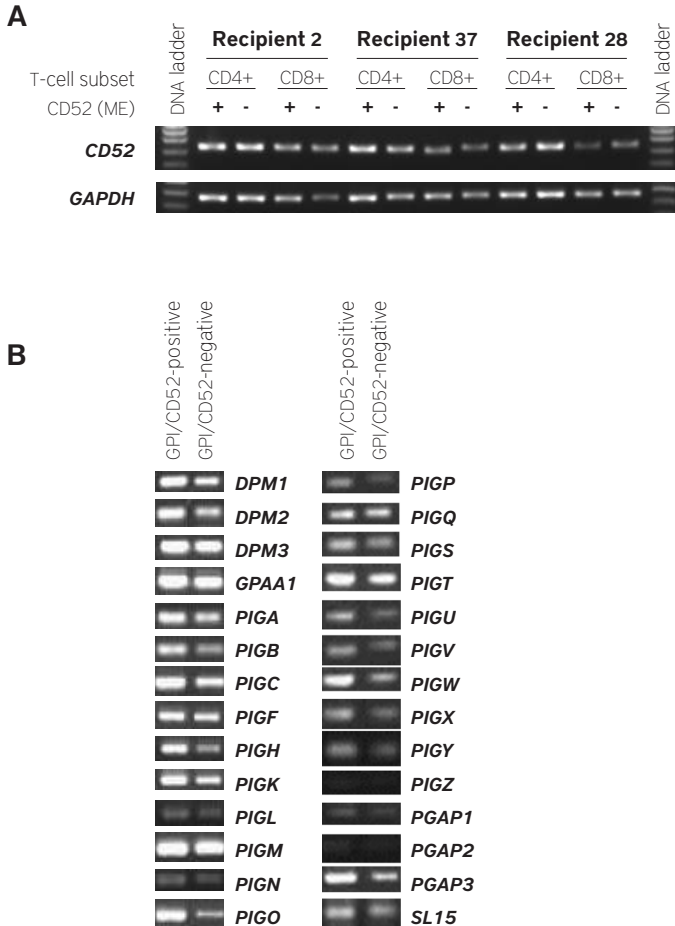| Recipient	HLA	Virus	Protein	Peptide
2	A*02:01	CMV	IE-1	VLEETSVML
28	B*35:01	CMV	pp65	IPSINVHHY
37	B*08:01	CMV	IE-1	QIKVRVDMV
37	B*08:01	EBV	BZLF1	RAKFKQLL

Figure S1. No loss of mRNA expression of CD52 or any of the GPI-anchor synthesis pathway genes in GPI/CD52-negative T cells

(A) Agarose gel electrophoresis results from a representative CD52 mRNA expression analysis of CD4 and CD8 T cells derived from recipients 2, 37, and 28 which were positive (+) or negative (-) for CD52 membrane expression (ME). CD52-negative and CD52-positive CD4 and CD8 T cells were purified by flow cytometric cell sorting, followed by mRNA isolation, cDNA synthesis, and a PCR amplification using specific primers (**Table S2**). Equimolar amounts of cDNA of the CD52-negative and CD52-positive samples were used for PCR amplification. As a control GAPDH was amplified. **(B)** Representative example of mRNA expression analysis for the GPI-anchor synthesis pathway genes performed on FACS purified GPI/CD52-negative and GPI/CD52-positive CD4 T cells from recipient 37. GPI/CD52-negative and GPI/CD52-positive CD4 T cells were purified by FACS, followed by mRNA isolation, and cDNA synthesis. PCR amplification was performed using primer sets specifically designed to individually amplify all 28 proteins involved in the GPI-anchor biosynthesis pathway. Equimolar amounts of cDNA were used for each amplification. Depicted is the agarose gel electrophoresis analysis from the resulting amplicons.

Floris C. Loeff[1]

Kevin Rijs[1]

Esther H.M. van Egmond[1]

Willem H. Zoutman[2]

Xiaohang Qiao[3]

Wilhelmina G.M. Kroes[4]

Sabrina A.J. Veld[1]

Marieke Griffioen[1]

Maarten H. Vermeer[2]

Jacques Neefjes[3,5]

J.H. Frederik Falkenburg[1]

Constantijn J.M. Halkes[1]*

Inge Jedema[1]*

CHAPTER 5

Loss of the GPI-anchor in B-lymphoblastic leukemia by epigenetic downregulation of *PIGH* expression

[1] Department of Hematology - Leiden University Medical Center - Leiden - the Netherlands
[2] Department of Dermatology - Leiden University Medical Center - Leiden - the Netherlands
[3] Division of Cell Biology - the Netherlands Cancer Institute - Amsterdam - the Netherlands
[4] Department of Clinical Genetics - Leiden University Medical Center - Leiden - the Netherlands
[5] Department of Chemical Immunology - Leiden University Medical Center - Leiden - the Netherlands
* C.J.H. and I.J. share senior authorship

ABSTRACT

Adult B-lymphoblastic leukemia (B-ALL) is a hematological malignancy characterized by genetic heterogeneity. Despite successful remission induction with classical chemotherapeutics and novel targeted agents, enduring remission is often hampered by disease relapse due to outgrowth of a pre-existing subclone resistant against the treatment. In this study, we show that small glycophosphatidylinositol (GPI)-anchor deficient CD52-negative B-cell populations are frequently present already at diagnosis in B-ALL patients, but not in patients suffering from other B-cell malignancies. We demonstrate that the GPI-anchor negative phenotype results from loss of mRNA expression of the *PIGH* gene, which is involved in the first step of GPI-anchor synthesis. Loss of *PIGH* mRNA expression within these B-ALL cells follows epigenetic silencing rather than gene mutation or deletion. The coinciding loss of CD52 membrane expression may contribute to the development of resistance to alemtuzumab (ALM) treatment in B-ALL patients resulting in the outgrowth of CD52-negative escape variants. Additional treatment with 5-aza-2'-deoxycytidine may restore expression of CD52 and revert ALM resistance.

INTRODUCTION

Despite introduction of new treatment modalities, such as immunotherapeutics and kinase inhibitors, the survival rate for adult patients with B-lymphoblastic leukemia (B-ALL) remains disappointing due to a high risk of relapse after initial successful induction of complete remission.[1] Relapse often results from outgrowth of subclones carrying mutations that confer resistance to therapy.[2,3]

Incorporation of alemtuzumab (ALM, Campath-1H) in treatment protocols can lead to successful disease control in a wide variety of hematological malignancies.[4-6] In contrast, introduction of ALM as a single drug treatment for B-ALL resulted in only modest clinical efficacy. Despite similarly high membrane expression of the glycophosphatidylinositol (GPI)-anchored ALM target antigen CD52 across all the B-ALL molecular subtypes (with t(4;11) as the only exception),[7] only a minority of the patients achieved an enduring complete remission due to early relapses.[8,9] This could be the result of outgrowth of CD52-negative B-ALL escape variants,[10,11] as demonstrated in a mouse model engrafted with human B-ALL.[10] These CD52-negative B-ALL cells displayed normal *CD52* gene expression, but remarkably loss of CD52 membrane expression coincided with loss of other GPI-linked proteins like CD55 and CD59, indicating that loss of GPI-anchor expression had been the underlying cause. This loss of GPI-anchor expression was not the result of mutations in the X-linked *PIGA* gene,[10] one of 28 genes essential for GPI-anchor synthesis,[12] which causes loss of GPI-anchor expression in paroxysmal nocturnal hemoglobinuria (PNH).[13,14]

The aim of this study was to unravel the mechanisms underlying loss of GPI-anchor expression and coinciding loss of CD52 membrane expression in B-ALL. We show that small pre-existing GPI/CD52-negative B-cell populations are frequently present in peripheral blood (PB) and bone marrow (BM) of B-ALL patients already at diagnosis, but not in patients suffering from other B-cell malignancies or in healthy donor B cells. We demonstrate that loss of mRNA expression of the *PIGH* gene, which is involved in the first step of GPI-anchor synthesis, was the underlying cause of loss of GPI-anchor expression in B-ALL cells. This loss of *PIGH* mRNA expression was not due to genetic aberrations, but rather due to epigenetic silencing. These data describe a new mechanism of loss of GPI-anchor expression. The resulting loss of CD52 membrane expression may confer ALM resistance to B-ALL patients due to the outgrowth of CD52-negative escape variants.

MATERIAL AND METHODS

Patient samples

Residual BM or PB samples from ALM-naive patients with B-ALL, chronic lymphocytic leukemia (CLL), hairy cell leukemia (HCL), or mantle cell lymphoma (MCL) which were taken at diagnosis and stored anonymously were used for this study. Mononuclear cells (MNC) were isolated by Ficoll-Isopaque separation and cryopreserved in Iscove's Modified Dulbecco's Media (IMDM, Lonza, Verviers, Belgium) supplemented with 25% fetal calf serum (FCS, Lonza) and 10% dimethyl sulfoxide (DMSO, Sigma-Aldrich, Zwijdrecht, the Netherlands). MNC isolated from PB of healthy donors were taken as control. The use of these materials for research was approved by the Leiden University Medical Center medical ethical committee.

For one patient (ALL-06), a PB sample taken 1 month after relapse that occurred after ALM-treatment was available. In this patient, successful ALM-treatment, as indicated by the absence of circulating lymphocytes 2 months after treatment initiation, was followed by an early relapse at month 4.

Flow cytometry and cell sorting

GPI-anchor expression was analyzed by flow cytometry on thawed MNC samples stained with the GPI-anchor specific inactivated toxin pro-aerolysin coupled to AlexaFluor488 (FLAER-ALX488, Sanbio, Uden, the Netherlands), allophycocyanin (APC)-conjugated anti-CD52 (ITK diagnostics, Uithoorn, the Netherlands), anti-CD3-phycoerythrin/cyanine7 (ITK) or anti-CD3-PacificBlue (BD, Becton Dickinson, Breda, the Netherlands), and phycoerythrin (PE)-conjugated anti-CD19 (BD) and analyzed on an LSRII (BD) (gating strategy in **Figure S1**). Samples containing FLAER-negative cells, were further characterized by staining with FLAER, anti-CD45-PE (BD), and anti-CD19-APC (BD). FACS-sorting was performed using the same antibodies on a FACSARIA III (BD).

Fluorescent in situ hybridization analysis

High–resolution karyotype analysis on primary B-ALL samples was performed by combined binary ratio labeling fluorescent in situ hybridization as described before.[15] Fluorescent in situ hybridization analysis specific for cytogenetic aberrations t(9;22) and del7q on FACS-sorted GPI-anchor negative (FLAER-) malignant B cells (CD19+/CD45dim) was performed using Vysis probe combinations LSI BCR/ABL ES and D7S486/CEP 7 (both Abbott Molecular, Des Plaines, IL, USA), respectively.

Expression analysis of GPI-anchor synthesis pathway genes

For each patient sample, equal numbers of GPI-anchor negative and positive B cells (range 3000 - 670,000 cells) were isolated from thawed MNC samples by FACS-sorting. mRNA was isolated using the RNAqueous-Micro Kit (Thermo Fisher scientific, Bleiswijk, the Netherlands), which included DNAse treatment, quantified using a spectrophotometer (ND-1000, Thermo Fisher scientific), and completely converted to cDNA using M-MLV transcriptase (Thermo Fisher) and oligo-dT primers. cDNA input was equalized for the different samples using the mRNA Nanodrop measurements as reference (minimum of 6 ng of converted mRNA per sample). PCR amplification was performed using specific primers for the 28 GPI-anchor synthesis genes (**Table S1**) and PWO SuperYield DNA polymerase with a touchdown protocol which consisted of initial denaturing at 95°C (2 min), 7 cycles at 95°C (15 sec), 65°C-58°C with a 1°C decrement per cycle (30 sec), and 72°C (60 sec), 25 cycles at 95°C (15 sec), 58°C (30 sec), and 72°C (60 sec + 5 sec/cycle), and a final extension step at 72°C (7 min).

Expression analysis of the full protein coding region of *PIGH* was performed by amplification using specific primers (**Table S2**) and Phusion Flash High-Fidelity PCR Master Mix (Thermo fisher scientific) with a touchdown protocol which consisted of initial denaturing at 98°C (2 min), 7 cycles at 98°C (1 sec), 65°C-58°C with a 1°C decrement per cycle (5 sec), and 72°C (30 sec), 30 cycles (*PIGH*) or 20 cycles (*GAPDH*) at 98°C (1 sec), 58°C (5 sec), and 72°C (60 sec), and a final extension step at 72°C (7 min). As cDNA loading control, *GAPDH* was amplified.

Cell culture conditions and generation of subcultures

Cell lines Leiden-ALL-BV and Leiden-ALL-HP were generated previously in our laboratory from primary B-ALL cells.[15] B-ALL cell lines were maintained in Iscove's Modified Dulbecco's Media (IMDM, Lonza) supplemented with 6 mg/mL human serum albumin (HSA, Sanquin, Amsterdam, the Netherlands), 10 µg/mL cholesterol, 1 µg/mL insulin, 50 µM 2-mercaptoethanol (all three from Sigma-Aldrich), 200 µg/mL human apo-transferrin (Invitrogen, Carlsbad, Ca, USA), 2 mM glutamine (Lonza), 0.5 µg/mL amphotericin (Bristol-Myers Squibb, Utrecht, the Netherlands) and 50 units/mL penicillin/streptomycin (Lonza).

GPI-anchor negative and GPI-anchor positive subcultures of Leiden-ALL-BV and Leiden-ALL-HP were generated by FACS-sorting using counterstaining with FLAER-ALX488 and APC-conjugated anti-CD52. Upon subsequent expansion the four new subcultures were termed Leiden-ALL-BV-GPI-positive (BV

GPI^{pos}), Leiden-ALL-BV-GPI-negative (BV GPI^{neg}), Leiden-ALL-HP-GPI-positive (HP GPI^{pos}), and Leiden-ALL-HP-GPI-negative (HP GPI^{neg}). Purity of the newly formed subcultures was analyzed by flow cytometry staining with FLAER-ALX488 and APC-conjugated anti-CD52.

Generation of *PIGH*, *PIGA*, and mock expression constructs and retroviral transduction

A construct encoding wt*PIGH* coupled via a GSG linker and a self-cleaving T2A peptide sequence to a truncated form of the nerve growth factor receptor (t*NGFR*), which served as a marker gene, were cloned into the LZRS plasmid. As controls, constructs encoding wt*PIGA* coupled to t*NGFR* (PIGA) or t*NGFR* only (mock) were used. The constructs were transfected into the ϕ-NX-A retroviral packaging cell line using Fugene HD Transfection Reagent (Roche, Woerden, the Netherlands). After 4 days, transfected cells were selected by addition of 2 µg/mL puromycin (Clontech, TaKaRa Bio, Mountain View, CA, USA) to the culture medium. After 24 h, selected cells were further expanded in absence of puromycin for several weeks before supernatant was collected and stored at -80°C.

Retroviral transduction was performed as described before.[16] Supernatant containing the retroviral particles was added to wells of a flat bottom non-tissue culture treated 24-well plate coated with human fibronectin fragments (CH-296, Retronectin, TaKaRa Bio) and centrifuged for 20 min at 3000 x g. After removal of the supernatant, 1.5×10^5 B-ALL cells were added per well and incubated for 24 h at 37°C and 5% CO_2. Transduced cells were transferred to tissue culture treated plates and allowed to expand for 5 days before analysis by flow cytometry, counterstaining with FLAER-ALX488, APC-conjugated anti-CD52, and PE-conjugated anti-NGFR (BD).

PIGH mRNA expression and mutational analysis

mRNA was isolated from 5.0×10^5 cells and partial *PIGH* transcription variants were amplified by PCR using specific primers (**Table S2**) and Phusion Flash High-Fidelity PCR Master Mix using the protocol described above.

For mutational analysis, DNA was isolated from 2.0×10^6 cells using the Gentra Puregene Cell Kit (Qiagen, Venlo, the Netherlands). Amplification of the 10 kbp *PIGH* genomic region was performed using specific primers (**Table S2**) and the Expand Long Template PCR System with the following parameters, initial denaturing at 94°C (5 min), 10 cycles at 94°C (30 sec), 59°C (30 sec), and 68°C (8 min), 30 cycles at

94°C (30 sec), 59°C (30 sec), and 68°C (8 min + 20 sec/cycle), and a final extension step at 72°C (7 min). The resulting product was analyzed by gel electrophoresis using the SmartLadder LF (Eurogentec) as a marker. The correctly sized bands were excised and cleaned using the Wizard SV Gel and PCR Clean-Up System (Promega, Leiden, the Netherlands). Nested PCR's were performed using specific primers (**Table S2**) and PWO SuperYield DNA polymerase with the following parameters, initial denaturing at 94°C (5 min), 10 cycles at 94°C (15 sec), 58°C (30 sec), and 72°C (150 sec), 25 cycles at 94°C (15 sec), 58°C (30 sec), and 72°C (150 sec), and a final extension step at 72°C (7 min). Products from the nested PCR's were analyzed for mutation in the promoter region, exon boundaries, and gene body by Sanger sequencing using the same primers. All Sanger sequencing was performed by Baseclear (Leiden, the Netherlands) and analyzed using Geneious 8 software (Biomatters limited, Auckland, New Zeeland).

Microarray analysis

Total RNA of 2×10^6 cells of subcultures BV GPI[pos], BV GPI[neg], HP GPI[pos], and HP GPI[neg] was isolated using an RNAqueous Total RNA Kit (Thermo Fisher scientific), cleaned using an RNeasy mini kit (Qiagen), and quality checked using Agilent RNA6000 chips and the Agilent Bioanalyser (Santa Clara, CA, USA). RNA was amplified using the TotalPrep RNA amplification kit (Ambion). Samples were analyzed using a whole-genome gene expression direct hybridization assay with Human HT-12 v4 Expression BeadChips on a BeadArray 500GX device (all Illumina, San Diego, CA, USA). Data was analyzed using R 2.15 as described before.[17]

ChIP-qPCR

Chromatin immunoprecipitation (ChIP) was performed as described before.[18] For each subculture 100×10^6 cells were fixed using 1% formaldehyde for 10 min at 20°C. Formaldehyde was quenched by addition of 1/20 volume 2.5 M glycine for 15 min at 20°C. Cells were washed twice using PBS, supernatant was discarded, and the cell pellet was snap frozen at -80°C. The cell pellet was thawed and resuspended in lysis buffer, sonicated twice for 15 min using a Bioruptor (30 sec ON/OFF interval, output high, Diagenode, Seraing, Belgium), and split into four identical samples of which three were incubated with 200 µL Dynabeads Protein G pre-incubated with 5 µg of either anti-histone H3, anti-histone H3K4me3 and anti-histone H3K27me3 overnight at 4°C. The fourth sample was used as untreated reference (refDNA). Beads were washed in a Dynamag-2 magnet (Thermo Fisher scientific) followed by elution (50 mM Tris-HCl, 10 mM EDTA, 1% SDS). All samples were reverse cross-linked by overnight heating at 65°C. DNA was purified using phenol-chloroform extraction. DNA was quantified using a ND-1000 spectrophotometer.

5

Per condition, 5 ng of DNA was analyzed in duplicate by qPCR using specific primers targeting *PIGH* (**Table S2**), FastStart Taq DNA polymerase (Roche), and Evagreen (Biotium, Fremont, CA, USA) using the following protocol, initial denaturing at 95°C (10 min), followed by 45 cycles at 95°C (10 sec), 65°C (30 sec), 72°C (20 sec), and a plate read. *GAPDH* (promoter region) and *MYOD*1 (gene body) were amplified as positive controls for histone marks H3K4me3 or H3K27me3, respectively. qPCR analysis was performed on a LightCycler-480 (Roche). An average Ct-value was calculated from the duplicate measurement. For the positive control genes an average Ct-value was calculated from the two primer sets. Presence of *PIGH* coding DNA in the histone mark ChIP DNA samples relative to refDNA and normalized for a positive control gene (*GAPDH* for H3K4me3, *MYOD1* for H3K27me3) was calculated using the $2^{-\Delta\Delta Ct}$ method,[19] where $\Delta\Delta Ct = (Ct_{PIGH} - Ct_{GAPDH \text{ or } MYOD1})_{refDNA} - (Ct_{PIGH} - Ct_{GAPDH \text{ or } MYOD1})_{ChIPDNA}$. The difference between the GPI^{neg} and GPI^{pos} subcultures of Leiden-ALL-BV or Leiden-ALL-HP were calculated by dividing the $2^{-\Delta\Delta Ct}$ from the GPI^{neg} sample by the $2^{-\Delta\Delta Ct}$ from the GPI^{pos} sample. Results were normalized for the GPI^{pos} subcultures.

Promoter methylation analysis

DNA was extracted using the QIAamp DNA Blood Mini Kit (Qiagen) and 1 µg was bisulfite-converted using the EZ DNA Methylation Kit (Zymo Research, Orange, CA, USA). Amplification and methylation specific melting curve analysis (MS-MCA) was performed by using specific primers (**Table S2**) on a CFX384 Touch Real-Time PCR Detection System (Bio-Rad, Veenendaal, the Netherlands) using a touchdown PCR protocol with the following parameters, initial denaturing at 95°C (30 sec), 7 cycles at 95°C (30 sec), 65°C-58°C with a 1°C decrement per cycle (40 sec), and 72°C (40 sec), following by 33 cycles at 95°C (30 sec), 60°C (40 sec), and 72°C (40 sec), and a final extension step at 72°C (3 min). Following amplification, melting curves were acquired in the presence of iQ SYBR Green Supermix (Bio-Rad) during a linear temperature transition from 65°C to 90°C with increments of 0.2°C/10 sec. Bisulfite converted CpGenome Universal Methylated DNA (Chemicon, Hampshire, United Kingdom) and unmethylated male DNA were used as references. Methylation levels of individual CpGs were analyzed by Sanger sequencing (ratio between height of cytosine signal relative to thymine signal).

Demethylation assay

For each subculture, 1.0×10^5 cells were cultured in 200 µL medium with or without 0.5 µM 5-aza-2'-deoxycytidine (5-aza, Vidaza, Pharmion Corporation, Boulder, CO, USA) for 15 days. Daily, 100 µL culture supernatant was replaced with 100 µL fresh medium containing 1.0 µM 5-aza. Presence of GPI-positive cells was evaluated by flow cytometry using counterstaining with FLAER-ALX488.

RESULTS

**GPI/CD52-deficient cells are commonly present in B-ALL,
but not in other B-cell malignancies**

To examine whether pre-existing populations of GPI/CD52-negative malignant B cells were already present at diagnosis in patients with B-ALL who had not previously received ALM-treatment, we screened primary PB (n = 13) or BM (n = 12) samples from 25 patients with B-ALL who carried various cytogenetic aberrations (**Table 1**). In 13/22 evaluable samples (both PB and BM) clear (>0.025%) GPI-anchor negative populations (median 0.25%) were detected within the B-cell compartment (representative examples in **Figure 1**; aggregated result in **Table 1**). These GPI-anchor negative B cells consistently lacked CD52 membrane expression. Detailed flow cytometric analysis demonstrated that the GPI-anchor negative B cells were present in the malignant (CD45dim) but not in normal B-cells (CD45bright) within the same sample (representative examples for three cases in **Figure S2**). The malignant nature of the GPI-anchor negative B cells was further confirmed for these three B-ALL cases by flow cytometric cell sorting of the GPI-anchor negative populations and subsequent FISH analysis. The GPI-anchor negative B cells contained the same cytogenetic aberrations as the bulk of the malignancy (del7q for ALL-03, and t(9;22) for ALL-05 and ALL-12) (data not shown). In the samples of three patients carrying a mixed-lineage leukemia (MLL) translocation t(4;11) (samples 23-25) an atypical pattern of low GPI-anchor expression was observed (**Figure S3**), hampering proper discrimination of potential GPI-anchor negative B cells. The GPI-anchor positive B-cells within the other B-ALL samples displayed broad, but clearly positive CD52 expression patterns (**Table 1**), with the exception of sample ALL-08. Whereas the presence of GPI/CD52-negative cells in the malignant B cell populations was a frequent event, within the T cells of the same samples no clear GPI/CD52-negative cells were detected (representative examples in **Figure 1**). No overt GPI/CD52-negative B-cells were found in PB samples from healthy donors (n = 6, representative examples in **Figure S4**). To investigate whether GPI/CD52-negative cells were common in patients carrying B-cell malignancies, we screened samples from patients with CLL (PB, n = 5), HCL (PB, n = 5; spleen, n = 1), and MCL (PB, n = 2; BM, n = 2) taken at diagnosis. No GPI/CD52-negative cells were detected within these malignant B cells (**Figure S5**).

For one patient (ALL-06), material taken at diagnosis and material of the relapse that occurred after ALM-treatment was available for analysis. An enlarged GPI/CD52-negative B-cell population (32.5%) was found in the sample taken 1 month after relapse (**Figure S6**).

These data demonstrate that the presence of GPI/CD52-negative B-cells is a frequent event in B-ALL, but not in other B-cell malignancies and in healthy donor B cells.

Loss of *PIGH* mRNA expression in GPI-anchor negative primary B-ALL cells

To unravel the underlying mechanism resulting in GPI-anchor deficiency within GPI/CD52-negative B-ALL cells, we performed mRNA expression analysis for all 28 genes that are essential for GPI-anchor synthesis in FACS purified GPI-anchor negative B-ALL cells (from ALL-01, ALL-04, and ALL-05), using GPI-anchor positive B cells from the same samples as controls. In all three cases, no *PIGH* mRNA expression was detected in the GPI-anchor negative cells, whereas normal *PIGH* mRNA expression was detected in the GPI-anchor positive cells (**Figure 1B**, representative example). Transcriptional activity for all other 27 GPI-anchor synthesis genes was observed in both the GPI-anchor negative and positive cell populations.

Table 1. GPI-anchor deficiency in B-lymphoblastic leukemia

Sample	Number of B-cells screened	GPI^{neg}/CD52^{neg} B-cells (%)*	CD52 expression of GPI^{pos} B cells (MFI)	Sample type	Cytogenetic abnormalities**
ALL-01	260,013	5.46	1139	PB	t(9;22)
ALL-02	1,163,689	3.99	999	PB	t(9;22)
ALL-03	262,365	2.26	707	PB	Del 7q
ALL-04	533,748	0.92	973	PB	
ALL-05	711,323	0.66	605	BM	t(9;22)
ALL-06	813,639	0.38	2033	BM	
ALL-07	369,534	0.25	1390	BM	t(9;22)
ALL-08	860,812	0.19	57	BM	Trisomy 5 and 20
ALL-09	500,711	0.10	775	PB	
ALL-10	298,157	0.04	1604	PB	Hypodiploid
ALL-11	1,073,541	0.04	1654	BM	t(9;22)
ALL-12	608,951	0.03	1333	BM	t(9;22)
ALL-13	736,663	0.03	1967	PB	t(9;22)
ALL-14	230,537	< 0.025	1172	PB	
ALL-15	621,516	< 0.025	628	BM	Hyperdiploid
ALL-16	334,908	< 0.025	754	BM	
ALL-17	303,145	< 0.025	1734	PB	t(9;22)
ALL-18	411,442	< 0.025	755	BM	t(9;22)
ALL-19	253,089	< 0.025	4563	BM	
ALL-20	481,892	< 0.025	1731	PB	t(9;22), hyperdiploid
ALL-21	643,042	< 0.025	236	BM	t(9;22)
ALL-22	856,455	< 0.025	1089	PB	
ALL-23	456,449	***	***	BM	t(4;11), MLL
ALL-24	596,098	***	***	PB	t(4;11), MLL
ALL-25	527,922	***	***	PB	t(4;11), MLL

MFI, median fluoresce intensity; BM, bone marrow; PB, peripheral blood

* A cut-off percentage of 0.025% was used to exclude back-ground events

** Most frequent cytogenetic aberration

*** Not able to discriminate (see **Figure S3***)*

To explore whether absence of *PIGH* mRNA expression was a common phenomenon in GPI-anchor negative B-ALL cells, mRNA expression analysis for the protein-coding region of *PIGH* was performed in purified GPI-anchor negative B-cells derived from PB (n = 4) or BM (n = 4) samples of eight patients. Absence of *PIGH* mRNA expression was observed within the GPI-anchor negative cells and not within the GPI-anchor positive cells for all patients (**Figure 1C**).

These data show that loss of *PIGH* mRNA expression is a common phenomenon and associated with the GPI-anchor negative phenotype in B-ALL cells.

GPI-anchor expression is restored by enforced *PIGH* expression

To assess whether absence of *PIGH* mRNA expression was the sole cause of the GPI-anchor negative phenotype in B-ALL cells, we restored *PIGH* expression by retroviral transduction. We used cell lines Leiden-ALL-BV and Leiden-ALL-HP which were generated from primary B-ALL cells of samples ALL-02 and ALL-06 (after relapse following ALM-treatment), respectively. These cell lines contained 10.4% (Leiden-ALL-BV) and 0.4% (Leiden-ALL-HP) GPI-anchor negative cells. GPI-anchor negative and GPI-anchor positive subpopulations were purified by FACS-sorting (**Figure S7**). The GPI-anchor phenotype of these subcultures was stable during culturing. Absence of *PIGH* mRNA within GPI-anchor negative, but not within GPI-anchor positive subcultures was shown by mRNA expression analysis (**Figure S8**). In contrast, identical transcriptional activity was observed between the GPI-anchor negative and positive subcultures for the remaining GPI-anchor synthesis genes (**Figure S9**). High levels of *CD52* mRNA were present in both the GPI-anchor negative and positive subcultures (**Figure S9**). Restored GPI-anchor and coinciding CD52 membrane expression was observed in the GPI-anchor negative subcultures upon retroviral transduction with a construct encoding *PIGH*, but not with *PIGA* or a mock construct (**Figure 2A**). In the GPI-anchor positive subcultures no effect on GPI-anchor or CD52 membrane expression was observed upon transduction (**Figure 2B**).

In conclusion, the GPI-anchor negative phenotype in B-ALL cells was solely mediated by absence of *PIGH* mRNA expression.

Loss of *PIGH* mRNA expression does not result from a genetic aberration

To investigate if genetic aberrations resulted in loss of *PIGH* mRNA expression in GPI-anchor negative B-ALL cells, we first tested whether the inability to detect *PIGH* mRNA expression in the GPI-anchor

Figure 1. Loss of GPI/CD52-expression is due to absence of *PIGH* mRNA expression in B-ALL samples at diagnosis

(A) Four representative flow cytometric analyses of GPI-anchor (FLAER) and CD52 membrane expression on B cells (CD19+CD3-, left panels) or T cells (CD3+CD19-, right panels) in MNC samples taken at diagnosis from patients with B-ALL. The percentages of GPI/CD52-negative cells are indicated. **(B)** Representative example of mRNA expression analysis for the 28 genes comprising the GPI-anchor synthesis pathway on equimolar amounts of cDNA from GPI/CD52-negative (GPI^{neg}) and GPI/CD52-positive (GPI^{pos}) B cells purified from MNC sample ALL-04. **(C)** mRNA expression analyses of the *PIGH* protein-coding region (717 bp) performed on equimolar amounts of cDNA from purified GPI^{neg} and GPI^{pos} B cells from PB (n = 4, left panels) or BM (n = 4, right panels) samples of patients with B-ALL, using *GAPDH* (351 bp) as a loading control (M defines the marker lane).

A

B cells   T cells

ALL-03
ALL-04
ALL-13
ALL-20

CD52 / FLAER
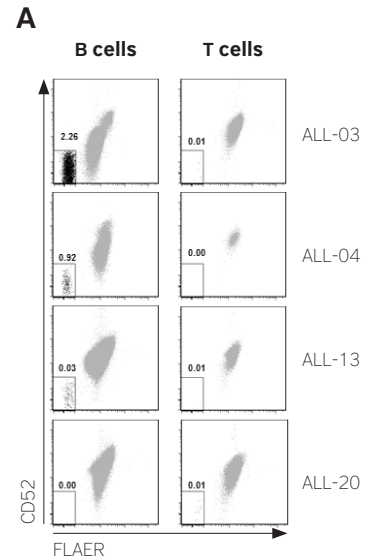
Figure 2. Retroviral transduction with *PIGH*, and genomic analysis of the *PIGH* gene loci in the GPI^{neg} and GPI^{pos} B-ALL subcultures

Flow cytometric analysis of GPI-anchor (FLAER) and CD52 membrane expression in **(A)** GPI^{neg} and **(B)** GPI^{pos} subcultures of cell lines Leiden-ALL-BV (BV-GPI^{neg} and BV-GPI^{pos}) and Leiden-ALL-HP (HP-GPI^{neg} and HP-GPI^{pos}) retrovirally transduced with an empty control construct (mock) or with constructs encoding *PIGA* or *PIGH*, coupled to *tNGFR* as marker gene. Transduction efficiency ranged between 13.6% and 52.9%. Dot plots are gated on tNGFR positive cells. **(C)** Schematic representation of analyses performed on DNA and mRNA isolated from GPI^{neg} and GPI^{pos} subcultures of cell lines Leiden-ALL-BV (BV-GPI^{neg} and BV-GPI^{pos}) and Leiden-ALL-HP (HP-GPI^{neg} and HP-GPI^{pos}). The *PIGH* genomic locus (chromosome 14:67601700-67588700, GRCh38.p7) is shown, numbered black boxes represent coding exons connected by straight black lines representing intronic regions. SNPs rs12893796 and rs11547225 (dbSNP build 144) are depicted by triangles.

A

Mock   *PIGA*   *PIGH*

BV GPI^{neg}
HP GPI^{neg}

CD52 / FLAER

B

Mock   *PIGA*   *PIGH*

BV GPI^{pos}
HP GPI^{pos}

CD52 / FLAER

PCR amplicons are numbered and indicated as stripped lines connecting the relevant primers (arrows). mRNA transcription variants are depicted by boxes connected with curved lines and identified by their Ensemble transcript number. The protein coding transcript is in black, predicted protein coding mRNA transcription variants are in grey. Closed boxes illustrate the protein coding region and open boxes the 5' and 3' untranslated regions.
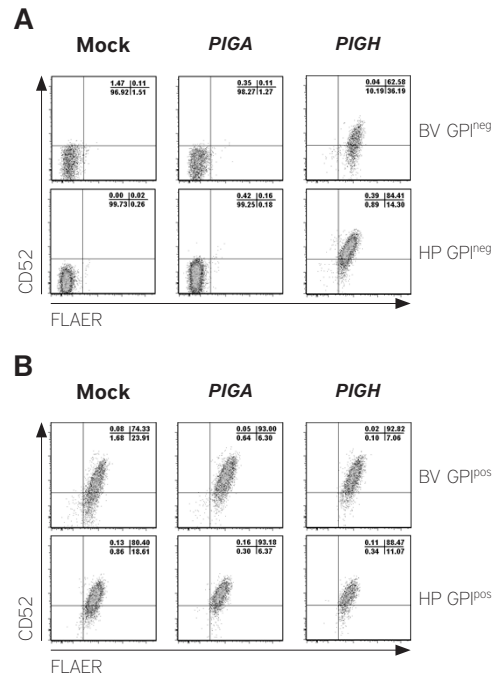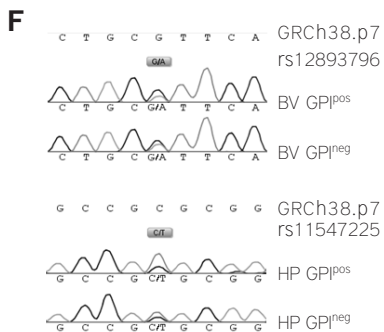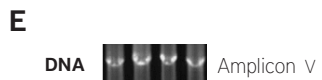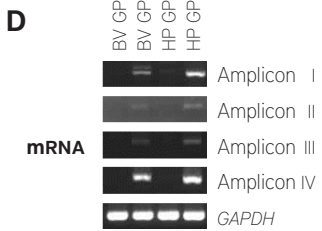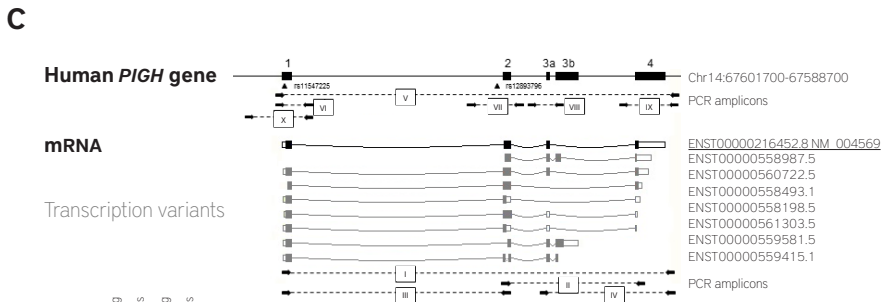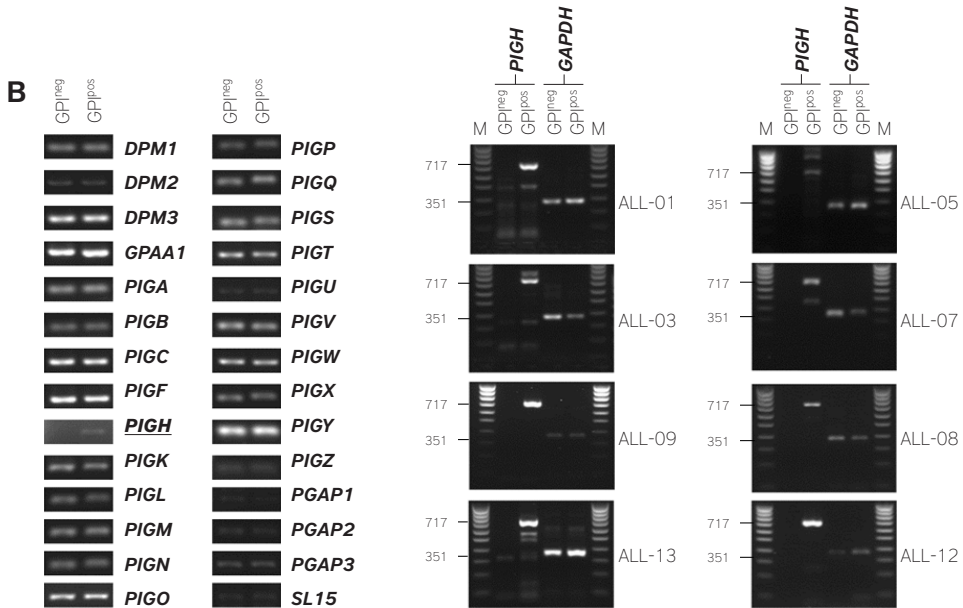
(D, E) Gel electrophoresis results for the indicated PCR amplifications on (D) mRNA or (E) DNA isolated from the GPI^neg and GPI^pos subcultures (*GAPDH* as loading control). (F) Sanger sequencing results from nested PCR amplifications VII (Leiden-ALL-BV) and VI (Leiden-ALL-HP) with assembly GRCh38.p7 as reference sequence. SNPs rs12893796 and rs11547225 are presented as grey boxes containing the allelic variants.

negative subcultures of the Leiden-ALL-BV and -HP cell lines was the result of loss of a primer binding site due to alternative splicing of the pre-mRNA. We performed PCR specific for sections of *PIGH* mRNA that include all possible transcription variants (**Figure 2C**, amplicons I-IV). No amplicons were generated for the GPI-anchor negative subcultures, whereas all amplicons were generated for the GPI-anchor positive subcultures (**Figure 2D**). This shows that inability to detect *PIGH* mRNA in GPI-anchor negative subcultures was due to complete absence of *PIGH* mRNA expression.

To examine if loss of *PIGH* mRNA expression in the GPI-anchor negative subcultures resulted from genomic deletion of *PIGH*, we performed PCR using primers designed to amplify the complete 10 kbp *PIGH* genomic region (**Figure 2C**, amplicon V). Amplicons of the correct size were obtained for both the GPI-anchor negative and positive subcultures (**Figure 2E**), indicating that the gene was present at the genomic level with no detectable deletions or insertions. Nested PCR (**Figure 2C**, amplicons VI-VII) followed by Sanger sequencing identified two single nucleotide polymorphisms (SNP, rs12893796 in Leiden-ALL-BV, rs11547225 in Leiden-ALL-HP) for which both allelic variants were detected in the GPI-anchor positive subcultures. Both allelic variants were also detected in the GPI-anchor negative subcultures (**Figure 2F**), indicating that both alleles of the *PIGH* gene had been amplified and thus were present at the genomic level. Absence of a focal genomic deletion was further implied by comparable transcriptional activity of genes proximal to the *PIGH* genetic locus in the GPI-anchor positive and negative subcultures (**Figure S10**).

To investigate if a mutation, small deletion, or insertion in the promoter region (starting 630 bp before the transcription start site), at one of the splice sites, or in the gene body was the cause of loss of *PIGH* mRNA expression, we examined these genetic loci by Sanger sequencing (**Figure 2C**, amplicons VII-X). No differences in DNA sequences were found between the GPI-anchor negative and positive subcultures. Within each amplicon, at least one known SNP was identified for which both allelic variants were detected (data not shown). These SNPs were always detected in both the GPI-anchor negative and positive subcultures, indicating that each analyzed amplicon originated from both alleles of the *PIGH* gene.

In summary, the intact *PIGH* gene was present in both GPI-anchor negative B-ALL subcultures, illustrating that loss of *PIGH* expression in these cells could not be explained by obvious genetic aberrations in the coding gene.

Loss of *PIGH* mRNA could be explained by epigenetic control of gene transcription

To explore whether loss of *PIGH* mRNA expression in GPI-anchor negative B-ALL cells resulted from epigenetic down regulation, we analyzed the presence of two predominant types of histone modifications at the *PIGH* gene locus. We considered histone mark H3K4me3, of which presence is strongly correlated with actively transcribed genes, and histone mark H3K27me3, of which presence correlates with transcriptional gene silencing.[20] We performed H3K4me3 and H3K27me3 specific ChIP on DNA isolated from the GPI-anchor negative subcultures, using the GPI-anchor positive subcultures as references, followed by qPCR to quantify the relative presence of these histone marks at the *PIGH* gene locus. Almost complete loss of histone mark H3K4me3 from the *PIGH* promoter region was found in both GPI-anchor negative subcultures (**Figure 3A**). In contrast, presence of histone mark H3K27me3 was increased in both GPI-anchor negative subcultures, with the largest effect between the Leiden-ALL-BV subcultures (**Figure 3A**). These data imply that the *PIGH* gene in the GPI-anchor negative subcultures was transcriptionally silenced.

Histone modifications are only one part of the interrelated epigenetic code that directs gene transcription. To further investigate whether loss of *PIGH* mRNA expression resulted from epigenetic down regulation of gene transcription, we analyzed the level of DNA methylation at the *PIGH* promoter region, which contains a CpG-island. We performed MS-MCA (**Figure 3B**) and Sanger sequencing (**Figure 3C**) on bisulfite converted DNA from the GPI-anchor negative and positive subcultures. In the GPI-anchor positive subcultures, mono-allelic DNA methylation (Leiden-ALL-BV) and unmethylated DNA (Leiden-ALL-HP) were observed by MS-MCA, compatible with transcriptional activity of at least one allele and expression of *PIGH* mRNA. Since Sanger sequencing cannot distinguish between individual alleles, average levels from the two alleles were measured resulting in mostly intermediate (Leiden-ALL-BV) and low (Leiden-ALL-HP) levels of methylation at individual CpGs. In the GPI-anchor negative subculture of Leiden-ALL-BV, a shift toward high level of DNA methylation was observed by MS-MCA and by Sanger sequencing, consistent with bi-allelic DNA methylation and loss of *PIGH* transcription. In the GPI-anchor negative subculture of Leiden-ALL-HP, a shift away from unmethylated was observed by MS-MCA, indicating partial methylation of the analyzed region, and Sanger sequencing analysis showed high levels of methylation in the region directly preceding the transcription start site (TSS) (CpG -11 to -6), but not in the bordering CpGs. Since high levels of methylation in this region were shared between the GPI-anchor negative subcultures of both Leiden-ALL-BV and Leiden-ALL-HP, CpGs at this position are likely to be essential for regulation of *PIGH* transcription and function as a so-called CpG "traffic light".[21]

No CpG methylation was detected at the *PIGH* promoter region in bisulfite converted DNA from purified healthy donor B cells, further highlighting the abnormal DNA methylation in B-ALL cells.

To test if *PIGH* promoter methylation is essential in retaining the GPI-anchor negative phenotype in B-ALL cells, we tested whether treatment of the GPI-anchor negative subcultures with the demethylating agent 5-aza would restore GPI-anchor expression. Gradual increase of the percentages of GPI-anchor positive cells was observed over time in samples treated with 5-aza in the GPI-anchor negative subcultures, and not in samples incubated without 5-aza (**Figure 3D**).

This illustrates that epigenetic down regulation of *PIGH* mRNA transcription results in loss of GPI-anchor expression in B-ALL cells and can be reverted by 5-aza treatment.
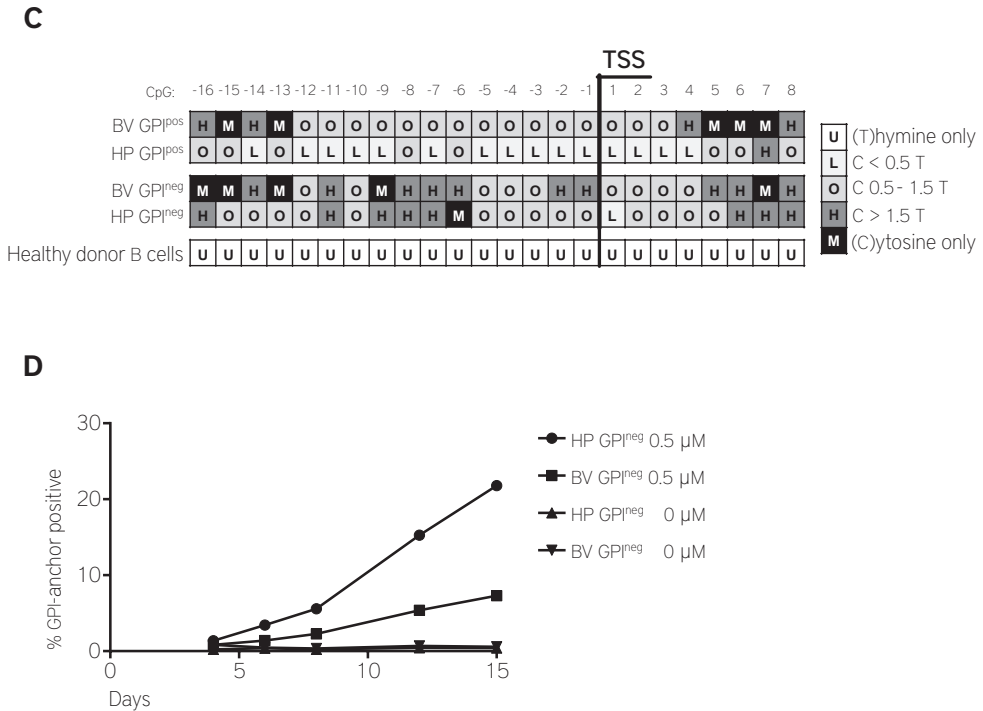
C

D
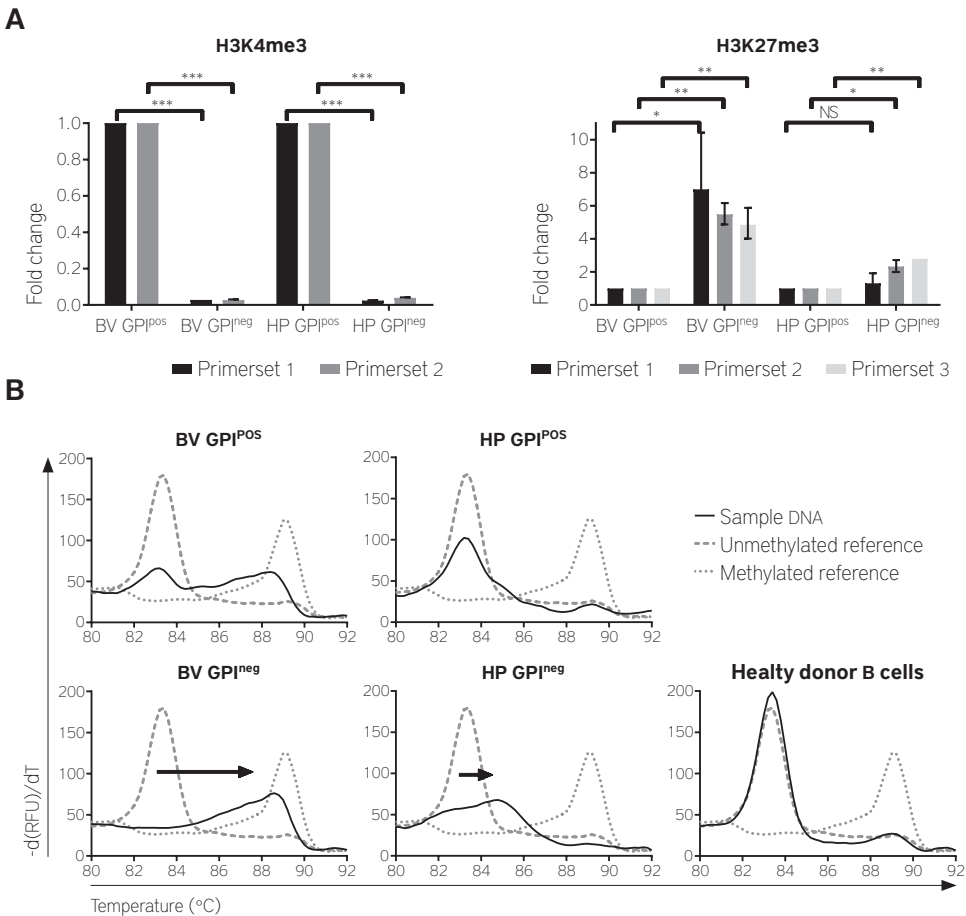
Figure 3. Epigenetic down regulation of *PIGH* gene transcription in GPI[neg] B-ALL subcultures

(A) ChIP–qPCR analysis of the relative presence of histone marks H3K4me3 and H3K27me3 at the *PIGH* gene location in the GPI[neg] subcultures compared to the GPI[pos] subcultures of Leiden-ALL-BV and Leiden-ALL-HP. *PIGH* DNA was quantified in H3K4me3 and H3K27me3 ChIP samples by qPCR and compared to a non-immunoprecipitated DNA reference sample (refDNA) and normalized for a positive control gene (*GAPDH* for H3K4me3 and *MYOD1* for H3K27me3). Bars represent the relative presence of *PIGH* DNA in the GPI[neg] compared to the GPI[pos] subcultures (whiskers represent standard deviation; * P < 0.05, ** P < 0.01, *** P < 0.001, NS = not significant; two-sided unpaired T-test). Primer set 1 (targeting the region 246 bp to 371 bp downstream of the TSS) and primer set 2 (329 bp to 496 bp downstream of the TSS) used for qPCR of H3K4me3 targeted the *PIGH* promoter region. Primer set 1 used for qPCR of H3K4me3 doubled as primer set 1 for qPCR of H3K27me3. Primer set 2 (4486 bp to 4570 bp downstream of the TSS) and primer set 3 (6261 bp to 6373 bp downstream of the TSS) used for qPCR of H3K27me3 targeted the *PIGH* gene body. **(B)** MS-MCA curves for the *PIGH* promoter region (-212 bp to +101 bp relative to the TSS, CpGs -19 to +15) on bisulfite converted DNA from the GPI[pos] and GPI[neg] B-ALL subcultures (solid black line). Bisulfite converted DNA from purified healthy donor B cells served as a control. MS-MCA curves for unmethylated reference DNA (striped gray line, peak Tm 83.4°C) and methylated reference DNA (dotted grey line, peak Tm 89.0°C) are plotted in each graph. **(C)** Sanger sequencing analysis of the methylation state of 24 individual CpGs in the *PIGH* promoter region (-161 bp to +51 bp relative to the TSS, CpGs -16 to +8) on bisulfite converted DNA from the GPI[pos] and GPI[neg] B-ALL subcultures and from purified healthy donor B cells. The levels of methylation of individual CpGs were determined by the ratio between the height of the cytosine signal and the thymine signal. **(D)** Percentages of GPI-anchor positive cells in the GPI[neg] B-ALL subcultures following treatment with or without 0.5 µM 5-aza for 15 days as analyzed by flow cytometry counterstaining with FLAER.

DISCUSSION

Durable remission in patients with B-ALL is often hampered by early disease relapse due to outgrowth of pre-existing subclones resistant to treatment.[2,3] In this study, we showed that small GPI/CD52-negative B-cell populations were found already at diagnosis in the majority of patients with B-ALL at frequencies that are in line with previous reports.[10,11] We showed that GPI-anchor negative B-cell populations were present in B-ALL patients carrying various cytogenetic abnormalities, implying that this phenotype can be acquired independent of the primary cause of malignant transformation. Nevertheless, these cells are part of the malignancy as demonstrated by their phenotype and genotype, and their presence within the cell lines generated from primary malignant B-ALL cells. No GPI-anchor negative B cells were detected in leukemic samples from patients suffering from mature B-cell malignancies such as CLL, HCL, and MCL, suggesting that the GPI-anchor negative phenotype in B-ALL develops as result of a cellular process that is part of the early stage of B-cell maturation in which B-ALL cells are arrested.

Considering the low frequencies of GPI-anchor negative cells in B-ALL, loss of GPI-anchor expression and coinciding loss of the GPI-anchor associated proteins unlikely provides a direct significant clonal growth advantage. This notion is supported by knock-out experiments in mice which demonstrated that GPI-anchor negative lymphocytes do not have intrinsic survival or growth benefits.[22,23] However, loss of the GPI-anchored protein CD52 renders the cells resistant to the CD52-targeting therapeutic antibody ALM, as demonstrated by outgrowth of GPI/CD52-negative escape variants mice engrafted with human B-ALL.[10] This may explain why ALM mono-therapy displays only limited efficacy in treatment of B-ALL.[8,9]

In PNH, lack of GPI-anchor expression is linked to a defect in the *PIGA* gene. We have previously shown that no mutations were present in *PIGA* in GPI-anchor negative B-ALL cells.[10] Here, we demonstrated that the GPI-anchor negative phenotype in B-ALL cells resulted from loss of *PIGH* mRNA expression. The *PIGH* gene is essential in GPI-anchor synthesis as was previously shown in a CRISPR-Cas9 knock-out screen.[12] Our study is the first to associate an anomaly related to the *PIGH* gene with a hematological disorder. Exploration of cancer genome databases did not yield an association between a genetic anomaly in *PIGH* and B-ALL (or any other malignancy), potentially as a result of the small contribution of the GPI-anchor negative cells to the total malignancy.

In contrast to the X-linked *PIGA*, *PIGH* is an autosomal gene located on chromosome 14q24.1, implying that two affected alleles are required for complete loss of *PIGH* mRNA expression. Molecular analysis revealed that epigenetic silencing rather than gene mutation or deletion resulted in loss of *PIGH* mRNA expression. Epigenetic silencing of tumor suppressor genes is a frequent event in cancer. B-ALL cells may be particularly affected by this mechanism as they are arrested in an early stage of B-cell development at which major epigenetic changes take place to lock-in the lineage commitment and to initiate and maintain allelic exclusion of one of the immunoglobulin genes.[24,25] Continued exposure to cellular processes triggering these epigenetic changes may lead to silencing of genes that are normally unaffected. In concordance, genome-wide *de novo* promoter DNA methylation was recently shown to be common in pediatric patients with B-ALL.[26,27]

Crosstalk between the various components of the epigenetic code and transcription factors renders it difficult to predict whether active gene silencing, via direct targeting by histone-modifying enzymes or DNA methyltransferases, or passive gene silencing, following the loss of an activating transcription factor or gain of a transcription repressor, had initiated silencing of *PIGH* gene transcription.[26,28-30] Irrespective of the mechanism, we demonstrated that silenced *PIGH* gene expression could be reversed in B-ALL cells, as illustrated by re-expression of the GPI-anchor following treatment with the epigenetic modifying agent 5-aza. Therefore, addition of epigenetic modifying drugs to ALM monotherapy may prevent ALM resistance.

In summary, the majority of patients with B-ALL harbor a small GPI/CD52-negative B-cell population already at diagnosis. These cells lost *PIGH* mRNA expression, a key component in GPI-anchor synthesis. This was not due to a genomic aberration, but rather to epigenetic silencing of *PIGH* gene transcription. Selective pressure provided by ALM-treatment may result in the outgrowth of GPI/CD52-negative escape variants in B-ALL patients and may be canceled by additional 5-aza-2'-deoxycytidine treatment.

REFERENCE LIST

1.	Fielding AK, Richards SM, Chopra R, et al. Outcome of 609 adults after relapse of acute lymphoblastic leukemia (ALL); an MRC UKALL12/ECOG 2993 study. *Blood*. 2007;109(3):944-950.

2.	Mullighan CG, Phillips LA, Su X, et al. Genomic analysis of the clonal origins of relapsed acute lymphoblastic leukemia. *Science*. 2008;322(5906):1377-1380.

3.	Hunger SP, Mullighan CG. Redefining ALL classification: toward detecting high-risk ALL and implementing precision medicine. *Blood*. 2015;125(26):3977-3987.

4.	Alinari L, Lapalombella R, Andritsos L, Baiocchi RA, Lin TS, Byrd JC. Alemtuzumab (Campath-1H) in the treatment of chronic lymphocytic leukemia. *Oncogene*. 2007;26(25):3644-3653.

5.	Moreton P, Hillmen P. Alemtuzumab therapy in B-cell lymphoproliferative disorders. *Semin Oncol*. 2003;30(4):493-501.

6.	Zinzani PL, Corradini P, Gallamini A, et al. Overview of alemtuzumab therapy for the treatment of T-cell lymphomas. *Leuk Lymphoma*. 2012;53(5):789-795.

7.	Golay J, Cortiana C, Manganini M, et al. The sensitivity of acute lymphoblastic leukemia cells carrying the t(12;21) translocation to campath-1H-mediated cell lysis. *Haematologica*. 2006;91(3):322-330.

8.	Angiolillo AL, Yu AL, Reaman G, Ingle AM, Secola R, Adamson PC. A phase II study of Campath-1H in children with relapsed or refractory acute lymphoblastic leukemia: a Children's Oncology Group report. *Pediatr Blood Cancer*. 2009;53(6):978-983.

9.	Gorin NC, Isnard F, Garderet L, et al. Administration of alemtuzumab and G-CSF to adults with relapsed or refractory acute lymphoblastic leukemia: results of a phase II study. *Eur J Haematol*. 2013;91(4):315-321.

10.	Nijmeijer BA, van Schie ML, Halkes CJ, Griffioen M, Willemze R, Falkenburg JH. A mechanistic rationale for combining alemtuzumab and rituximab in the treatment of ALL. *Blood*. 2010;116(26):5930-5940.

11.	Araten DJ, Sanders KJ, Anscher D, Zamechek L, Hunger SP, Ibrahim S. Leukemic blasts with the paroxysmal nocturnal hemoglobinuria phenotype in children with acute lymphoblastic leukemia. *Am J Pathol*. 2012;181(5):1862-1869.

12.	Koike-Yusa H, Li Y, Tan EP, Velasco-Herrera Mdel C, Yusa K. Genome-wide recessive genetic screening in mammalian cells with a lentiviral CRISPR-guide RNA library. *Nat Biotechnol*. 2014;32(3):267-273.

13.	Ware RE, Rosse WF, Howard TA. Mutations within the Piga gene in patients with paroxysmal nocturnal hemoglobinuria. *Blood*. 1994;83(9):2418-2422.

14.	Rosse WF. Paroxysmal nocturnal hemoglobinuria as a molecular disease. *Medicine (Baltimore)*. 1997;76(2):63-93.

15.	Nijmeijer BA, Szuhai K, Goselink HM, et al. Long-term culture of primary human lymphoblastic leukemia cells in the absence of serum or hematopoietic growth factors. *Exp Hematol*. 2009;37(3):376-385.

16. Loeff FC, van Egmond HME, Nijmeijer BA, Falkenburg JHF, Halkes CJ, Jedema I. Complement-dependent cytotoxicity induced by therapeutic antibodies in B-cell acute lymphoblastic leukemia is dictated by target antigen expression levels and augmented by loss of membrane-bound complement inhibitors. *Leuk Lymphoma*. 2017;58(9):1-14.

17. Pont MJ, Honders MW, Kremer AN, et al. Microarray Gene Expression Analysis to Evaluate Cell Type Specific Expression of Targets Relevant for Immunotherapy of Hematological Malignances. *PLoS One*. 2016;11(5):e0155165.

18. Schmidt D, Wilson MD, Spyrou C, Brown GD, Hadfield J, Odom DT. ChIP-seq: using high-throughput sequencing to discover protein-DNA interactions. *Methods*. 2009;48(3):240-248.

19. Livak KJ, Schmittgen TD. Analysis of relative gene expression data using real-time quantitative PCR and the 2(-Delta Delta C(T)) Method. *Methods*. 2001;25(4):402-408.

20. Barski A, Cuddapah S, Cui K, et al. High-resolution profiling of histone methylations in the human genome. *Cell*. 2007;129(4):823-837.

21. Medvedeva YA, Khamis AM, Kulakovskiy IV, et al. Effects of cytosine methylation on transcription factor binding sites. *BMC Genomics*. 2014;15:119.

22. Kulkarni S, Bessler M. The effect of GPI-anchor deficiency on apoptosis in mice carrying a Piga gene mutation in hematopoietic cells. *J Leukoc Biol*. 2002;72(6):1228-1233.

23. Keller P, Tremml G, Rosti V, Bessler M. X inactivation and somatic cell selection rescue female mice carrying a Piga-null mutation. *Proc Natl Acad Sci U S A*. 1999;96(13):7479-7483.

24. Cedar H, Bergman Y. Epigenetics of haematopoietic cell development. *Nat Rev Immunol*. 2011;11(7):478-488.

25. Lee ST, Xiao Y, Muench MO, et al. A global DNA methylation and gene expression analysis of early human B-cell development reveals a demethylation signature and transcription factor network. *Nucleic Acids Res*. 2012;40(22):11339-11351.

26. Burke MJ, Bhatla T. Epigenetic modifications in pediatric acute lymphoblastic leukemia. *Front Pediatr*. 2014;2(2296-2360 (Electronic)):42.

27. Lee ST, Muench MO, Fomin ME, et al. Epigenetic remodeling in B-cell acute lymphoblastic leukemia occurs in two tracks and employs embryonic stem cell-like signatures. *Nucleic Acids Res*. 2015;43(5):2590-2602.

28. Cedar H, Bergman Y. Linking DNA methylation and histone modification: patterns and paradigms. *Nat Rev Genet*. 2009;10(5):295-304.

29. McCabe MT, Brandes JC, Vertino PM. Cancer DNA methylation: molecular mechanisms and clinical implications. *Clin Cancer Res*. 2009;15(12):3927-3937.

30. Tycko B. Epigenetic gene silencing in cancer. *J Clin Invest*. 2000;105(4):401-407.
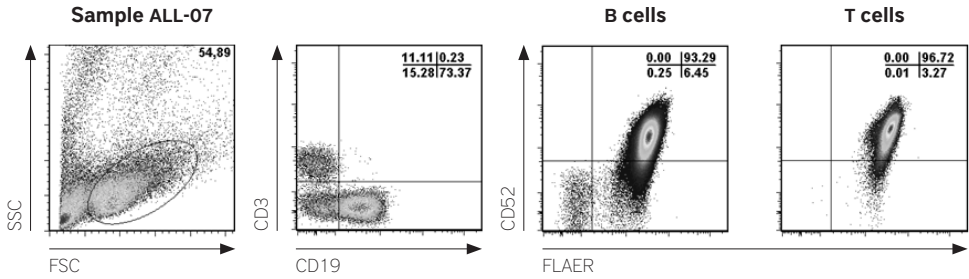
5

SUPPLEMENTAL DATA

Figure S1. Gating strategy for detection of GPI/CD52 negative B cells in primary samples
Representative example of flow cytometric analysis to detect and quantify the presence of GPI/CD52 negative cells in primary samples. Shown is the analysis for sample ALL-07. Lymphocytes were selected based on forward scatter (FSC) and side scatter (SSC) (25,000 events shown). Within the lymphocyte gate, B cells were defined as CD19+/CD3- and T cells as CD3+/CD19- (25,000 events shown). Within these gates GPI/CD52 negative cells were defined as FLAER/CD52 negative (lower left quadrant) (all 369,534 events shown).
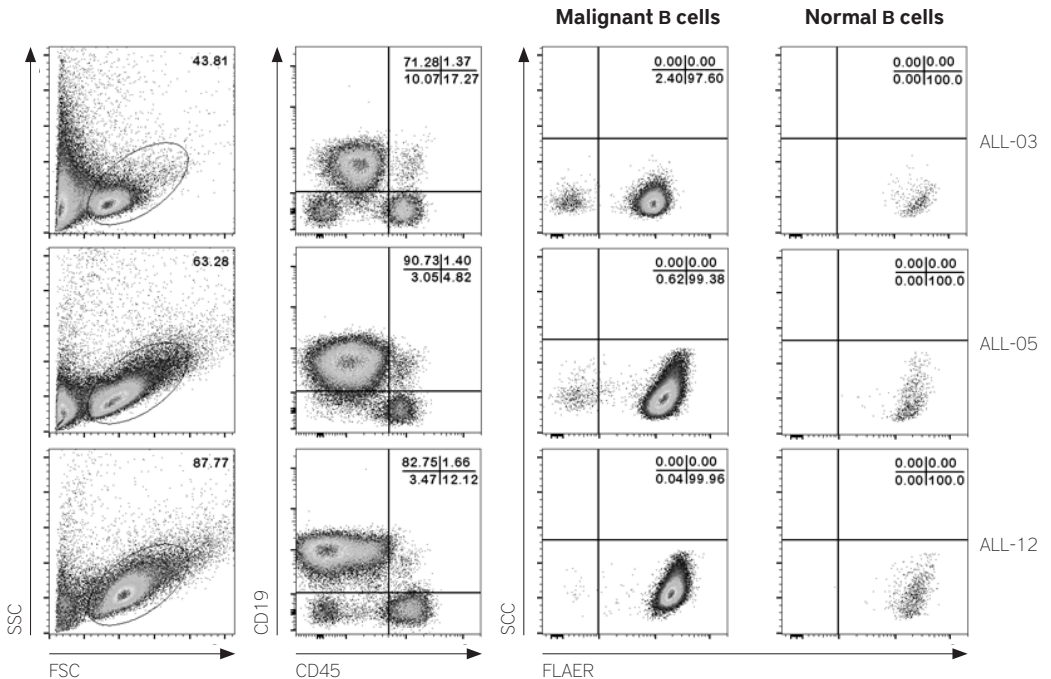

Figure S2. GPI-anchor negative B cells were present in the malignant and absent in normal B-cells within the same sample
Representative examples of flow cytometric analysis of primary B-ALL samples ALL-03, ALL-05, and ALL-12. Horizontally distributed panels belong to the same sample. Lymphocytes were selected based on forward scatter (FSC) and side scatter (SSC). Within the lymphocyte gate, malignant B cells were defined as CD19+/CD45^{dim} and normal B cells as CD19+/CD45^{bright}. Within these gates FLAER-staining is shown, showing GPI-negative cells in the lower left quadrant.
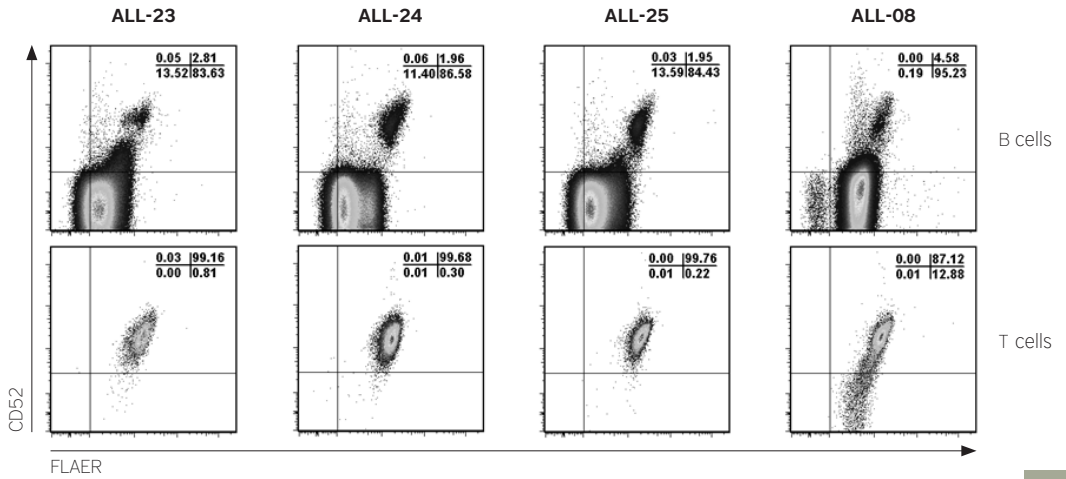
Figure S3. GPI-anchor and CD52 expression in B-ALL cells carrying t(4;11) MLL translocation and in sample ALL-08
Flow cytometric analysis of GPI-anchor expression (FLAER) and expression of CD52 on samples from patients carrying the t(4;11) MLL translocation (Sample ALL-23, ALL-24, and ALL-25) and from non-MLL sample ALL-08. Shown are cells within the lymphocyte gate that were CD19+CD3- (B cells, upper panels) or CD3+CD19- (T cells, lower panels). Numbers indicate the percentage of cells within the quadrants.
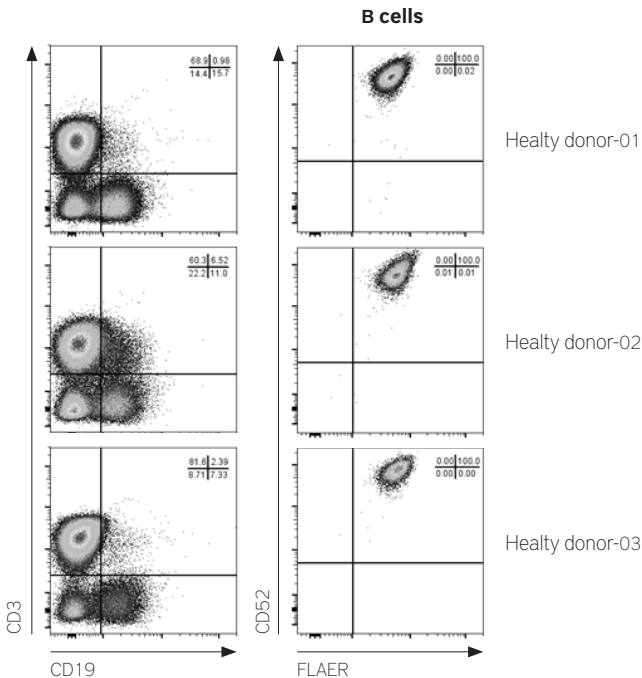

Figure S4. GPI-anchor and CD52 expression in PB samples from healthy donors
Flow cytometric analysis of GPI-anchor expression (FLAER) and expression of CD52 on PB samples from healthy donors. Shown are all cells within the lymphocyte gate (left panels) and cells within the lymphocyte gate that were CD19+CD3- (B cells, right panels). Numbers indicate the percentage of cells within the respective quadrant.
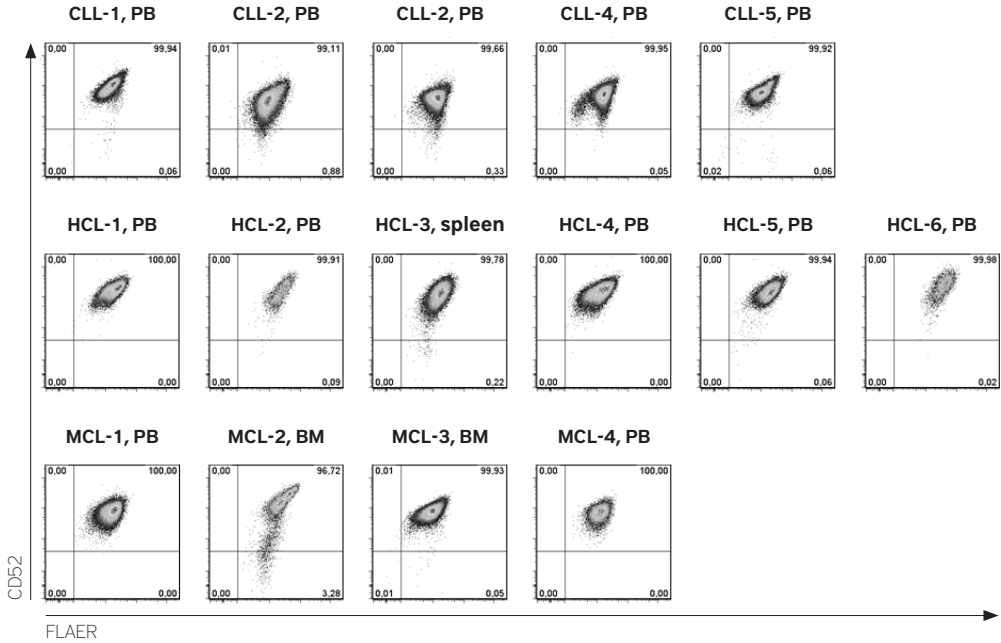
Figure S5. GPI-anchor and CD52 expression in samples from patients with CLL, HCL, or MCL

Flow cytometric analysis for GPI-anchor expression (FLAER) and expression of CD52 on PB, BM, or spleen samples from patients with CLL, HCL, or MCL. Shown are cells within the lymphocyte gate that were positive for CD19 and negative for CD3 (B cells). Numbers indicate the percentage of cells within the respective quadrant.
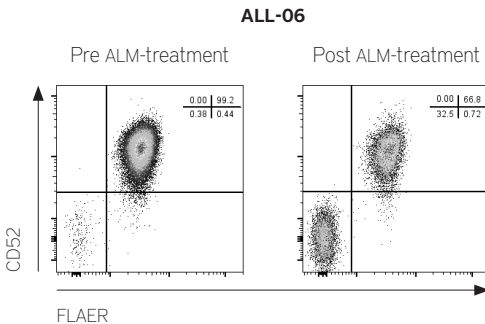

Figure S6. GPI-anchor and CD52 expression before and after ALM-treatment in patient ALL-06

Flow cytometric analysis of GPI-anchor expression (FLAER) and expression of CD52 on samples taken 3 months before start of ALM-treatment (left) and 1 month after secession of treatment due to relapse (right). Shown are cells within the lymphocyte gate that were positive for CD19 and negative for CD3 (B cells). Numbers indicate the percentage of cells within the respective quadrant.
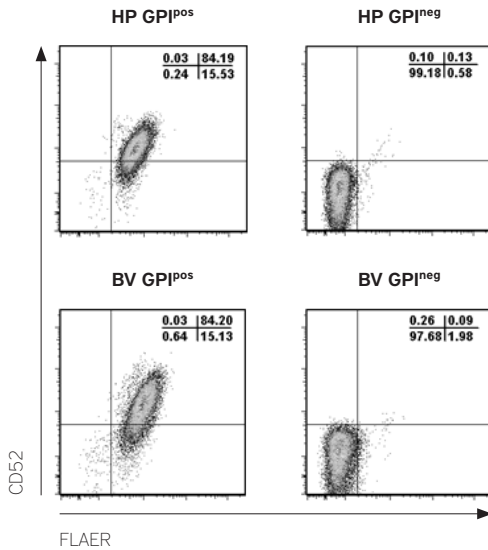
Figure S7. GPI-anchor and CD52 expression on the subcultures of cell lines Leiden-ALL-BV and Leiden-ALL-HP
Flow cytometric analysis of GPI-anchor (FLAER) and CD52 membrane expression in the GPI^{neg} and GPI^{pos} subcultures of B-ALL cell lines Leiden-ALL-HP (HP GPI^{neg} and HP GPI^{pos}, respectively) and Leiden-ALL-BV (BV GPI^{neg} and BV GPI^{pos}, respectively). Numbers indicate the percentage of cells within the quadrants.
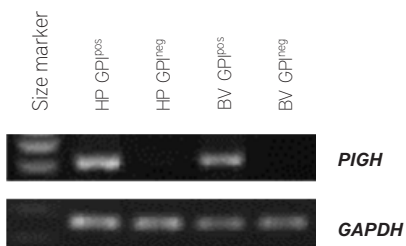

Figure S8. Loss of *PIGH* mRNA expression in GPI-anchor negative B-ALL subcultures
Gel electrophoresis results for *PIGH* mRNA expression analysis in the GPI^{neg} and GPI^{pos} subcultures of cell lines Leiden-ALL-HP (HP GPI^{neg} and HP GPI^{pos}, respectively) and Leiden-ALL-BV (BV GPI^{neg} and BV GPI^{pos}, respectively). Equimolar amounts of cDNA were used for PCR amplification. GAPDH was used as a loading control.
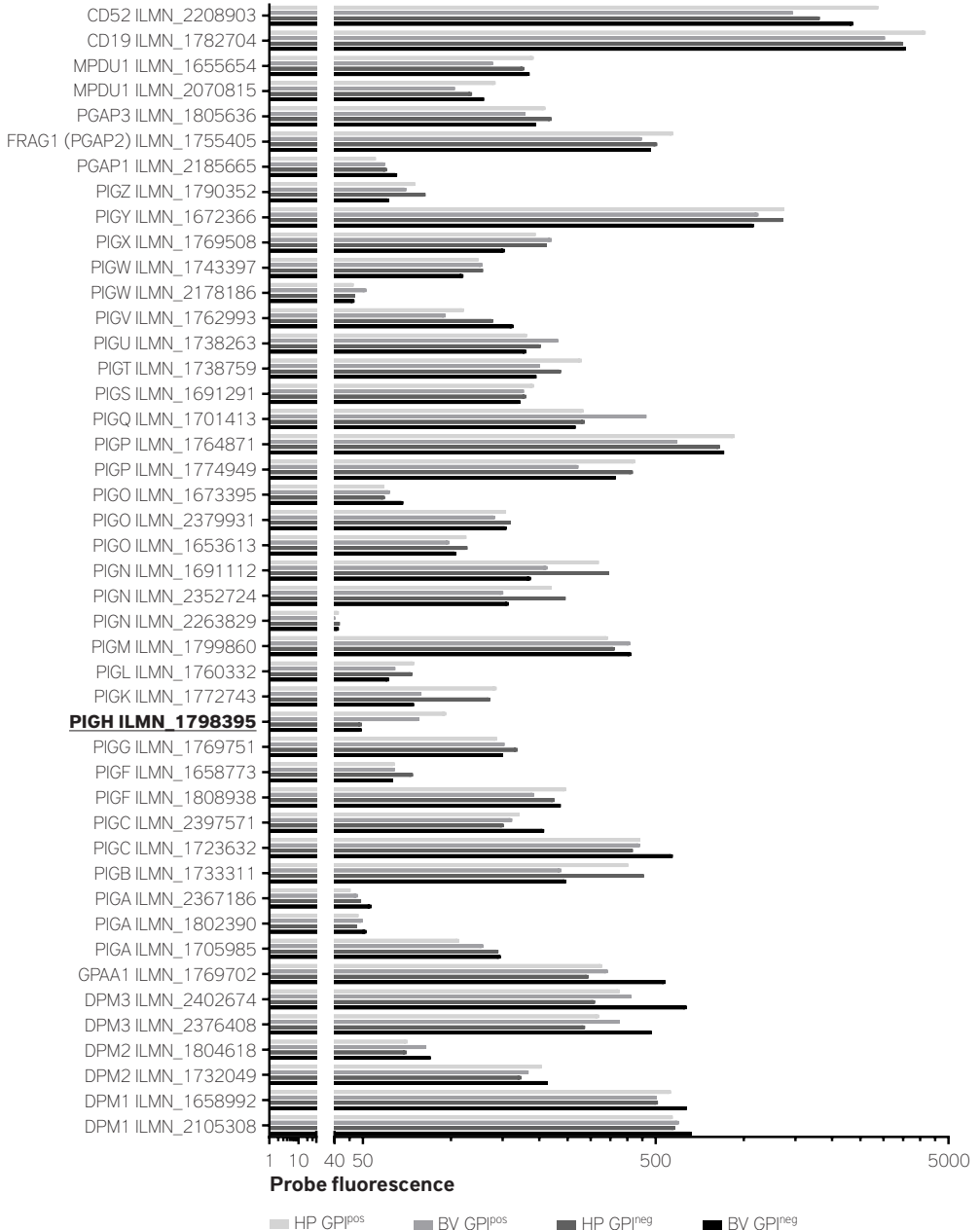
Figure S9. Global mRNA expression analysis of the GPI-anchor synthesis genes in the GPI/CD52-negative and GPI/
CD52-positve cell cultures

Global mRNA expression analysis of the GPI-anchor synthesis genes, CD19, and CD52 in cell cultures BV GPI^neg, HP
GPI^neg, BV GPI^pos, and HP GPI^pos as determined by microarray analysis. Probe background fluorescence is generally
between 40-60.[17]
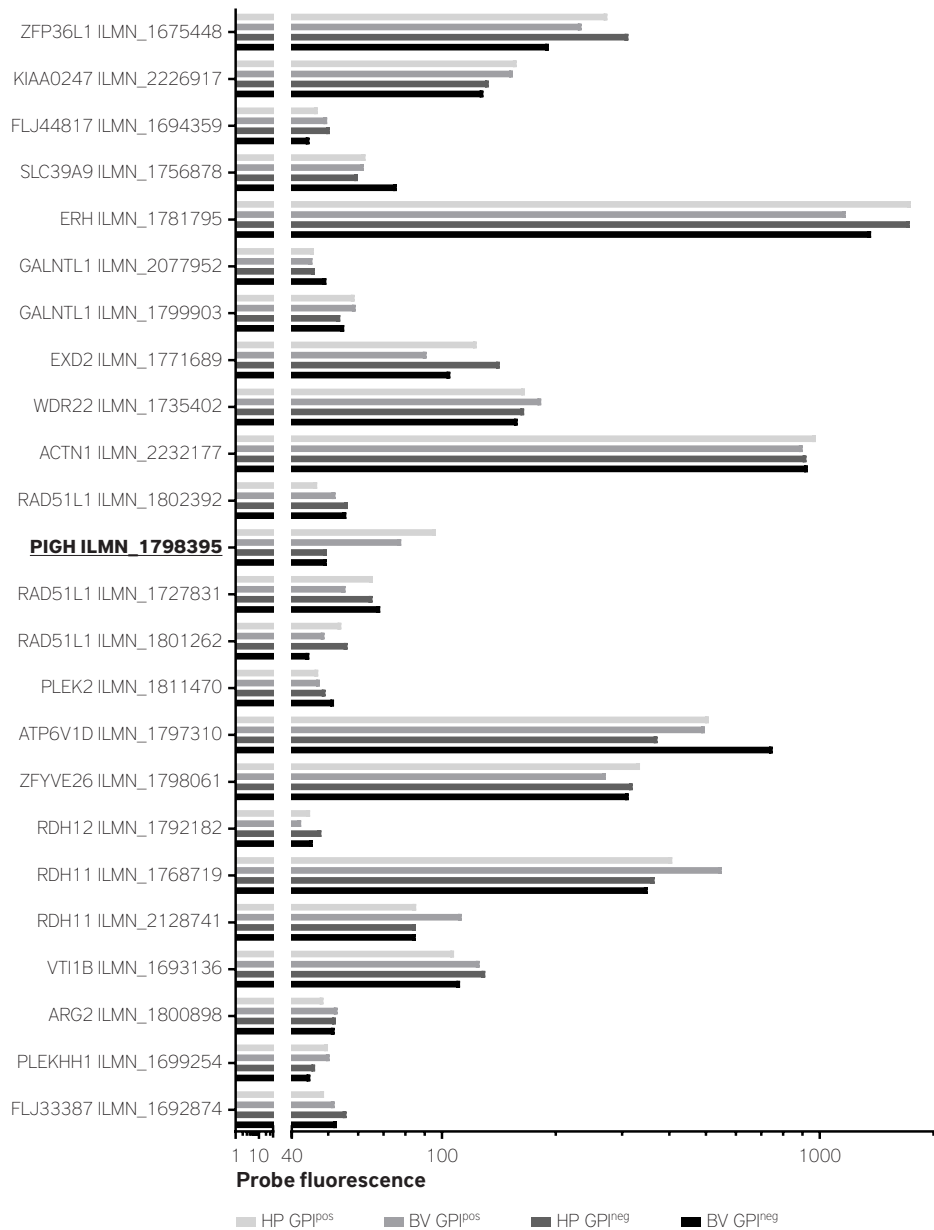
Figure S10. No difference in expression of genes proximal to *PIGH* in GPI/CD52-negative cell cultures compared to GPI/CD52-positve cell cultures

Global mRNA expression analysis of genes proximal (1.1 Mbp upstream to 1.2 Mbp downstream) to the *PIGH* chromosomal location in cell cultures BV GPI^neg, HP GPI^neg, BV GPI^pos, and HP GPI^pos as determined by microarray analysis. Nearest 10 genes for which probes were present on the Human HT-12 v4 chip are depicted.

Table S1. Primer sequences for mRNA expression analysis

| Primers set	Gene name	Forward primer	Reverse primer	Amplicon size
1	*PIGA*	GTTCGGGAGAGAGTCACGATA	GCTTGTTTGTAAGCACCGAGC	157
2	*PIGB*	CTTACCCTTCTTTATTCATGGCTG	GGTTAATGAGTATCCACAGAACAC	169
3	*PIGC*	CTGCGCAACCCTAGGAACTC	GAAGAAGCCAGACCAGTCCC	510
4	*PIGF*	GTAGTTCCCCGCTTCCCTTC	CTCCAAGCCATGCTCCTACA	567
5	*PIGH*	GCCATTTACATGCAGAAGGT	GACTGTGTCCACCTGATGGT	289
6	*PIGK*	GGGAAGTCTGAAGCCGGTAA	CTAGGTGGGATCCTCCCAGT	447
7	*PIGL*	TACCTAAAGGGTGCTCTGTG	CCGGGAGAAGATAATGTAGAGG	209
8	*PIGM*	TCACCGCTTTCCTCTTATACC	TGGGAAGGATGTAAGTCACTG	255
9	*PIGN*	AGAAGTGAAGAAACCAAGCC	TCAACACTGATACAACAAGGTC	188
10	*PIGO*	TCGTTGCCCTGAAGAGACAC	ATGCCAATGGATGGCTGGAA	838
11	*PIGP*	GGTGGAAAATTCACCGTCGC	TGGATGGAGTCGAGTGGAGA	261
12	*PIGQ*	CTGTGGATCAGCTACATCCA	CCAGGTCATAGGAACAGGAG	271
13	*PIGS*	GCGGCTACACACCTAGAGG	CTGGGAGTAAGGCAACGAGG	132
14	*PIGT*	GCGGGAGGAACTTGTCATCA	CAAGAGCTTCTTCCAGGGGG	490
15	*PIGU*	TTCATTTCCGAGCGGGTGG	TGCGGGGATGAAATCCCAAG	690
16	*PIGV*	CATGTTCAGGTTCTCACCAG	GCCTAGAATGTATCGTGTGAC	228
17	*PIGW*	AGCCATCTCCTGTTTCCGTG	TGCACACCAGCCATGTGTAT	582
18	*PIGX*	CATAACAGAGGCAGTGATGG	CATTCTCCAAAGCACAAGGGG	342
19	*PIGY*	TGTTCTACTCAGCCTCTGTGG	CCCATCCAAGTCCAAAGGTG	133
20	*PIGZ*	GCCCTGGGAGTTTTACCCC	GAAGGTGGAACCAGAGATCAGC	73
21	*DPM1*	ACAGAATTCTTCTAAGACCACG	CTCCATTTCCTTTGTAGCGA	204
22	*DPM2*	TTAGCCTGATCATCTTCACCT	ATGAACAGTCCCACAAACAG	160
23	*DPM3*	ATGACGAAATTAGCGCAGTGG	TTAGGCTGTCAGAAGCGCAG	287
24	*GPAA1*	CCACGAGCGCTATATGGTGT	ATTGATGCCACGCAGGGTTA	616
25	*PGAP1*	TTCTATGTGCCTGCAAGGGG	ACCTCGTACCGACAGTCTGA	519
26	*PGAP2*	TCCCACTACCACTGGATCGG	GTGTGCTTCTTGGTCAACCG	685
27	*PGAP3*	ACCTGTCGGGACGACTGTAA	AAGAGCGGTGGGAAGTCAAG	647
28	*SL15*	CGTTCAGTGGGACTTGCTTC	GTGTGCCCGTTGTGGTAGTT	465

Table S2. Primer sequences for construct generation, mutational screening, and bisulfite sequencing

	Forward primer	Reverse primer
PIGH mRNA expression Analysis		
Protein coding region *PIGH*	TCTGGAGCGGGCGAGAC	ACGGAAAACCAGCCCCTATG
GAPDH	ATGTTCGTCATGGGTGTGAACCA	TGGCAGGTTTTTCTAGACGGCAG
PIGH mRNA primers		
Exon 1-4, amplicon I	TCTGGAGCGGGCGAGAC	CCCATGTCTGAAAACCAAAGTCC
Exon 2-4, amplicon II	AGGTCTGCTTGGTTATCTCCAT	ACGGAAAACCAGCCCCTATG
Exon 1-2, amplicon III	TCTGGAGCGGGCGAGAC	GACAATATCCTTGACCTTGCCC
Exon 3-4, amplicon IV	CCCAAGTAGTACCCGTCTTCC	CCCATGTCTGAAAACCAAAGTCC
PIGH DNA mutation screening		
Full *PIGH* gene 10 kbp, amplicon V	TCTGGAGCGGGCGAGAC	ACGGAAAACCAGCCCCTATG
Exon 1, amplicon VI	TCTGGAGCGGGCGAGAC	AGGGTGAAGAGTCCGTAGGC
Exon 2, amplicon VII	TGCTGAGGGAGTGTGAAAGG	TGCCAGTGATAATTTTGAAGTTGGT
Exon 3, amplicon VIII	GAGTTTCACTTAGACTTTGCTATT	ACATTTGCCTCAGAGAGGAAC
Exon 4, amplicon IX	ACAAGCTGTGCTGTAAGCCT	AAAACTGCGAGGCCAGAACT
Promoter region, amplicon X	GGCTTAGAGAAATCGGCTTGC	TGAGGAGCAGAAGGGATGGA
qPCR ChIP		
H3K4me3 *PIGH* primer set 1	CTCTTCACCCTCTGCGAGGTAAT	CTGTAGGAGGGGCCGACCA
H3K4me3 *PIGH* primer set 2	GTCTTTGGTCGAGCCCGGA	TCCAGGAGCACACATTTCACTA
H3K27me3 *PIGH* primer set 2	GTGTGCCCTACTTGTCCTCC	CCAGACCCAGTGGAGAGCTA
H3K27me3 *PIGH* primer set 3	ATGTTCCCCTCATTGCCTGG	AGGGTGATGAAGATGGCAGC
H3K4me3 *GAPDH* primer set 1	GAAAGCCTGCCGGTGACTAA	GCATCACCCGGAGGAGAAAT
H3K4me3 *GAPDH* primer set 2	GCCAATCTCAGTCCCTTCCC	TAGTAGCCGGGCCCTACTTT
H3K27me3 *MYOD1* primer set 1	GGCCTTTGAGACACTCAAGC	AGGCCCTCGATATAGCGGAT
H3K27me3 *MYOD1* primer set 2	TAGGAGAGGCGGGAGAACTG	CAATGGGTCTCCGAGAAGGG
Methylation Assay primers		
Promoter amplicon	GGTTTTTTAGTGTTGGATTATAGGTTTGA	CTCCGCTCATCCTCCATAAC

5

CHAPTER 6

Summary and general discussion
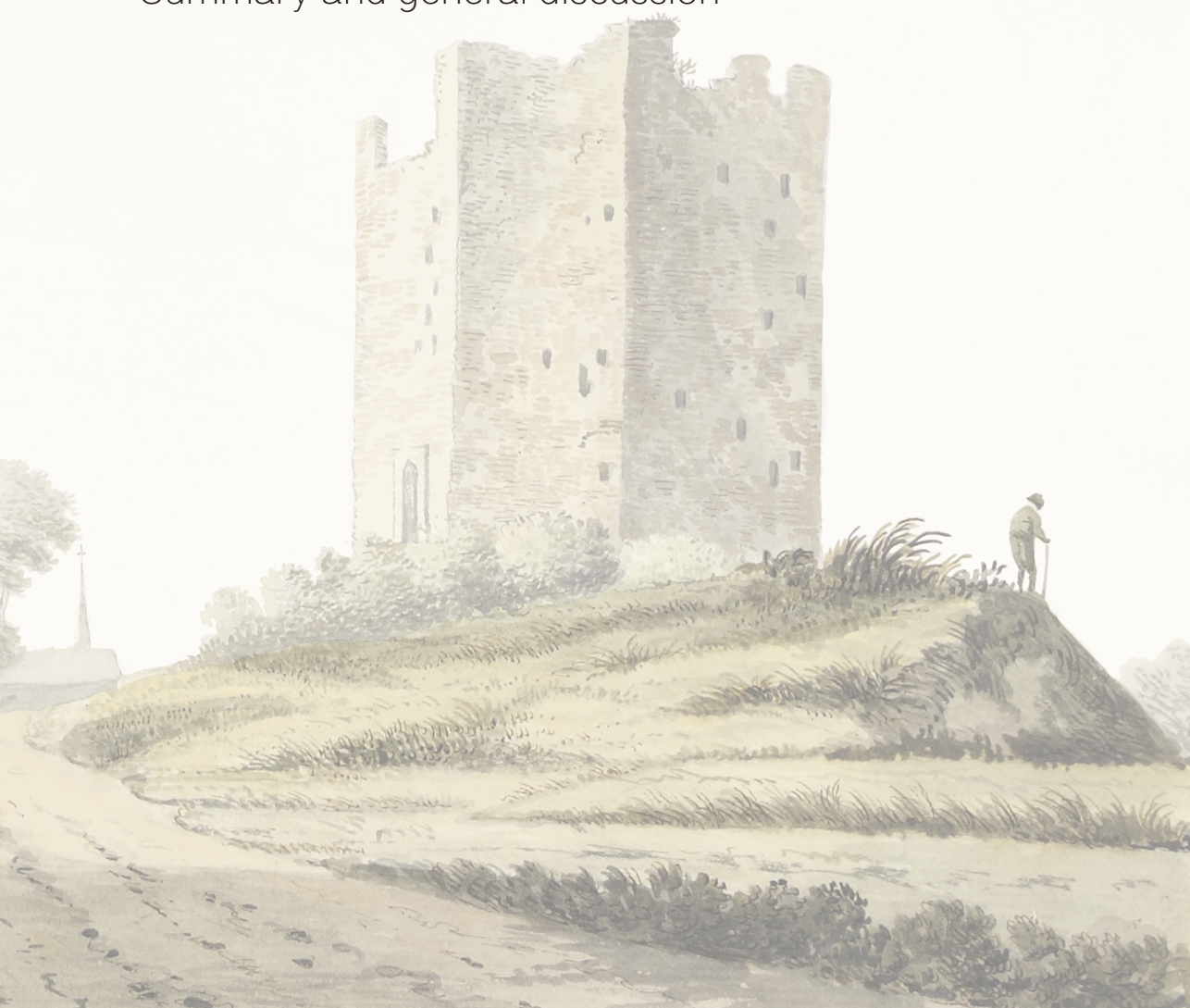
SUMMMARY

Alemtuzumab (ALM) is a cytotoxic monoclonal antibody that is used as a therapeutic agent in a variety of clinical settings. The target antigen for ALM is CD52, which is highly expressed on the membrane of mature lymphocytes, but not or only marginally on hematopoietic stem cells, red blood cells, and non-hematopoietic tissues. As such, ALM can be administered for the purpose of lymphocyte depletion with no or only minimal toxicity to other tissues. In this thesis, the mechanism of action of ALM was investigated in the context of two clinical settings, i.e. T-cell depletion before allogeneic stem cell transplantation (alloSCT) and depletion of malignant cells in B lymphoblastic leukemia (B-ALL).

ALM-based T-cell depletion before allogeneic stem cell transplantation is applied to prevent the highly destructive side effect of graft versus host disease (GvHD). To obtain insight into ALM pharmacokinetics and its effect on the circulating T cells in patients who received alloSCT with a T-cell depleted graft by addition of ALM "to the bag" with or without prior ALM as part of the conditioning regimen, we analyzed in a prospective study ALM plasma levels and the number of circulating T cells in a cohort of 36 patients. Results from this analysis are described in **CHAPTER 2**. We observed considerable variation in inter-patient peak ALM plasma levels after graft infusion. This variation was demonstrated to depend on plasma volume rather than the number of circulating lymphocytes present before the start of ALM treatment. Effective T-cell depletion was observed in all patients. Patients with peak ALM plasma levels above 6.5 µg/ml did not develop severe GvHD. Continued presence of ALM prevented reconstitution of CD52-positive T cells when post-transplantation ALM plasma levels were above 0.7 µg/mL. Despite this, none of the patients had major complications related to Epstein-Barr virus (EBV) or cytomegalovirus (CMV). This outcome likely relates to the immunoprotective effect of early reconstitution of CD52-negative T cells which we demonstrated was not affected by enduring ALM exposure after transplantation.

In **CHAPTER 3** we examined the relative contribution of various factors that influence the efficiency of antibody-induced complement dependent cytotoxicity (CDC), one of the mechanisms employed by antibodies to induce target-cell lysis, using ALM together with exemplar therapeutic antibodies rituximab (RTX) and ofatumumab (OFA) (both targeting CD20) against a panel of B-ALL cell lines and primary B-ALL samples. We demonstrated that the sensitivity of target cells for antibody-induced CDC was predominantly determined by the level of target antigen expression and by antibody concentration. Purified glycosylphosphatidylinositol (GPI)-anchor negative subcultures from two B-ALL cell lines

were found to be especially sensitive to CDC induced by RTX and OFA, due to the lack of expression of membrane-bound complement inhibitors CD55 and CD59. Forced expression of CD55 and CD59 allowed us to demonstrate that both inhibitors were able to individually constrain CDC. This inhibiting effect was only observed within a specific range for target antigen expression and antibody concentration, indicating that the effect of CD55 and CD59 acts secondary to these parameters. Using primary B-ALL samples, we demonstrated that the natural variation of CD55 and CD59 could not be used as a single factor to predict sensitivity to CDC.

Early reconstitution of T cells that lack CD52 membrane expression may convey an immunoprotective effect after ALM-based T-cell depleted alloSCT. In **CHAPTER 4** we performed a comprehensive analysis to investigate the extent to which these CD52-negative T cells contribute to early T-cell reconstitution. Also, we elucidated the mechanism resulting in loss of CD52 membrane expression. In a consecutive cohort of 89 patient who had received an alloSCT for a variety of malignant and non-malignant hematological diseases, we showed that in the majority of patients the bulk of CD4 T cells and a substantial fraction of the CD8 T cells were negative for CD52 membrane expression at week 6 after graft infusion. In contrast, no obvious CD52-negative cell population was found within the NK or B cells from the same individuals. Direct staining of the GPI-anchor confirmed that loss of CD52 membrane expression was due to loss of GPI-anchor expression, as suggested by previous reports. Targeted sequence analysis on mRNA from clonally expanded GPI/CD52-negative and positive T cells from three alloSCT recipients demonstrated that a highly polyclonal mutational landscape in the *PIGA* gene had resulted in the loss of GPI-anchor and coinciding absence of CD52 membrane expression. Forced re-expression of wildtype *PIGA* in the GPI/CD52-negative T-cell clones restored the GPI/CD52-positive phenotype. The GPI/CD52-negative cells after alloSCT were mainly of donor origin as demonstrated by chimerism analysis. In cells collected from two donors, GPI/CD52-negative T cells were already present at low frequencies. *PIGA*-specific sequence analysis on mRNA from clonally expanded donor T cells indicated the presence of a similar highly mutational landscape in the *PIGA* gene as found in the recipient. Only a minority of mutations were found in both the donor and the matched recipient, probable due to the limited depth of our analysis. Functional analysis of the GPI/CD52-negative T-cell population showed that this population contained multiple functional virus-specific T cells, supporting the hypothesis that these cells have a beneficial role in early immune protection after ALM-based T-cell depleted alloSCT.

When ALM was applied as a monotherapy for the treatment of B-ALL, initial clinical responses were frequently followed by early relapse due to the outgrowth of a CD52-negative subclone resistant to the therapy. In **CHAPTER 5** we aimed to elucidate the mechanism resulting in loss of CD52 expression in B-ALL. We demonstrated that the lack of CD52 membrane expression was the result of loss of GPI-anchor expression. Analysis of a cohort of patients with B-ALL showed that malignant cells with this GPI/CD52-negative phenotype were already present at low frequencies before the initiation of ALM-treatment. An unbiased mRNA expression analysis of the genes involved in GPI-anchor synthesis indicated that synthesis of the GPI-anchor within these cells was defective due to lack of *PIGH* mRNA expression. To further investigate what caused the loss of *PIGH* expression, we exploited the two purified GPI/CD52-negative B-ALL subcultures used in **CHAPTER 3** that were generated from primary B-ALL samples. Forced expression of *PIGH* mRNA restored GPI-anchor expression and coinciding CD52 membrane expression in these subcultures confirming that absence of *PIGH* mRNA expression was the primary underlying reason for the GPI/CD52-negative phenotype. Epigenetic silencing rather than gene mutation or deletion had resulted in loss of *PIGH* mRNA expression within these B-ALL cells, as demonstrated by in-depth mutational and epigenetic analysis. Treatment with the epigenetic modifying drug 5-aza-2′-deoxycytidine was able to revert the GPI/CD52-negative phenotype in these malignant B-ALL cells, illustrating potential clinical synergy with ALM treatment.

GENERAL DISCUSSION

Optimizing ALM treatment

Proper CD52 antigen expression and a sufficient ALM level were demonstrated in this thesis to be the major determinants for successful ALM-induced target cell depletion. In contrast, membrane-bound complement inhibitors CD55 and CD59 were shown to convey protection against CDC-mediated depletion. Manipulation of these factors in the clinical setting may improve treatment outcome of ALM-therapy.

Regulating the peak ALM level after alloSCT

In **CHAPTER 3** we demonstrated that antibody concentration was one of the primary factors that determines the efficiency of CDC-induced target cell lysis. The same applies for antibody-dependent cellular cytotoxicity (ADCC).[1,2] Control of the in-vivo antibody concentration could be a potent tool to ensure successful depletion of donor T cells during alloSCT. The current paradigm for ALM dosing in both in-vivo and in-vitro T-cell depletion in alloSCT is flat dosing for adults patients and dosing per kg body weight in the pediatric setting. At the Leiden University Medical Center, all adult patients within a specific conditioning regimen receive the same ALM schedule and dosing regardless of patient characteristics. This dosing schedule consist of 30 mg ALM intravenously as part of in-vivo conditioning and 20 mg ALM added "to the bag" containing the graft, except for MA-conditioned patients with a sibling donor who only receive 20 mg of ALM added to the bag. In **CHAPTER 2** we showed that peak ALM plasma levels varied widely between recipients. Importantly, an ALM peak level below 6.5 µg/mL was associated with the development of mild GvHD, whereas higher levels were shown to prevent GvHD. Together this argues for the introduction of individualized dosing. A user friendly ALM level predication tool in the form of a dashboard system loaded with a relevant pharmacokinetics (PK)-model,[3] such as generated in **CHAPTER 2**, could be employed to adjust the final ALM dose at the moment of graft infusion. Patient specific covariates such as length, weight, and hematocrit (to estimate the patients' plasma volume) together with an accurate ALM plasma measurement taken before graft infusion, likely suffice as input to estimate the peak ALM plasma level after graft infusion. One goal of dose adjustment guided based on the PK-model would be to achieve a peak ALM plasma level of at least 6.5 µg/mL to prevent GvHD. On the other hand, since in most patients the current dose of 20 mg ALM added "to the bag" resulted in a peak level higher than 6.5 µg/mL, downward dose adjustment may also be envisioned. Hereby

6

the goal would be to limit unnecessary ALM exposure after transplantation which results in delayed reconstitution, while maintaining a peak ALM level higher than 6.5 µg/mL to prevent GvHD. Before clinical implementation, the assay used for the ALM plasma measurement and the predictive power of the PK-model presented in this thesis need to be validated. The latter may be done initially as an observational study in a patient cohort with standard conditioning protocols, followed by a prospective interventional study. Whether this dose adjustment approach will also be applicable in MA-conditioned patients with a sibling donor who do not receive ALM as part of the conditioning regimen, restricting PK prediction solely to covariates without a pre-graft infusion ALM measurement, needs to be evaluated.

Optimizing the ALM level for the treatment of malignancies

No formal dose optimization studies were performed when ALM was introduced for the treatment of hematological malignancies. The first two patients that were treated with ALM (Campath-H1) for non-Hodgkin lymphoma (NHL) were dosed based on tolerability of the infusion reaction and on the amount of ALM available.[4] Based on the results from that study, various phase II studies were conducted in patients with chronic lymphocytic leukemia (CLL), NHL, and T-cell prolymphocytic leukemia (T-PLL) using similar approaches; a starting dose of 3 mg daily, increased to 10 mg daily as soon as infusion reactions were tolerated, followed by 30 mg infusions trice weekly for up to 12 weeks.[5-8] This strategy was subsequently selected for the accelerated U.S. Food and Drug Administration approval of ALM for the treatment of CLL and has not been challenged in large trials. Although pharmacokinetic studies have since demonstrated that responders have higher circulating ALM levels compared to non-responders,[9,10] this may simply be a reflection of the initial tumor burden. As demonstrated in **CHAPTER 3** for CDC, higher antibody concentrations are required to induce lysis of cells with low antigen expression. Considering the heterogeneity of antigen expression within most tumors, this would suggest an aim to achieve high circulating ALM levels to also deplete malignant cells with the lowest antigen expression. However, since CD52 is also expressed at low levels on NK-cells and macrophages that induce ADCC and antibody-dependent cellular phagocytosis, respectively, high ALM levels may result in abrogation of these effector mechanisms thereby decreasing the efficacy of the treatment. Thus, the optimal ALM dose for eradication of the malignant cells may not be found until the relative contributions of its in-vivo mechanisms of action become clear. In addition, depletion of CD52 expressing immune cells may put patients at risk of developing life threatening infections which should be considered for the overall effectiveness of the treatment.

Increasing sensitivity to ALM-treatment by blocking complement inhibitors

A potential option to increase the efficiency of ALM-induced target cell lysis mediated via CDC would be elimination of the protective effect provided by complement inhibitors. In **CHAPTER 3** we demonstrated that overexpression of GPI-linked membrane-bound complement regulatory proteins (mCRP) CD55 and CD59 individually increased protection of B-ALL cells from CDC, whereas loss of GPI-anchor synthesis and coinciding loss of membrane expression of CD55 and CD59 expression sensitized B-ALL cells for CDC. Although our study was limited to analyzing the protective effect of CD55 and CD59, various other membrane-bound and soluble complement inhibiters also convey protection against antibody induced-CDC.[11] Blocking the function of membrane-bound complement inhibitors is likely preferred over blocking soluble inhibitors. First, because the generally high serum concentrations of soluble complement inhibitors such as factor I (35 μg/mL) and factor H (300 μg/mL) would probably hamper effective blocking.[12-14] Second, therapies targeting soluble complement inhibitors would induce systemic dysregulation of the complement system which may result in extensive side effects that are normally associated with diseases of the complement system, such as angioedema. In contrast, mCRP, such as CD55, CD59, complement receptor 1 (CD35), and membrane cofactor protein (CD46), could be blocked specifically on the targeted cells by using a bi- or multispecific antibody construct designed to block the mCRP with one domain, while engaging an antigen expressed only on the targeted cell with another domain.[15] It could also be envisioned to design an mCRP-blocking treatment targeted to an antigen with broader tissue expression to increase its clinical applicability. For example, an mCRP blocking treatment targeting CD52 expressing cells might be beneficial in conjunction with CD20, CD19, and CD38 targeting CDC-inducing antibody therapeutics thereby being applicable for treatment against multiple B-cell malignancies. Some bystander lysis of healthy cells targeted by the mCRP-blocking treatment, but not the antibody therapeutic, may be expected and should be monitored to assess the overall safety of such combination treatment.

Reverting loss of CD52 membrane expression in B-ALL

Patients with B-ALL are particularly prone to develop treatment resistant relapse, due to the genetic intra-tumor heterogeneity. In **CHAPTER 5** we showed that in the majority of patients with B-ALL, small CD52/GPI-negative malignant cell populations are present already at diagnosis. In one patient from whom pre- and post-ALM treatment blood samples were available, outgrowth of the pre-existing CD52/GPI-negative clone was demonstrated. To mitigate the chance of developing treatment resistant relapse in B-ALL, therapies combining multiple treatment modalities, such as chemotherapeutic agents,

targeted agents like tyrosine kinase inhibitors, and monoclonal antibodies, could be employed. Our group and others have previously shown that a combination of ALM and the CD20-targetting antibody RTX may result in reciprocal treatment synergy in B-ALL due to (1) loss of mCRP expression on the CD52/GPI-negative cells, increasing their sensitivity for RTX-induced lysis and (2) upregulation of CD52 expression on the RTX-resistant cells making them more prone to ALM-induced lysis.[16,17] The combination of ALM and RTX has already shown clinical success in patients with previously untreated or refractory CLL.[18-20] Unfortunately, CD20-positive malignant cells are only present in half of B-ALL patients and often constitute only a subfraction of the malignant cells.[16,21,22] As such, design of other combination treatments remains desired. Since loss of CD52 membrane expression in B-ALL cells results from epigenetic downregulation of *PIGH* expression and subsequent loss of the GPI-anchor, epigenetic modifying drugs may restore the expression of CD52 and revert ALM resistance. In **CHAPTER 5** we demonstrated that the DNA demethylating agent 5-aza-2'-cytidine can revert the CD52/GPI-anchor-negative phenotype in B-ALL cells. A similar effect may be induced by other epigenetic modifying drugs that promote gene expression, such as the DNA demethylating agent decitabine, the histone deacetylase inhibitors valproic acid and vorinostat, and the DNA and histone demethylating agent cladribine. Interestingly, the addition of cladribine with or without vorinostat or valproic acid to ALM-treatment of patients with T-PLL overcame ALM-resistance.[23] This effect was observed in the absence of apoptosis of T-PLL cells, suggesting absence of a direct toxic effect induced by the epigenetic modifying drug. The mechanism of loss of CD52 expression and subsequent ALM-resistance in T-PLL is currently unknown,[24-26] but ALM treatment had no effect on CD52 mRNA levels suggesting involvement of the GPI-anchor.[23] The observation that ALM-resistance in these cells could be prevented by epigenetic modifying drug suggest that a mechanism similar to what we found in the B-ALL cells was at play, as opposed to for example a crippling mutation of the *PIGA* gene. Importantly, this study in T-PLL shows that combining ALM with epigenetic modifying drugs is safe and may have a synergistic effect.

The effect of ALM-treatment on the immunobiology of alloSCT

Following alloSCT there are three major complications that may cause unfavorable treatment outcome, including development of GvHD, relapse resulting from inadequate graft versus tumor (GvT) effect, and infections. ALM-based T-cell depletion may affect all three processes. The activation and effector function of T cells is mediated via the interaction between T-cell receptors (TCR) expressed on the cell surface of T cells and small protein sequences (peptides) presented in human leukocyte antigen (HLA) molecules expressed on the surface of stimulator/target cells. Normally, during maturation in the

thymus, T cells are negatively selected when their TCR interacts with high affinity with self-peptide-HLA complexes.[27] Because of genetic differences between patient and donor within either the HLA (major histocompatibility antigen) or in the presented peptides (minor histocompatibility antigens, MiHA), mature donor T cells infused with the graft may recognize peptide-HLA complexes presented on patient cells as non-self and eliminate these cells resulting in the detrimental GvHD or the beneficial GvT reactivity. Recognition of pathogen-derived peptides presented in self-HLA may result in immunoprotection.

The effect of CD52/GPI-negative T cells on GvHD and GvT

As shown in **CHAPTER 4**, CD52/GPI-negative T cells found in recipients of ALM-based T-cell depleted alloSCT are predominantly donor-derived T cells with a memory phenotype. Unless the donor has been exposed to alloantigens through blood transfusion, organ transplantation, or pregnancy, this memory phenotype must have been the result of an antigenic challenge by past infections in the donor. In an HLA-matched transplantation, these pathogen-specific CD52/GPI-negative memory T cells are not expected to contribute to either GvHD or GvT. This is in contrast to CD52/GPI-negative naive T cells that, being trained in the thymus of the donor not to recognize self-peptide in self-HLA, would be able to recognize MiHA and contribute to GvHD and GvT. In the (partially) HLA-mismatched setting, besides the CD52/GPI-negative naive T cells, the pathogen-specific CD52/GPI-negative memory T cells may still induce GvHD and GvT.[28] This may result from cross-reactivity of these memory cells towards any peptide in nonself-HLA, a combination that was obviously not present during thymic selection in the donor, that by chance may be present in the pathogen-specific CD52/GPI-negative memory T-cell repertoire. Whether this mechanism is a potent driver of GvHD and GvT remains to be established. Although we did establish the dynamics of CD52/GPI-negative T cells following alloSCT with a T-cell depleted graft by addition of ALM "to the bag" with or without prior ALM as part of the conditioning regimen in **CHAPTER 2**, this study was limited in the number of patients and only three developed mild GvHD. Of these patients that developed GvHD, one had received myeloablative condition and a graft from a sibling donor, one had received myeloablative conditioning and a graft from an unrelated donor (10/10 match), and one had received non-myeloablative conditioning and a graft from a sibling donor. The contribution of CD52/GPI-negative cells to GvHD in these patients was not studied. However, since they all had low ALM plasma peak levels, it is likely that naive donor T cells that had escaped ALM conditioning contributed to the development of GvHD. Conclusively demonstrating that CD52/GPI-negative donor T cells do not (dominantly) take part in the processes of GvHD or GvT is difficult since only the opposite can be proven. However, utilizing the large numbers of MiHA that have currently been identified, screens could be developed using peptide-

MHC-multimers to assess the relative frequency of alloreactive T cells in the CD52/GPI-negative and CD52/GPI-positive T-cell populations.[29] The ongoing effort to identify novel MHC-II restricted MiHA and the improvement of MHC-II multimer technology will likely be essential to the success of such screen,[30-32] since CD52/GPI-negative cells were more abundantly present in the CD4 T-cell than in the CD8 T-cell compartment (**CHAPTER 4**).

The effect of CD52/GPI-negative T cells on infectious complications

Infectious complications are one of the major causes of morbidity associated with alloSCT. Since immune protection is prominently mediated via T cells, depletion of donor T cells may increase the risk of infection. Following T-cell depleted alloSCT, this risk is in part mitigated by the lack for need of post-transplantation application of immunosuppressive drugs, which is typically given to prevent the occurrence of GvHD after infusion of an unmanipulated graft, allowing for an unrestrained immune response. Following ALM-based T-cell depletion, enduring exposure to ALM may prevent reconstitution of adaptive immune cells that express high levels of CD52. In contrast, reconstitution of innate immune cells, such as neutrophils, NK-cells, and monocytes, which typically have low CD52 expression levels is relatively unaffected. In **CHAPTER 2** we showed that reconstitution of T cells with a CD52/GPI-negative phenotype was unaffected by residual ALM. In **CHAPTER 4** we showed that these polyclonal CD52/GPI-negative T-cell populations contained virus-specific T cells with a functional potential comparable to that of CD52/GPI-positive T cells, suggesting that they may contribute to early immune protection. Since they are of memory phenotype they do not require stimulation by professional antigen presenting cells (APC) for their activation, which renders them ideal effectors in the cell deprived environment shortly after alloSCT. To conclusively demonstrate that CD52/GPI-negative T cells contribute to early immune protection, the relative fraction of pathogen-specific CD52/GPI-negative and -positive T cells could be followed during an infection by flow cytometry using labeled MHC-multimers loaded with pathogen-derived peptides.

An interesting and relatively recently defined population of T cells that may be of specific importance in the early immune protection of tissue are the tissue resident memory T cells. Despite their high levels of CD52 expression, they were not cleared from skin following high-dose ALM treatment (180 mg cumulative dose) in patients with mycosis fungoides.[33,34] Analogously, addition of ALM (20-50 mg cumulative dose) to the conditioning regimen of alloSCT recipients is unlikely to extensively deplete these cells. This is supported by our own observation of the slow replacement of patient T cells with

donor T cells in dermal tissue following ALM-based T-cell depleted alloSCT.[35] Upon infusion of an unmanipulated graft, tissue resident memory T cells may be depleted as a result of the donor T-cell mediated alloimmune response. Thus, depletion of donor T cells from the graft may counterintuitively contribute to early immune protection, by sparing of the tissue resident memory T cells.

Effect of ALM-based depletion on APC

One cell type that is of high importance in all these processes are the APC, such as dendritic cells (DC). Whereas memory T cells can become activated solely by recognition of their target antigen, DC are essential in priming naive T cells during the initial phase of the immune response. Unlike circulating DC that express CD52 at varying levels, tissue "resident" DC such as epidermal Langerhans cells and small intestine DC do not express CD52 and are thus likely to survive ALM-induced cytotoxicity.[36,37] Typically GvHD sensitive tissues, such as gut, skin, liver, and lung contain especially large populations of tissue "resident" DC. Mouse models have demonstrated that recipient DC that survive conditioning are essential to initiate GvHD.[38-40] However, recipient DC have also been demonstrated to be powerful mediators of GvT resulting from the presentation of hematopoiesis-associated MiHa.[41,42] In transplantation protocols without ALM-based T-cell depletion, tissue resident DC will initially be mainly of recipient origin before being replaced by DC from donor hematopoietic origin over the course of several months.[43] Whether these dynamics are similar after ALM-based T-cell depleted alloSCT is currently not known. Specific targeting of tissue DC during conditioning may prevent GvHD, however, may also diminish GvT and immunoprotection.

Concluding remarks

The expression pattern of CD52 has made ALM a unique therapeutic antibody with broad clinical applicability. The combined results presented in this thesis add to the continuing expansion of our understanding of factors that regulate the sensitivity of target cells for depletion by ALM. This knowledge is relevant for the ongoing use of ALM as a treatment against hematological malignancies, for its use as a T-cell depleting agent to prevent GvHD after alloSCT, for new applications of ALM such as the treatment of multiple sclerosis, and more broadly for other and future cytolytic antibody therapeutics. Antigen escape resulting in treatment resistance is a continuing challenge for antibody therapeutics and has recently been demonstrated to also affect chimeric antigen receptor T cell therapy.[44-46] Our demonstration of non-traditional pathways of escape, by epigenetic dysregulation and by a polyclonal mutational landscape, may allow others to identify new pathways more rapidly. Finally, the insights

gained into the pharmacokinetics of ALM following alloSCT and the recognition of the abundance and function of CD52/GPI-negative T cells may aid timing of cellular interventions and may help to fine tune future T-cell depleting strategies.

6

REFERENCE LIST

1.   Riechmann L, Clark M, Waldmann H, Winter G. Reshaping human antibodies for therapy. *Nature*. 1988;332(6162):323-327.

2.   Holgate RG, Weldon R, Jones TD, Baker MP. Characterisation of a Novel Anti-CD52 Antibody with Improved Efficacy and Reduced Immunogenicity. *PLoS One*. 2015;10(9):e0138123.

3.   Mould DR, Dubinsky MC. Dashboard systems: Pharmacokinetic/pharmacodynamic mediated dose optimization for monoclonal antibodies. *J Clin Pharmacol*. 2015;55 Suppl 3:S51-59.

4.   Hale G, Dyer MJ, Clark MR, et al. Remission induction in non-Hodgkin lymphoma with reshaped human monoclonal antibody CAMPATH-1H. *Lancet*. 1988;2(8625):1394-1399.

5.   Lim SH, Davey G, Marcus R. Differential response in a patient treated with Campath-1H monoclonal antibody for refractory non-Hodgkin lymphoma. *Lancet*. 1993;341(8842):432-433.

6.   Pawson R, Dyer MJ, Barge R, et al. Treatment of T-cell prolymphocytic leukemia with human CD52 antibody. *J Clin Oncol*. 1997;15(7):2667-2672.

7.   Keating MJ, Flinn I, Jain V, et al. Therapeutic role of alemtuzumab (Campath-1H) in patients who have failed fludarabine: results of a large international study. *Blood*. 2002;99(10):3554-3561.

8.   Osterborg A, Dyer MJ, Bunjes D, et al. Phase II multicenter study of human CD52 antibody in previously treated chronic lymphocytic leukemia. European Study Group of CAMPATH-1H Treatment in Chronic Lymphocytic Leukemia. *J Clin Oncol*. 1997;15(4):1567-1574.

9.   Mould DR, Baumann A, Kuhlmann J, et al. Population pharmacokinetics-pharmacodynamics of alemtuzumab (Campath) in patients with chronic lymphocytic leukaemia and its link to treatment response. *Br J Clin Pharmacol*. 2007;64(3):278-291.

10.   Hale G, Rebello P, Brettman LR, et al. Blood concentrations of alemtuzumab and antiglobulin responses in patients with chronic lymphocytic leukemia following intravenous or subcutaneous routes of administration. *Blood*. 2004;104(4):948-955.

11.   Meyer S, Leusen JH, Boross P. Regulation of complement and modulation of its activity in monoclonal antibody therapy of cancer. *MAbs*. 2014;6(5):1133-1144.

12.   Wu B, Ouyang Z, Lyon CJ, et al. Plasma Levels of Complement Factor I and C4b Peptides Are Associated with HIV Suppression. *ACS Infect Dis*. 2017;3(12):880-885.

13.   Tseng MH, Lin SH, Wu CY, et al. Serum complement factor I is associated with disease activity of systemic lupus erythematosus. *Oncotarget*. 2018;9(9):8502-8511.

14.   Pouw RB, Brouwer MC, Geissler J, et al. Complement Factor H-Related Protein 3 Serum Levels Are Low Compared to Factor H and Mainly Determined by Gene Copy Number Variation in CFHR3. *PLoS One*. 2016;11(3):e0152164.

15.   Macor P, Secco E, Mezzaroba N, et al. Bispecific antibodies targeting tumor-associated antigens

and neutralizing complement regulators increase the efficacy of antibody-based immunotherapy in mice. *Leukemia*. 2015;29(2):406-414.

16.   Nijmeijer BA, van Schie ML, Halkes CJ, Griffioen M, Willemze R, Falkenburg JH. A mechanistic rationale for combining alemtuzumab and rituximab in the treatment of ALL. *Blood*. 2010;116(26):5930-5940.

17.   Cruz RI, Hernandez-Ilizaliturri FJ, Olejniczak S, et al. CD52 over-expression affects rituximab-associated complement-mediated cytotoxicity but not antibody-dependent cellular cytotoxicity: preclinical evidence that targeting CD52 with alemtuzumab may reverse acquired resistance to rituximab in non-Hodgkin lymphoma. *Leuk Lymphoma*. 2007;48(12):2424-2436.

18.   Badoux XC, Keating MJ, Wang X, et al. Cyclophosphamide, fludarabine, alemtuzumab, and rituximab as salvage therapy for heavily pretreated patients with chronic lymphocytic leukemia. *Blood*. 2011;118(8):2085-2093.

19.   Frankfurt O, Ma S, Gordon L, et al. Phase II study of alemtuzumab-rituximab therapy in previously untreated patients with chronic lymphocytic leukemia: short- and long-term outcomes. *Leuk Lymphoma*. 2015;56(2):315-323.

20.   Zent CS, Call TG, Shanafelt TD, et al. Early treatment of high-risk chronic lymphocytic leukemia with alemtuzumab and rituximab. *Cancer*. 2008;113(8):2110-2118.

21.   Pituch-Noworolska A, Hajto B, Mazur B, et al. Expression of CD20 on acute lymphoblastic leukemia cells in children. *Neoplasma*. 2001;48(3):182-187.

22.   Yang S, Wang J, Zhao T, et al. CD20 expression sub-stratifies standard-risk patients with B cell precursor acute lymphoblastic leukemia. *Oncotarget*. 2017;8(62):105397-105406.

23.   Hasanali ZS, Saroya BS, Stuart A, et al. Epigenetic therapy overcomes treatment resistance in T cell prolymphocytic leukemia. *Sci Transl Med*. 2015;7(293):293ra102.

24.   Tuset E, Matutes E, Brito-Babapulle V, Morilla R, Catovsky D. Immunophenotype changes and loss of CD52 expression in two patients with relapsed T-cell prolymphocytic leukaemia. *Leuk Lymphoma*. 2001;42(6):1379-1383.

25.   Dearden CE, Matutes E, Cazin B, et al. High remission rate in T-cell prolymphocytic leukemia with CAMPATH-1H. *Blood*. 2001;98(6):1721-1726.

26.   Birhiray RE, Shaw G, Guldan S, et al. Phenotypic transformation of CD52(pos) to CD52(neg) leukemic T cells as a mechanism for resistance to CAMPATH-1H. *Leukemia*. 2002;16(5):861-864.

27.   Klein L, Hinterberger M, Wirnsberger G, Kyewski B. Antigen presentation in the thymus for positive selection and central tolerance induction. *Nat Rev Immunol*. 2009;9(12):833-844.

28.   Amir AL, van der Steen DM, Hagedoorn RS, et al. Allo-HLA-reactive T cells inducing graft-versus-host disease are single peptide specific. *Blood*. 2011;118(26):6733-6742.

29.   Hadrup SR, Bakker AH, Shu CJ, et al. Parallel detection of antigen-specific T-cell responses by multidimensional encoding of MHC multimers. *Nat Methods*. 2009;6(7):520-526.

6

30. Bentzen AK, Hadrup SR. Evolution of MHC-based technologies used for detection of antigen-responsive T cells. *Cancer Immunol Immunother*. 2017;66(5):657-666.

31. Kong YY, Kwok WW. Identification of Human Antigen-Specific CD4(+) T-Cells with Peptide-MHC Multimer Technologies. *Methods Mol Biol*. 2019;1988:375-386.

32. van Balen P, van Bergen CAM, van Luxemburg-Heijs SAP, et al. CD4 Donor Lymphocyte Infusion Can Cause Conversion of Chimerism Without GVHD by Inducing Immune Responses Targeting Minor Histocompatibility Antigens in HLA Class II. *Front Immunol*. 2018;9:3016.

33. Clark RA, Watanabe R, Teague JE, et al. Skin effector memory T cells do not recirculate and provide immune protection in alemtuzumab-treated CTCL patients. *Sci Transl Med*. 2012;4(117):117ra117.

34. Watanabe R, Gehad A, Yang C, et al. Human skin is protected by four functionally and phenotypically discrete populations of resident and recirculating memory T cells. S*ci Transl Med*. 2015;7(279):279ra239.

35. van Balen P, van der Zouwen B, Kruisselbrink AB, et al. Tissue Damage Caused by Myeloablative, but Not Non-Myeloablative, Conditioning before Allogeneic Stem Cell Transplantation Results in Dermal Macrophage Recruitment without Active T-Cell Interaction. *Front Immunol*. 2018;9:331.

36. Buggins AG, Mufti GJ, Salisbury J, et al. Peripheral blood but not tissue dendritic cells express CD52 and are depleted by treatment with alemtuzumab. *Blood*. 2002;100(5):1715-1720.

37. Rao SP, Sancho J, Campos-Rivera J, et al. Human peripheral blood mononuclear cells exhibit heterogeneous CD52 expression levels and show differential sensitivity to alemtuzumab mediated cytolysis. *PLoS One*. 2012;7(6):e39416.

38. Shlomchik WD, Couzens MS, Tang CB, et al. Prevention of graft versus host disease by inactivation of host antigen-presenting cells. *Science*. 1999;285(5426):412-415.

39. Matte CC, Liu J, Cormier J, et al. Donor APCs are required for maximal GVHD but not for GVL. *Nat Med*. 2004;10(9):987-992.

40. Markey KA, Banovic T, Kuns RD, et al. Conventional dendritic cells are the critical donor APC presenting alloantigen after experimental bone marrow transplantation. *Blood*. 2009;113(22):5644-5649.

41. Levenga H, Schaap N, Maas F, et al. Partial T cell-depleted allogeneic stem cell transplantation following reduced-intensity conditioning creates a platform for immunotherapy with donor lymphocyte infusion and recipient dendritic cell vaccination in multiple myeloma. *Biol Blood Marrow Transplant*. 2010;16(3):320-332.

42. Levenga H, Woestenenk R, Schattenberg AV, et al. Dynamics in chimerism of T cells and dendritic cells in relapsed CML patients and the influence on the induction of alloreactivity following donor lymphocyte infusion. *Bone Marrow Transplant*. 2007;40(6):585-592.

43. Mielcarek M, Kirkorian AY, Hackman RC, et al. Langerhans cell homeostasis and turnover after nonmyeloablative and myeloablative allogeneic hematopoietic cell transplantation. *Transplantation*. 2014;98(5):563-568.

44.   Fischer J, Paret C, El Malki K, et al. CD19 Isoforms Enabling Resistance to CART-19 Immunotherapy Are Expressed in B-ALL Patients at Initial Diagnosis. *J Immunother*. 2017;40(5):187-195.

45.   Sotillo E, Barrett DM, Black KL, et al. Convergence of Acquired Mutations and Alternative Splicing of CD19 Enables Resistance to CART-19 Immunotherapy. *Cancer Discov*. 2015;5(12):1282-1295.

46.   Orlando EJ, Han X, Tribouley C, et al. Genetic mechanisms of target antigen loss in CAR19 therapy of acute lymphoblastic leukemia. *Nat Med*. 2018;24(10):1504-1506.

6

ADDENDUM

NEDERLANDSE SAMENVATTING

Alemtuzumab; de mechanismen van differentiële gevoeligheid en resistentie

Het afweersysteem, ook wel het immuunsysteem genoemd, heeft zich geëvolueerd tot een zeer efficiënt systeem dat als doel heeft ziektes te voorkomen. Dit doet het door herkenning en vernietiging van gevaarlijke lichaamsvreemde entiteiten en van ontregelde lichaamseigen cellen. In uitzonderlijke gevallen faalt het afweersysteem. Therapieën die erop gericht zijn direct invloed uit te oefenen op het afweersysteem, door stimulatie of juist onderdrukking, zijn in de laatste decennia zeer effectief gebleken in de genezing van een breed scala aan ziekten waarbij het natuurlijke afweer onvoldoende was.

Alemtuzumab is een medicijn dat gebaseerd is op een molecuul, een antilichaam, dat van nature deel uitmaakt van het afweersysteem. Antilichamen zijn eiwitten die met hoge specificiteit hun doelwit binden. Dit doen zij met hun variabele domeinen. Antilichamen worden geproduceerd door B cellen, waarbij elke B-cel kloon een antilichaam produceert met een uniek variabel domein. Door de grote diversiteit aan B-cel klonen is het afweersysteem in staat om een breed scala aan doelwitten te herkennen. Naast de variabele domeinen bevatten antilichamen ook een constant domein, dat gelijk is tussen verschillende antilichamen. Via dit constante domein zijn antilichamen in staat tot het rekruteren en het activeren van andere componenten van het afweersysteem, die vervolgens in staat kunnen zijn tot vernietiging van het doelwit. Voor het antilichaam-geïnduceerde vernietigen van lichaamscellen is van de volgende mechanismen bekend dat zij hieraan bijdragen; complement gemedieerde lysis (CDC), antilichaam-afhankelijke celgemedieerde cytotoxiciteit, en antilichaam-afhankelijke celgemedieerde fagocytose. De efficiëntie van deze mechanismen wordt beïnvloed door diverse factoren zoals de concentratie van het antilichaam, de mate van aanwezigheid van het doelwit(eiwit), en in het geval van CDC, de aanwezigheid van complement en complement-inhibitoren.

Alemtuzumab is een monoklonaal antilichaam, wat betekent dat alle antilichamen in dit medicijn van een enkele B-cel kloon afkomstig zijn en identieke domeinen hebben. Het doelwit voor alemtuzumab is CD52, een eiwit dat indirect geankerd is aan het buitenmembraan van cellen door een covalente binding te vormen met het glycolipide glycosylfosfatidylinositol (GPI). CD52 wordt tot expressie gebracht op het celmembraan van rijpe lymfocyten, maar niet op bloedvormende stamcellen, rode bloedcellen, of op niet-bloedvormende cellen. Door deze unieke distributie zal het toedienen van alemtuzumab

leiden tot de vernietiging van rijpe lymfocyten zonder dat het schade toebrengt aan overige weefsels. Rijpe lymfocyten is de verzamelnaam van een brede set aan gedifferentieerde witte bloedcellen die een zeer potent onderdeel van het afweersysteem vormen. Belangrijke voorbeelden van rijpe lymfocyten zijn T cellen en B cellen. En zijn verscheidene klinische toepassingen waarbij het doel is om rijpe lymfocyten te vernietigen doormiddel van de toediening van alemtuzumab. Twee toepassingen die worden beschreven in dit proefschrift zijn T-cel depletie voor allogene stamceltransplantatie (alloSCT) en depletie van maligne B cellen.

AlloSCT is een in opzet curatieve therapie voor patiënten met ziekten die hun oorsprong hebben in het bloedvormend systeem. Het doel van alloSCT is om de bloedvormende stamcellen van de patiënt te vervangen door stamcellen van een gezonde donor om daarmee een normale, van de donor stamcellen afkomstige, bloedcelontwikkeling te introduceren. In het stamcel transplantaat (graft) dat afgenomen is bij de donor zitten naast stamcellen ook rijpe lymfocyten. Zowel het positieve therapeutische effect van alloSCT alsmede de ongewenste bijwerkingen worden met name veroorzaakt door donor T cellen die in het transplantaat aanwezig zijn op het moment van infusie bij de patiënt. Deze donor T cellen zijn in staat om cellen van de patiënt te herkennen en te vernietigingen. In het geval van vernietiging van maligne cellen die de voorbehandeling van de patiënt hebben overleefd zal dit leiden tot het therapeutische 'graft-versus-tumor' (GvT)-effect. In het geval van herkenning van gezond patiëntweefsel (bijvoorbeeld huid, lever, of darm) zal dit leiden tot orgaanschade, een toxisch en potentieel dodelijk proces dat 'graft-versus-host'-ziekte (GvHD) wordt genoemd. Depletie van donor T cellen door directe toevoeging van alemtuzumab aan het transplantaat voor infusie in de patiënt kan er voor zorgen dat zowel het GvT-effect als de GvHD een halt wordt toegeroepen. Deze vorm van voorbehandeling van het transplantaat heeft bewezen de incidentie van GvHD sterk te reduceren. Desalniettemin ontwikkelt een klein deel van patiënten nog steeds GvHD. Alemtuzumab dat aanwezig is in de zak van het transplantaat, al dan niet gebonden aan cellen, wordt samen met de stamcellen per infuus aan de patiënt gegeven. Het is waarschijnlijk dat deze infusie van alemtuzumab in de patiënt de vroege ontwikkeling van rijpe lymfocyten negatief beïnvloedt, wat vervolgens een negatieve impact kan hebben op de kracht van het afweersysteem. Details van dit proces waren echter onduidelijk.

Een tweede klinische toepassing van alemtuzumab is de behandeling van maligniteiten in bloedvormende cellen die CD52 tot expressie brengen. Een voorbeeld hiervan is B-cel acute lymfatische leukemie (B-ALL), een ziekte waarbij ongeremde groei van voorloper B cellen de normale vorming van bloedcellen

in het beenmerg verdrukt. B-ALL cellen van vrijwel alle sub-classificeringen brengen CD52 tot expressie op het membraan. Toediening van alemtuzumab kan daardoor celdood van de maligne B-ALL cellen tot gevolg hebben. Helaas is echter gebleken dat bij veel patiënten kort na een succesvolle behandeling met alemtuzumab de ziekte terugkomt. Deze teruggekomen vorm van de ziekte bleek in veel gevallen niet langer gevoelig voor behandeling met alemtuzumab doordat de B-ALL cellen CD52 expressie hadden verloren. De oorzaak van afwezigheid van CD52 op deze cellen was onbekend.

Dit proefschrift

Om de klinische toepassingen van alemtuzumab te optimaliseren is het van belang om te weten welke factoren invloed uitoefenen op de efficiëntie waarmee alemtuzumab vernietiging van doelwitcellen kan induceren. Ook is het van belang om te achterhalen via welk(e) mechanisme(n) doelwitcellen kunnen ontsnappen aan alemtuzumab.

Om de potentieel ernstige gevolgen van GvHD na alloSCT te voorkomen worden T cellen uit het stamceltransplantaat verwijderd doormiddel van alemtuzumab-geïnduceerde T-cel depletie. Om inzicht te krijgen in de kinetiek van alemtuzumab en zijn effect op circulerende T cellen in patiënten die een alloSCT hebben ondergaan met een stamceltransplantaat waarvan de T cellen waren gedepleteerd doormiddel van toevoeging van alemtuzumab, waarbij in de voorbehandeling van de patiënt ook of juist geen alemtuzumab was gebruikt, hebben we in een prospectieve studie de concentratie alemtuzumab in plasma en het aantal circulerende T cellen na alloSCT gemeten in een cohort van 36 patiënten. De resultaten van deze analyse staan beschreven in **HOOFDSTUK 2**. We laten zien dat de hoogste concentratie alemtuzumab gemeten na transplantatie substantieel verschilt tussen de patiënten. Dit verschil was met name toe te schrijven aan verschillen in plasma volume en niet aan de hoeveelheid T cellen die aanwezig waren voor de start van alemtuzumab behandeling. De depletie van T cellen was efficiënt in alle patiënten. Patiënten die een alemtuzumab concentratie boven de 6,5 μg/mL bereikten ontwikkelden geen ernstige GvHD. De aanwezigheid van alemtuzumab na alloSCT in een plasma concentratie boven de 0,7 μg/mL belemmerde CD52-positieve T cellen om in aantal te herstellen. Desondanks had geen van de patiënten zware complicaties als gevolg van het Epstein-Barr-virus of het cytomegalovirus, wat aangeeft dat ze nog voldoende anti-virale T-cel immuniteit hadden. Dit heeft waarschijnlijk te maken met het beschermende effect van het uitgroeien van CD52-negatieve T cellen, hetgeen niet beïnvloed werd door de aanwezigheid van alemtuzumab na transplantatie.

CDC is een van de mechanismen waarvan wordt gedacht dat zij belangrijk is voor het vernietigen van door therapeutisch antilichaam gebonden doelwitcellen. In **HOOFDSTUK 3** hebben we de relatieve bijdrage bestudeerd van verschillende factoren op de efficiëntie van antilichaam-geïnduceerde CDC. We hebben gebruik gemaakt van alemtuzumab en de representatieve therapeutische antilichamen rituximab en ofatumumab (beide anti-CD20) om CDC te induceren van een selectie van B-ALL cellijnen en primaire B-ALL samples. We laten zien dat de gevoeligheid van doelwitcellen voor antilichaam-geïnduceerde CDC voornamelijk afhankelijk is van de antilichaam concentratie en van de dichtheid van het doelwiteiwit van het antilichaam op de cel. Gezuiverde GPI-anker negatieve celculturen van twee B-ALL cellijnen bleken extra gevoelig te zijn voor CDC geïnduceerd door rituximab en ofatumumab, omdat zij geen expressie hadden van de membraangebonden complement inhibitoren CD55 en CD59. Door CD55 en CD59 geforceerd tot expressie te brengen hebben we laten zien dat beide inhibitoren onafhankelijk van elkaar in staat zijn om CDC te beperken. Dit beperkende effect was alleen aanwezig binnen een begrensde spreiding van expressie van het doelwiteiwit van de antilichamen en binnen een begrensde antilichaam concentratie, wat impliceert dat het effect van CD55 en CD59 ondergeschikt is aan deze factoren. Door gebruik te maken van primaire B-ALL samples hebben we laten zien dat de natuurlijke variatie van CD55 of CD59 expressie niet kan worden gebruikt als een individuele factor voor het voorspellen van de gevoeligheid van doelwitcellen voor CDC.

Een relatief vroeg herstel van het aantal circulerende T cellen is te zien na een alloSCT met een transplantaat gedepleteerd van T cellen doormiddel van toevoeging van alemtuzumab. Dit komt omdat er, in tegenstelling tot een niet-gedepleteerde alloSCT, minder gebruik wordt gemaakt van medicatie die de uitgroei van afweercellen remt. Een deel van deze circulerende T cellen is negatief voor CD52 membraanexpressie, zoals beschreven en uitgelegd in **HOOFDSTUK 2**. Deze CD52-negatieve T cellen leveren mogelijk een positieve bijdrage aan het afweersysteem vroeg na een alloSCT. In **HOOFDSTUK 4** laten we een uitgebreide analyse zien van de mate waarin CD52-negatieve T cellen een bijdrage leveren aan het vroege herstel in het aantal T cellen. Daarnaast helderen we op wat het mechanisme is dat resulteert in het verlies van CD52 expressie van het membraan van deze cellen. In een cohort van 89 patiënten die een alloSCT hadden ondergaan voor verschillende maligne en niet-maligne aandoeningen aan het bloedvormend systeem, hebben we laten zien dat 6 weken na infusie van het transplantaat in de meerderheid van patiënten het grootste deel van de CD4-positieve T cellen en een substantieel deel van de CD8-positieve T cellen negatief waren voor CD52 membraanexpressie. Binnen de NK en B cellen van dezelfde patiënten waren daarentegen geen duidelijk CD52-negatieve cel populaties detecteerbaar.

Directe kleuring van het GPI-anker bevestigde dat verlies van CD52 membraanexpressie het resultaat was geweest van verlies van GPI-anker expressie, wat in voorgaande publicaties al gesuggereerd werd. Doelgerichte sequentieanalyse op mRNA van klonaal geëxpandeerde GPI/CD52-negatieve en -positieve T cellen van drie patiënten die een alloSCT hadden ondergaan liet zien dat een zeer polyklonale diversiteit aan mutaties in het *PIGA* gen de oorzaak was van het verlies van het GPI-anker en de samenvallende afwezigheid van CD52 membraanexpressie. Geforceerde expressie van wildtype *PIGA* in de GPI/CD52-negatieve T-cel klonen herstelde het GPI/CD52-positieve fenotype. De GPI/CD52-negatieve cellen die aanwezig waren na alloSCT hadden hun oorsprong voornamelijk vanuit de donor, wat aangetoond werd door chimerisme analyse. In cellen afkomstig van twee donoren waren GPI/CD52-negatieve T cellen reeds aanwezig in lage frequenties. Sequentie analyse van het *PIGA* gen op mRNA van klonaal geëxpandeerde T cellen van de donor liet zien dat een zeer polyklonale diversiteit aan mutaties in het *PIGA* gen aanwezig was, die gelijkenis vertoonde met die van de patiënten die een alloSCT hadden ondergaan. Niettemin waren slechts enkele identieke mutaties aanwezig in zowel de donor als de gematchte patiënt, wat waarschijnlijk het gevolg is van de beperkte diepte van onze analyse. Functionele analyse van de GPI/CD52-negatieve T-cel populaties toonde aan dat deze meerdere functionele virus-specifieke T cellen bevatten, wat een ondersteuning biedt voor de hypothese dat deze cellen een heilzame rol kunnen vervullen vroeg na alloSCT met een transplantaat gedepleteerd van T cellen doormiddel van toevoeging van alemtuzumab.

Behandeling van B-ALL met enkel alemtuzumab resulteert in eerste instantie in goede klinische responsen, echter deze worden frequent gevolgd door een snelle terugkeer van de ziekte door uitgroei van een deel van de maligne cellen die negatief zijn voor CD52 en daardoor resistent zijn tegen de behandeling. In **HOOFDSTUK 5** tonen we het mechanisme waardoor deze B-ALL cellen negatief worden voor CD52 expressie. We hebben laten zien dat de afwezigheid van CD52 membraanexpressie het resultaat was van verlies van GPI-anker expressie. Analyse van een cohort patiënten met B-ALL toont aan dat maligne cellen met een GPI/CD52-negatief fenotype al in een lage frequentie aanwezig waren voor de start van de behandeling met alemtuzumab. Een onvooringenomen analyse van mRNA expressie van genen die betrokken zijn bij de vorming van het GPI-anker bracht aan het licht dat afwezigheid van *PIGH* expressie de oorzaak was van de afwezigheid van het GPI-anker. Om de diepere oorzaak van het verlies van *PIGH* expressie te onderzoeken hebben we gebruik gemaakt van twee gezuiverde GPI/CD52-negatieve celculturen die afkomstig waren van primaire B-ALL samples en die reeds gebruikt werden in de experimenten beschreven in **HOOFDSTUK 3**. Geforceerde expressie van *PIGH* mRNA in deze

celculturen herstelde expressie van het GPI-anker en de samenvallende membraanexpressie van CD52, wat bevestigde dat afwezigheid van *PIGH* mRNA expressie de primaire onderliggende oorzaak was van het GPI/CD52-negatieve fenotype. Epigenetische onderdrukking van gen expressie en niet een mutatie in of deletie van het *PIGH* gen was de oorzaak van verlies van *PIGH* mRNA expressie in deze B-ALL cellen, bleek na een diepte analyse. Behandeling met 5-aza-2'-deoxycytidine, een medicijn dat effect heeft op de epigenetica van cellen, herstelde het GPI/CD52-positieve fenotype in de maligne B-ALL cellen, wat erop duidt dat dit medicijn potentieel synergie kan opleveren wanneer het wordt gegeven in combinatie met alemtuzumab behandeling.

Samenvattend

Het patroon van CD52 expressie maakt alemtuzumab een uniek therapeutisch antilichaam met een brede klinische inzetbaarheid. De resultaten beschreven in dit proefschrift dragen bij aan het vergroten van onze kennis over de factoren die de gevoeligheid van doelwitcellen voor vernietiging door alemtuzumab beïnvloeden. Deze kennis is relevant voor huidige behandelingen van maligniteiten met alemtuzumab, voor het gebruik van alemtuzumab voor depletie van T cellen voor alloSCT om GvHD te voorkomen, voor nieuwe toepassingen van alemtuzumab zoals de behandeling van multiple sclerosis, en breder bekeken voor andere en toekomstige therapeutische antilichamen die celdood induceren. Ontsnapping aan therapie door verlies van expressie van het doelwiteiwit van het membraan van doelwitcellen is een voortdurende uitdaging voor therapeutische antilichamen en is recent ook beschreven voor chimere antigeenreceptor T-cel therapie. De in dit proefschrift beschreven niet-traditionele mechanismen van ontsnapping van doelwitcellen, doormiddel van epigenetische onderdrukking of door een zeer polyklonale diversiteit aan mutaties, stelt andere onderzoekers in staat om nieuwe ontsnappingsmechanismen sneller te identificeren. Tot slot, het inzicht dat we hebben gekregen in de kinetiek van alemtuzumab na alloSCT en de erkenning van de overvloed en functie van CD52/GPI-negatieve T cellen zou het correct timen van cellulaire interventies kunnen bevorderen en zou toekomstige T-cel depletie strategieën kunnen optimaliseren.

DANKWOORD

"*Alles wat een ander kan, kun jij ook! Hoogstens, duurt het wat langer*", sprak   mijn vader regelmatig uit. Er is geen treffendere beschrijving voor mijn promotietraject.

Bij de totstandkoming van dit proefschrift zijn veel mensen direct en indirect betrokken geweest. Ik ben hen zeer erkentelijk voor alle hulp en steun die ik heb mogen ontvangen. Voor een aantal personen in het bijzonder is een simpel 'dagge bedaankt zij, dah witte war', zoals op z'n Brabants gezegd, niet voldoende om recht te kunnen doen aan hun betekenisvolle bijdrage. Vandaar dat ik hen specifiek wil bedanken.

Allereerst mijn promotor Prof.dr. Fred Falkenburg en copromotoren Dr. Stijn Halkes en Dr. Inge Jedema voor hun wetenschappelijke inzichten en begeleiding. Zij weten elkaar op een natuurlijke wijze te completeren, waardoor ik bijzonder veel van hun supervisie heb mogen leren. Op momenten was het intimiderend om tegen zoveel wetenschappelijk meesterschap te moeten opboksen. Desalniettemin ben ik, ten gevolge van de beproevingen, boven mezelf uitgestegen en durf ik met bescheiden trots te stellen dat het me juist daardoor is gelukt om het proefschrift in zijn huidige vorm neer te zetten.

Daarnaast alle (oud-)collega's van het laboratorium voor experimentele hematologie. Samen zorgen zij voor een vertrouwde werksfeer, die fungeert als een grote familie. Dit bemerk je aan de oprechte interesse in elkaars onderzoek en de zeer grote mate van bereidheid om mee te helpen en om mee te denken. Ik mis de gezelligheid 'op de brug' en misschien nog wel het meest de ongemakkelijke toespraakjes voor jarigen. In het bijzonder wil ik de kamergenoten op C5 benoemen; Aicha, Boris, Hetty, Ilona, Lisa, Lorenz, Margot, Marthe, Matthijs, Pleun, en Sanja, met wie ik regelmatig diepzinnige gesprekken voerde over 'het hoe' en 'het waarom' van een promotie.

Kevin, leverde als student een essentiële bijdrage aan het 5de hoofdstuk van dit proefschrift. Hem wens ik succes in zijn verdere carrière.

Mijn paranimfen, Esther en Lois. Beiden hebben bergen werk voor mij verzet voor de onderzoeken beschreven in dit proefschrift, ik ben hen dan ook zeer dankbaar. Ik waardeer het zeer dat zij naast mij willen staan tijdens mijn verdediging.

Mijn vrienden wil ik zowel danken voor het luisterend oor en de afleiding op de momenten dat het promoveren stroef verliep, als voor het meebeleven van de momenten waarop successen te vieren waren.

Mijn broers, schoonzussen, en tantes voor de onuitputtelijke interesse in de vorderingen van dit bijzondere avontuur. Mijn oma, bij wie ik op de zaterdagen als ontsnapping aan de hectiek mijn klassieke-auto-hobby mocht uitoefenen.

Mijn vader en moeder voor de liefdevolle, onbezorgde jeugd die de basis vormde om mezelf te kunnen ontwikkelen tot de persoon die ik ben, voor de vrijheid om mijn eigen keuzes te maken en voor hun onuitputtelijke aanmoediging. Pa, jouw liefdevolle karakter was uniek en de herinnering hieraan leeft voort in alle mensen die jouw pad hebben mogen kruisen.

Mijn allerliefste Aukje, zij verbreedt mijn perspectief op het leven en laat mij zien wat het betekent om ultiem gelukkig te zijn. Zonder haar bijdrage zou dit proefschrift niet zo mooi zijn. Het was een genot om dit avontuur met haar te mogen delen.

CURRICULUM VITAE

Floris Loeff werd geboren op 5 november 1986 te Willemstad, Noord-Brabant. Na het behalen van het VWO-diploma aan het Altena College te Sleeuwijk, werd in 2004 begonnen aan de Bachelor Bio-medische Wetenschappen aan de Universiteit van Utrecht. Deze studie werd door hem in 2007 afgerond en werd vervolgd met de Master Immunity and Infection, eveneens aan de Universiteit van Utrecht. Masterstages werden uitgevoerd op de afdeling Infectieziekten en Immunologie van de Faculteit Diergeneeskunde aan de Universiteit van Utrecht (begeleid door van Dr. D. Zaiss) en de afdeling Proces Ontwikkeling van het Nederlands Vaccin Instituut te Bilthoven (begeleid door Ir. Y.E. Thomassen). De Masterthesis werd door hem geschreven op de afdeling Pathologie van het VU Medisch Centrum te Amsterdam (begeleid door Dr. J.J.M. Hoozemans). In 2011 heeft hij deze Masterstudie afgerond. In datzelfde jaar is hij gestart met het in dit proefschrift beschreven promotieonderzoek uitgevoerd op het Laboratorium voor Experimentele Hematologie, welk onderdeel is van de Afdeling Hematologie in het Leids Universitair Medisch Centrum onder begeleiding van Dr. Inge Jedema, Dr. Stijn Halkes, en Prof Dr. Fred Falkenburg. Van augustus 2017 tot mei 2020 is hij werkzaam geweest als onderzoeker bij Sanquin Research in het laboratorium onder leiding van Dr. Theo Rispens, waar hij onder meer onderzoek deed aan immunogeniciteit van biologicals. Dit onderzoek werd uitgevoerd in nauwe samenwerking met het Biologics laboratorium van Sanquin Diagnostiek onder leiding van Annick de Vries. Vanaf februari 2020 kreeg hij als onderzoeker een gedeelde aanstelling, voor zowel Sanquin Research als Sanquin Diagnositiek. Per mei van datzelfde jaar werd de volledige overstap gemaakt naar het Biologics laboratorium, waar hij nu zijn passie voor therapeutische antistoffen voortzet.

LIST OF PUBLICATIONS

Loeff FC, van Egmond EHM, Moes DJAR, Wijnands C, Von Dem Borne PA, Veelken H, Falkenburg JHF, Jedema I, Halkes CJM. Impact of alemtuzumab pharmacokinetics on T-cell dynamics, graft-versus-host disease and viral reactivation in patients receiving allogeneic stem cell transplantation with an alemtuzumab-based T-cell-depleted graft. *Transplant Immunology*. 2019 Jun 14. pii: S0966-3274(19)30041-3.

Loeff FC, van Egmond HME, Nijmeijer BA, Falkenburg JHF, Halkes CJ, Jedema I. Complement-dependent cytotoxicity induced by therapeutic antibodies in B-cell acute lymphoblastic leukemia is dictated by target antigen expression levels and augmented by loss of membrane-bound complement inhibitors. *Leukemia & Lymphoma*. 2017 Sep;58(9):1-14.

Loeff FC, Falkenburg JHF, Hageman L, Huisman W, Veld SAJ, van Egmond HME, van de Meent M, von dem Borne PA, Veelken H, Halkes CJM, Jedema I. High mutation frequency of the *PIGA* gene in T cells results in reconstitution of GPI anchor-/CD52- T cells that can give early immune protection after alemtuzumab-based T cell-depleted allogeneic stem cell transplantation. *The Journal of Immunology*. 2018 Mar 15;200(6):2199-2208.

Loeff FC, Rijs K, van Egmond EHM, Zoutman WH, Qiao X, Kroes WGM, Veld SAJ, Griffioen M, Vermeer MH, Neefjes J, Frederik Falkenburg JH, Halkes CJM, Jedema I. Loss of the GPI-anchor in B-lymphoblastic leukemia by epigenetic downregulation of *PIGH* expression. *American Journal of Hematology*. 2019 Jan;94(1):93-102.

Publications not in the this thesis

Steenhuis M, van Mierlo G, Derksen NIL, Ooijevaar-de Heer P, Kruithof S, **Loeff FC**, Berkhout LC, Linty F, Reusken C, Reimerink J, Hogema B, Zaaijer H, van de Watering L, Swaneveld F, van Gils MJ, Bosch BJ, van Ham SM, ten Brinke A, Vidarsson G, van der Schoot EC, Rispens T. Dynamics of antibodies to SARS-CoV-2 in convalescent plasma donors. *MedRχiv*. Posted January 06, 2021 doi: 10.1101/2021.01.06.20249035.

Jacobse J, Ten Voorde W, Tandon A, Romeijn SG, Grievink HW, van der Maaden K, van Esdonk MJ, Moes DJAR, **Loeff FC**, Bloem K, de Vries A, Rispens T, Wolbink G, de Kam M, Ziagkos D, Moerland M, Jiskoot W, Bouwstra J, Burggraaf J, Schrier L, Rissmann R, Ten Cate R. Comprehensive evaluation of microneedle-based intradermal adalimumab delivery vs. subcutaneous administration: results of a randomized controlled clinical trial. *British Journal of Clinical Pharmacology*. 2021 Jan 5. doi: 10.1111/bcp.14729. [Online ahead of print]

Vogelzang EH*, **Loeff FC***, Derksen NIL, Kruithof S, Ooijevaar-de Heer P, van Mierlo G, Linty F, Mok JY, van Esch W, de Bruin S, Vlaar APJ; Amsterdam University Medical Center COVID-19 Biobank Study Group,, Seppen B, Leeuw M, van Oudheusden AJG, Buiting AGM, Jim KK, Vrielink H, Swaneveld F, Vidarsson G, van der Schoot CE, Wever PC, Li W, van Kuppeveld F, Murk JL, Bosch BJ, Wolbink GJ, Rispens T. Development of a SARS-CoV-2 total antibody assay and the dynamics of antibody response over time in hospitalized and nonhospitalized patients with COVID-19. *The Journal of Immunology*. 2020 Dec 15;205(12):3491-3499. doi: 10.4049/jimmunol.2000767.
*E.H.V. and **F.C.L**. contributed equally.

Großerichter-Wagener C, Kos D, van Leeuwen A, Dijk L, Jeremiasse J, **Loeff FC**, Rispens T. Biased anti-idiotype response in rabbits leads to high-affinity monoclonal antibodies to biologics. *MAbs*. Jan-Dec 2020;12(1):1814661. doi: 10.1080/19420862.2020.1814661.

Loeff FC, Tsakok T, Dijk L, Hart MH, Duckworth M, Baudry D, Russell A, Dand N, van Leeuwen A, Griffiths CEM, Reynolds NJ, Barker J, Burden AD, Warren RB, de Vries A, Bloem K, Wolbink GJ, Smith CH, Rispens T; on behalf of the BADBIR and BSTOP Study Groups and the PSORT Consortium. Clinical impact of antibodies against ustekinumab in psoriasis: an observational,

cross-sectional, multicenter study. *The Journal of Investigative Dermatology*. 2020 Apr 10 doi: 10.1016/j.jid.2020.03.957.

Atiqi S, Hooijberg F, **Loeff FC**, Rispens T, Wolbink GJ. Immunogenicity of TNF-Inhibitors. *Frontiers in Immunology*. 2020 Feb 26 11:312 doi: 10.3389/fimmu.2020.00312.

Pan S, Tsakok T, Dand N, Lonsdale DO, **Loeff FC**, Bloem K, de Vries A, Baudry D, Duckworth M, Mahil S, Pushpa-Rajah A, Russell A, Alsharqi A, Becher G, Murphy R, Wahie S, Wright A, Griffiths CEM, Reynolds NJ, Barker J, Warren RB, David Burden A, Rispens T, Standing JF, Smith CH; BADBIR Study Group, the BSTOP Study Group, the PSORT Consortium. Using real-world data to guide ustekinumab dosing strategies for psoriasis: A prospective pharmacokinetic-pharmacodynamic study. *Clinical and Translational Science*. 2020 Mar;13(2):400-409. doi: 10.1111/cts.12725.

Tsakok T, Wilson N, Dand N, **Loeff FC**, Bloem K, Baudry D, Duckworth M, Pan S, Pushpa-Rajah A, Standing JF, de Vries A, Alsharqi A, Becher G, Murphy R, Wahie S, Wright A, Griffiths CEM, Reynolds NJ, Barker J, Warren RB, Burden AD, Rispens T, Stocken D, Smith C; British Association of Dermatologists Biologic and Immunomodulators Register (BADBIR) Study Group and the Psoriasis Stratification to Optimise Relevant Therapy (PSORT) Consortium. Association of serum ustekinumab levels with clinical response in psoriasis. *JAMA Dermatology*. 2019 Sep 18. doi: 10.1001/jamadermatol.2019.1783. [Epub ahead of print]

Berkhout LC, Vogelzang EH, Hart MM, **Loeff FC**, Dijk L, Derksen NIL, Wieringa R, van Leeuwen WA, Krieckaert CLM, de Vries A, Nurmohamed MT, Wolbink GJ, Rispens T. The effect of certolizumab drug concentration and anti-drug antibodies on TNF neutralisation. *Clinical and Experimental Rheumatology*. 2019 Aug 30. [Epub ahead of print]

Alford SE, Kothari A, **Loeff FC**, Eichhorn JM, Sakurikar N, Goselink HM, Saylors RL, Jedema I, Falkenburg JH, Chambers TC. BH3 Inhibitor Sensitivity and Bcl-2 dependence in primary acute lymphoblastic leukemia cells. *Cancer Research*. 2015 Apr 1;75(7):1366-75.